



Universidade do Minho  
Escola de Engenharia

Ana Alexandra Gonçalves Figueiredo

Evaluation of Temperature Influence on  
Embedded Kinematic System





Universidade do Minho  
Escola de Engenharia

Ana Alexandra Gonçalves Figueiredo

Evaluation of Temperature Influence on  
Embedded Kinematic System

Dissertação de Mestrado  
Ciclo de Estudos Integrados Conducentes ao  
Grau de Mestre em Engenharia Mecânica

Trabalho efectuado sob a orientação do  
Professor Doutor José Filipe Bizarro Meireles  
Engenheiro Pedro Miguel de Sousa Bernardo

## DECLARAÇÃO

Nome: Ana Alexandra Gonçalves Figueiredo

Endereço eletrónico: a62869@alunos.uminho.pt Telefone: 911530742

Cartão do Cidadão: 13922058

Título da dissertação: Evaluation of Temperature Influence on Embedded Kinematic System

Orientador:

Professor Doutor José Filipe Bizarro Meireles

Engenheiro Pedro Miguel de Sousa Bernardo

Ano de conclusão: 2015

Mestrado Integrado em Engenharia Mecânica

É AUTORIZADA A REPRODUÇÃO INTEGRAL DESTA DISSERTAÇÃO APENAS PARA EFEITOS DE INVESTIGAÇÃO, MEDIANTE DECLARAÇÃO ESCRITA DO INTERESSADO, QUE A TAL SE COMPROMETE.

Universidade do Minho, \_\_\_\_/\_\_\_\_/\_\_\_\_

Assinatura:

"Alone we can do so little, together we can do so much."

Helen Keller

## ACKNOWLEDGMENTS

I would like to start my acknowledgements by saying that I was a very lucky person since I was surrounded by amazing people who were fundamental to me throughout this entire project. The knowledge shared paired with my devotion and commitment were the basic elements to accomplish this hard task.

Firstly, I would like to thank to the company Bosch Car Multimedia S.A. for sheltering me and providing me all the equipment, software and services necessary to fulfil the execution of the assignments.

It is also important to show my deep appreciation for all the members of the mechanical development section (END) for welcoming me and making me feel I belonged there. To my colleagues Pedro Moreira, Nuno Pinto, Pedro Filipe Moreira and Filipe Loureiro I want to thank for all the times they made me laugh and all the bad days they changed into something better with their humour. They have no idea how important that was to me. Their guidance and patience to help me were indispensable for the conclusion of my dissertation.

Next, I would like to thank profusely to José Azevedo, head of the mechanical development section and also Pedro Bernardo, my mentor for receiving and accepting me in their team. They believed in my capabilities and gave me this opportunity which is something I will never forget. Their patience and advice were also essential to solve the problems I have been encountered during my path and they always did their best to find a solution.

It is a genuine pleasure to express my gratitude to my supervisor Professor José Meireles for his commitment and full dedication to my work. His knowledge and words of wisdom made all the difference and his persistent help guided me during the execution of this dissertation. In those moments when I lost my temper, I really appreciate for making me believe that I have much potential and I am capable of overcoming all the obstacles in my way.

I could not forget to thank to my colleague Ricardo Campos for his availability, commitment and patience. For several times he was the only one to whom I could turn to. Although he thinks he was just a little help, I truly do not know how I could have finished my work if it was not for his tremendous contribution.

I would also like to present my gratitude to the project HMIExcel n° 36265/2013 (2013-2015) for providing me this opportunity and turn a possibility into reality.

My family is a fundamental support as they encourage me to do more and be better every single day. My parents are my heroes, the ones who fought really hard for everything I have, they are undoubtedly an example to me, the people I admire the most. My sister is my best friend and is always prepared to say exactly what I need to hear in a kindly manner and no one else can understand me like she does. My little and adorable niece is the cure for all the bad moments because her kisses, hugs and smiles make me forget all the problems of my life.

I would like to give a special thank you to my boyfriend, Filipe Marques, my confident and best friend who was always there for me, in the best and worst moments. He is essential in my life and always was an unconditional support. I would not have overcome this difficult phase of my life if it had not been for him.

Last but not least, I would like to say a very big thank you for all my colleagues who were by my side in the last 5 years. In a special way, Henrique and Carlos Grenha left their mark in my life, they are like brothers to me, thank you so much for all the companionship and the memorable moments we spent together.

## ABSTRACT

The present dissertation was developed within the course of Integrated Master in Mechanical Engineering, its title is “Evaluation of Temperature Influence in Embedded Kinematic System” and it was executed at the company Bosch Car Multimedia during the last few months. The main objective is to display the results of the search performed, as well as the decisions drawn along the way. This work includes the study, analysis and simulation of a proposed problem. The motivation in choosing this theme is related with a problem of Bosch and, for that reason, they would like to investigate and, consequently, find a solution.

Initially, it is necessary to perform some research about gear history, since its discovery until nowadays, including its importance in society and examples of application. Next, it is studied what have already been done in this field by other engineers, namely thermal simulations on gears and thermal-stress simulations on diverse products. Then, the theoretical introduction is presented not only the thermal and mechanical phenomena but also the methods used to formulate a model and solve the problem in software ANSYS v16.0 (ANSYS, 2015).

It is fundamental to present the component in study, its specifications and characteristics as well as developing a kinematic and dynamic analyses. It is important to show and explain what was implemented in the programme highlighting the most relevant aspects, such as, materials, mesh, boundary conditions and the results, which can be of thermal or mechanical nature.

Next, it is described with detail the experiment performed on the component, which is constituted by two phases. The obtained results are analysed based on what was determined through the numerical results, followed by a comparison of both. Possible error sources of the experimental activity are also referred as well as others from the simulation point of view.

At last, the final conclusions of the project are displayed, highlighting the most important points and what could be improved in the future. Moreover, the objectives of the work are reviewed and it is concluded what was possible to achieve along with the aspects which were not totally solved.

## KEYWORDS

Simulation

Kinematic System

Temperature

Displacements

ANSYS

Polymers

Gear

Heat Transfer

Finite Element Analysis



## RESUMO

A presente dissertação foi desenvolvida no âmbito do curso Mestrado Integrado em Engenharia Mecânica, tem como título “Avaliação da Influência da Temperatura em Sistemas Cinemáticos Incorporados” e foi realizada na empresa Bosch Car Multimedia nos últimos meses. Esta tem como objetivo mostrar os resultados da pesquisa efetuada bem como os caminhos seguidos para a concretização do projeto. Este trabalho visa o estudo, análise e simulação de um problema proposto. A motivação para a escolha deste tema reside num problema que a Bosch possui e, desse modo, gostaria de investigar e, conseqüentemente, encontrar uma solução para o mesmo.

Inicialmente é necessário realizar uma pesquisa relativa à história das rodas dentadas, desde a sua descoberta até aos dias de hoje, incluindo também a sua importância na sociedade e exemplos de aplicação. Seguidamente é estudado o que já foi efetuado nesta área por outros engenheiros, nomeadamente simulações térmicas em rodas dentadas ou simulações térmico-mecânicas em diversos produtos. Posteriormente, estudam-se os fundamentos teóricos relativos não só aos fenómenos térmicos e mecânicos envolvidos mas também aos métodos para formular um modelo e resolver o problema em estudo no software ANSYS v16.0 (ANSYS, 2015).

É fundamental apresentar o componente que se encontra a ser estudado, as suas especificações e características bem como estudá-lo através de uma análise cinemática e uma dinâmica. É importante também mostrar e explicar o que foi implementado no programa, enaltecendo os aspetos mais relevantes, como os materiais, a malha, condições de fronteira e os resultados, o qual podem ser de natureza térmica ou mecânica.

Seguidamente é descrita de forma detalhada a experiência realizada aos componentes, o qual é constituída por duas fases. Os resultados obtidos são analisados com base no que se determinou através dos resultados numéricos, elaborando também uma comparação entre os mesmos. Referem-se possíveis fontes de erro quer da parte da atividade experimental quer do ponto de vista da simulação.

Por fim, são apresentadas as conclusões finais do trabalho onde se enaltece os pontos mais importantes e o que poderia ser melhorado no futuro. Assim, os objetivos do trabalho são revistos e conclui-se o que foi possível concretizar bem como os aspetos que não foram completamente resolvidos.

## PALAVRAS-CHAVE

Simulação

Sistema Cinemático

Temperatura

Deslocamentos

ANSYS

Polímeros

Roda Dentada

Transferência de Calor

Análise de Elementos Finitos

# TABLE OF CONTENTS

Acknowledgments .....	iii
Abstract .....	v
Keywords .....	vi
Resumo .....	vii
Palavras-Chave .....	viii
Table of Contents .....	ix
List of Figures .....	xiii
List of Tables .....	xvii
List of Symbols .....	xix
Acronyms .....	xxiii
1. Introduction .....	1
1.1. Theme Context/Motivation .....	2
1.2. Company Presentation .....	3
1.3. Objectives .....	6
1.4. Work Methodology .....	6
1.5. Overview of Dissertation Content .....	7
2. Background .....	9
2.1. Technical Component .....	12
2.1.1. The History of Gears and Its Importance in the Quotidian .....	12
2.1.2. The Application of Gears in Industry .....	15
2.2. Technological Component .....	21
2.2.1. Thermal Simulations Performed on Gears .....	21
2.2.2. Coupled Simulations Performed on Diverse Components .....	24
3. Theoretical Introduction .....	29
3.1. Finite Element Analysis .....	30
3.1.1. Problem Classification .....	31
3.1.2. Modelling .....	32
3.1.3. Discretisation .....	33
3.1.4. Solving a Problem .....	33

3.2. Finite Volume Method.....	35
3.2.1. Discretisation .....	36
3.3. Heat Transfer Phenomena.....	37
3.3.1. Conduction .....	38
3.3.2. Convection .....	38
3.4. Mechanical Phenomena .....	40
3.4.1. Deformation .....	41
3.4.2. Stress .....	41
3.5. Methods and Types of Elements used on the Mesh.....	42
3.5.1. Global Mesh Controls .....	43
3.5.2. Local Mesh Controls.....	44
3.5.3. Evaluation of Mesh Quality .....	47
3.6. Models used in Simulations .....	49
3.6.1. Steady-State Thermal .....	49
3.6.2. Static Structural.....	50
3.6.3. Fluid-Structure Interaction .....	52
3.7. Experimental Technology.....	54
4. Industrial Application.....	57
4.1. Presentation and Study.....	58
4.1.1. Description of the Navigation System C-HUD.....	58
4.1.2. Specifications of the Kinematics.....	62
4.1.3. Kinematic and Dynamic Analysis.....	66
4.2. Numerical Simulations .....	72
4.2.1. Initial Considerations .....	73
4.2.2. Software Validation .....	78
4.2.3. Simulations on the Total Assembly .....	85
4.2.4. Simulations on One Gear .....	90
4.2.5. Simulations on the Assembly of Gears .....	99
4.2.6. Comparison and Discussion of the Numerical Results .....	105
5. Experimental Validation .....	111
5.1. Description of the Experiment .....	112
5.2. Presentation of the Results.....	114
5.3. Comparison of the Numerical and Experimental Results.....	119
5.3.1. Recommendations for the Functional Dimensions of Manufacturing .....	124

6. Concluding Remarks .....	129
References .....	133
Appendices .....	143
Appendix A.....	145
Appendix B.....	149
Appendix C.....	153
Appendix D.....	157



## LIST OF FIGURES

Figure 1 - Bosch Car Multimedia (Bosch S.A., 2011).....	4
Figure 2 - Types of products developed and produced at Bosch Braga (Bosch Group, 2014)..	4
Figure 3 - Organisational Chart (Bosch Group, 2014).....	5
Figure 4 - Primitive Gear (Branco et al., 2009) .....	13
Figure 5 - Gear Illustrations of Leonardo da Vinci (Drago, 1988) .....	13
Figure 6 - Issus Coleoptratus (Mechanical Gears Seen for the First Time in Nature, 2013)...	15
Figure 7 - Example of Gears (Flores & Claro, 2007).....	16
Figure 8 - Movement Transmission Systems by Intermediate Connection: (a) four bar mechanism; (b) transmission by belt; (c) transmission by chain; (Flores & Claro, 2007) .....	16
Figure 9 - (a) Rotating movement transmission for rotation; (b) Rotating movement transmission for translation (Flores & Gomes, 2015) .....	17
Figure 10 - (a) Gearing with Parallel Shafts; (b) Gearing with Concurrent Shafts; (c) Gearing with Non-Coplanar Shafts (Flores & Gomes, 2015).....	18
Figure 11 - (a) Gears of a mixer; (b) Gears of a toy (Flores & Gomes, 2015) .....	18
Figure 12 - (a) Mechanical Watch; (b) Automobile Differential; (c) Pinion-Rack; (d) Large gear; (e) Counter; (f) Reduction Gear; (g) Industrial Mixer; (h) Manual Reduction Gear of a Car (Flores & Gomes, 2015) .....	19
Figure 13 - A two-dimensional model of a gear tooth (Cook et al., 2002) .....	31
Figure 14 - Mesh for finite volumes: (a) cell-centred; (b) cell-vertex (Moukalled et al., 2015) .....	37
Figure 15 - Axial Forces applied in a Bar (Moaveni, 1999) .....	42
Figure 16 – Tetrahedron with 4 nodes (left) and 10 nodes (centre); Hexahedron with 20 nodes (right) (ANSYS Inc., 2013).....	47
Figure 17 - Triangle Aspect Ratio Calculation (ANSYS Inc., 2013) .....	47
Figure 18 - Aspect Ratios for Triangles (ANSYS Inc., 2013) .....	48
Figure 19 - Maximum Corner Angles for Triangles (ANSYS Inc., 2013) .....	48
Figure 20 - (a) Equilateral Triangle; (b) Highly Skewed Triangle (ANSYS Inc., 2013).....	48
Figure 21 - Principle of Triangulation Technology (LMI Technologies, 2013).....	56
Figure 22 – Unit of Head-Up Display (Bosch Car Multimedia, 2014).....	59

Figure 23 – Representation of Combiner Head-Up Display (Bosch Car Multimedia, 2014)..	59
Figure 24 - Components of C-HUD (Technical Drawings of the Combiner Head-Up Display)	
.....	61
Figure 25 - Components of the Kinematics Module .....	62
Figure 26 - Kinematics System .....	63
Figure 27 - Nomenclature of Gears .....	64
Figure 28 - Representation of the Train .....	66
Figure 29 - Lead Angle of a Worm .....	68
Figure 30 - Forces Applied on a Worm Gear (Gopinath & Mayuram).....	68
Figure 31 - Forces Applied on Spur Gears.....	70
Figure 32 - Assembly in Study.....	74
Figure 33 - Parts of the Assembly .....	74
Figure 34 - View in Detail about Picture Generator Unit .....	75
Figure 35 - Gears of the Assembly.....	75
Figure 36 - Coupled Simulation Steady-State Thermal and Static Structural.....	79
Figure 37 - Geometry and Mesh of the Bar .....	80
Figure 38 - Geometry and Mesh of the Bar with Holes .....	81
Figure 39 - Fixed Bar at both Ends .....	81
Figure 40 - Fixed Bar at both Holes .....	82
Figure 41 - Results for Bar 1 .....	82
Figure 42 - Results for Bar 2 .....	83
Figure 43 - Assembly in Study: (a) Outside; (b) Inside .....	85
Figure 44 - Mesh: (a) Outer Parts; (b) Inner Components .....	86
Figure 45 – Power of the LED .....	87
Figure 46 - Results of Temperature at 20 °C .....	88
Figure 47 - Temperature Distribution at 20 °C .....	88
Figure 48 - Temperature of the LED at 20 °C.....	89
Figure 49 - Results for the Simulation at 90 °C .....	90
Figure 50 - Geometry of the Gear on the Front (left) and on the Back (right) .....	91
Figure 51 - Gear Mesh on the Front and on the Rear.....	91
Figure 52 – Details about the Mesh Teeth .....	92
Figure 53 - Total Deformation for Material POM .....	93
Figure 54 - Total Deformation for Material PP.....	93
Figure 55 - Geometry of the Gear with Enclosure and Respective Mesh.....	94



Figure 56 - Method of Spheres of Influence .....	95
Figure 57 - Residuals of the Simulation.....	96
Figure 58 - Temperature of the Gear.....	97
Figure 59 - Results for the material POM .....	97
Figure 60 - Results for the Material PP .....	98
Figure 61 - Representation of the Assembly Geometry .....	99
Figure 62 - Mesh of the Assembly (Front).....	100
Figure 63 - Mesh of the Assembly (Back) .....	101
Figure 64 - Details about the Mesh .....	102
Figure 65 - Results of Total Deformation for Material POM .....	103
Figure 66 - Von-Mises Stresses for POM Simulation.....	103
Figure 67 - Results of Total Deformation for Material PP .....	104
Figure 68 - Von-Mises Stresses for PP Simulation.....	105
Figure 69 - Comparison of the Software Module .....	107
Figure 70 - Comparison of the Materials .....	107
Figure 71 - Results about Convergence of the Mesh .....	109
Figure 72 - Equipment used in the Experimental Activity (STEINBICHLER - Inspiring Innovation, s.d.).....	112
Figure 73 - Experimental Activity of the Gear at 20 °C .....	113
Figure 74 - Experimental Activity of the Gear at 90 °C .....	114
Figure 75 - Experimental Results for the Teeth at 20 °C .....	115
Figure 76 - Experimental Results for the Teeth at 90 °C .....	116
Figure 77 - Experimental Results for the Path of the Pin at 20 °C .....	116
Figure 78 - Experimental Results for the Path of the Pin at 90 °C .....	117
Figure 79 - Experimental Results for other part of the Pin Path at 20 °C.....	117
Figure 80 - Experimental Results for other part of the Pin Path at 90 °C.....	118
Figure 81 - Experimental Results for the Angular Adjustment Component at 20 °C.....	118
Figure 82 - Experimental Results for the Angular Adjustment Component at 90 °C.....	119
Figure 83 - Teeth Displacement Results .....	120
Figure 84 - Angular Adjustment Component Displacements .....	123



## LIST OF TABLES

Table 1 - Parameters to determine h.....	40
Table 2 - Evaluation of Mesh Quality .....	49
Table 3 - Characteristics of Gears .....	65
Table 4 - Gear Speed.....	67
Table 5 - Values for Air Density at Different Temperatures .....	76
Table 6 - Materials Properties .....	77
Table 7 - Properties of Materials.....	80
Table 8 - Comparison between Theoretical and Numerical Results .....	84
Table 9 - Results of the Radial Displacements .....	106
Table 10 - Number of Mesh Cells and Results .....	108
Table 11 - Comparison between Numerical and Experimental Teeth Results .....	120
Table 12 - Comparison of the Numerical and Experimental Path Results.....	121
Table 13 - Comparison of the Numerical and Experimental Angle Adjustment Component Results .....	122
Table 14 - Tolerances Applied on the Gears .....	124



## LIST OF SYMBOLS

### Latin Symbols

Symbol	Description	Unit
A	Cross-Sectional Area	mm <sup>2</sup>
B	Strain-Displacement Matrix	-
c	Total Clearance	mm
c <sub>r</sub>	Radial Clearance	mm
c <sub>t</sub>	Transversal Clearance	mm
d	Nodal Displacements Vector	mm
d <sub>e</sub>	External Diameter	mm
d <sub>i</sub>	Internal Diameter	mm
d <sub>p</sub>	Primitive Diameter	mm
d <sub>n</sub>	Pitch Diameter of Gear n	mm
e	Width of Space	mm
E	Young's Modulus	MPa
E <sub>CV</sub>	Energy in the Control Volume	J
E <sub>E</sub>	Constitutive Matrix	Pa
f <sub>xy</sub>	Coefficient of Friction between Gears x and y	-
F	Force	N
F <sup>a</sup>	Axial Component of the Force	N
F <sub>B</sub>	Body Forces	N/m <sup>3</sup>
F <sub>E</sub>	External Body Forces Vector	N/m <sup>3</sup>
F <sup>r</sup>	Radial Component of the Force	N
F <sup>t</sup>	Tangential Component of the Force	N
g	Gravitational Acceleration	m/s <sup>2</sup>
g <sub>F</sub>	Fluid Acceleration Vector	m/s <sup>2</sup>
Gr	Grashof Number	-
$\bar{h}$	Average Heat Transfer Coefficient	W/(m <sup>2</sup> .K)
h	Heat Transfer Coefficient	W/(m <sup>2</sup> .K)
h <sub>a</sub>	Radial Distance from the Pitch Circle until the Beginning of the	mm

	Teeth (Addendum)	
$h_f$	Radial Height of the Gear Teeth (Dedendum)	mm
$h_j$	Heat Transfer of Species j	J
$i$	Transmission Ratio	-
$J_j$	Diffusion Flux Vector of Species j	kg/(m <sup>2</sup> .s)
$k$	Heat Flow Matrix	-
$k_{eff}$	Effective Conductivity	W/(m.K)
$k_T$	Thermal Conductivity of the Fluid	W/(m.K)
$K$	Element Stiffness Matrix	-
$l_a$	Length of Approach	mm
$l_r$	Length of Recess	mm
$L$	Length	mm
$L_C$	Characteristic Length	m
$Nu$	Nusselt Number	-
$p$	Pitch	mm
$p_s$	Static Pressure	Pa
$P$	Engine Power	W
$P_A$	Axial Load	N
$Pr$	Prandalt Number	-
$Q$	Thermal Conductance Vector	W
$r_e$	Nodal Loads Vector	N
$r_x$	Radius of Gear x	mm
$Ra$	Rayleigh Number	-
$s$	Tooth Thickness	mm
$S_h$	Source of Heat	J
$S_m$	Source of Mass	kg
$T$	Temperature	°C
$T_s$	Surface Temperature	°C
$T_\infty$	Bulk Temperature	°C
$v$	Flow Velocity Vector	m/s
$Z_n$	Number of Teeth of Gear n	-

## Greek Symbols

Symbol	Description	Unit
$\alpha$	Coefficient of Thermal Expansion	K <sup>-1</sup>
$\alpha_n$	Pressure Angle	°
$\beta$	Lead Angle	°
$\beta_v$	Volumetric Thermal Expansion Coefficient	-
$\delta$	Deformation/Displacement	mm
$\delta\varepsilon$	Virtual Strains	-
$\delta u$	Virtual Displacements	m
$\eta$	Efficiency	-
$\nu$	Kinematic Viscosity	m <sup>2</sup> /s
$\rho$	Fluid Density	kg/m <sup>3</sup>
$\sigma$	Stress	MPa
$\tau$	Stress Tensor	Pa
$\tau_{eff}$	Effective Stress Tensor	Pa
$\Phi$	Surface Traction	Pa
$\omega_n$	Angular Velocity of Gear n	rpm





## ACRONYMS

2D – Two-Dimensional

3D – Three-Dimensional

ANSYS – ANalysis SYStem

AR-HUD – Augmented Reality Head-Up Display

CAD – Computer Aided Design

CAE – Computer Aided Engineering

CATIA – Computer-Aided Three-Dimensional Interactive Application

CFD – Computational Fluid Dynamics

CFX – ANSYS Module for CFD Analysis

C-HUD – Combiner Head-Up Display

CM – Car Multimedia

DEFORM – Engineering Software

DFMA – Design For Manufacturing Assembly

DOF – Degrees Of Freedom

END – Mechanical Development Section

ENG – Engineering Department

FEA – Finite Element Analysis

FEM – Finite Element Method

FVM – Finite Volume Method

HUD – Head-Up Display

ICCG – Incomplete Cholesky Conjugate Gradient

ILC – Intelligent Light Control

ITER – Iterative Solver Option

JCG – Jacobi Conjugate Gradient

LCD – Liquid Crystal Display

LED – Light-Emitting Diode

MUSCL – Monotone Upstream-Centred Schemes for Conservation Laws

NX – Design Modelling Software

PCB – Printed Circuit Board

PCG – Preconditioned Conjugate Gradient  
PDE – Partial Differential Equations  
PGU – Picture Generator Unit  
PISO – Pressure-Implicit with Splitting of Operators  
POM – PolyOxyMethylene  
PP – PolyPropylene Material Reinforced with Carbon and Stainless Steel Fibres  
PRESTO – PREssure STaggering Option  
QUICK – Quadratic Upwind Interpolation for Convective Kinematics  
RNG – Re-Normalisation Group  
RSM – Reynolds Stress Model  
SIMPLE – Semi-Implicit Method for Pressure-Linked Equations  
SIMPLEC – Semi-Implicit Method for Pressure-Linked Equations Consistent  
SST – Shear-Stress Transport

“It always seems impossible until it is done.”

Nelson Mandela

## 1. INTRODUCTION

In recent times, metal gears are being replaced by the plastic ones in a wide range of applications. This is happening due to the enhancement of their characteristics as a result of researches and studies which have accomplished new discoveries. In addition, plastics are contrasting with metals as they are progressing whether in properties as well as processes while metals present a much higher level of development and, consequently, there are few advancements in this area.

On the other hand, when there is a mathematical model to be solved, the first approach is to do an analytical study where it is intended to find a solution to the set of equations. The problem is that this tends not to function when there are complicated models. For more complex models, the math becomes impossible to solve manually. Then, the alternative is to use numerical methods for solving the problems in study. A computer must be used to perform the thousands of repetitive calculations involved. The result is a gradient of what the solution is, where the applied scale allows to understand the results reached.

There is also a middle ground between these two methods. There are many important non-linear equations for which it is not possible to find an analytic solution. However, there are techniques where you can find approximate analytic solutions that are close to the true solution,

at least within a certain range.

### 1.1. THEME CONTEXT/MOTIVATION

The motivation to choose this theme is related with the necessity of solving a problem which appeared at Bosch through client complaints. There is a component which has been returned several times due to its noise of some pieces inside it. The situation is that there are only suspicions about what could be the problem. Moreover, it was defined that the company should investigate about the root of the problem in order to improve this part. Consequently, it was established to study the behaviour of plastic elements, namely gears, as they could be interfering among them at high temperatures and be causing the disturbing noise.

The use of plastics has been increasing in gears in the recent times. Plastics present diverse advantages when compared to other metals, i.e. steel. They possess the capability to absorb shocks and vibrations (Geethamma et al., 2014) as a result of their elastic compliance. It is also important to mention that they are low density and low inertia materials and produce a relatively low coefficient of friction (Subramanian et al., 2006; Lima et al., 2013). The tolerances of polymers are, usually, less critical than for metal gears, due in part to their greater resilience (Luo et al., 2014; Huson & Maxwell, 2006). Regarding the processes, it is possible to operate with minimum or no lubrication (Pogolian et al., 2010; Hu, 1998), due to inherent lubricity and, in what concerns the production of components, they have a silent behaviour on duty. Other advantage is the fact they are resistant to corrosion which means there is no necessity of using plating or protective coatings. Finally, in the injection-moulding process there is a good relation between cost and effectiveness in large production.

Although plastics are favourable materials to work with, design engineers should be familiar with the limitations of plastic gears relative to metal gears. Firstly, they present less capacity to carry loads (Umanskii et al., 1990; Zhigun, 1991), due to lower yield and ultimate tensile strength and the greater compliance of plastic gears may also produce stress concentrations. Moreover, these mechanisms cannot generally be moulded having the same accuracy as high precision machined metal gears. A very critical characteristic is that plastic gears are subjected to greater dimensional instabilities (Gauruva & Shankar, 2015; Malkin, 2008; Ranjbaran, 2010), as they feature larger coefficient of thermal expansion and moisture absorption. Bearing that in mind, there is a reduced ability to operate at elevated (and low) temperatures which states that operations are limited to less than 120°C. In the beginning of a process, when the engineer is designing gears and intends to produce them, there is a high mould cost in developing correct

tooth form and dimensions. Lastly, if some mistake is made during the process of moulding tools or idealising the manufacturing procedure, residual internal stresses at the tooth roots can be produced resulting in over stressing and/or distortion with aging.

Considering all these motives, it is essential to study and analyse the behaviour of plastics due to its unpredictability and dimensional sensitiveness. The more engineers know about this type of materials, the best they can produce using them without the necessity of wasting money and time in errors.

## 1.2. COMPANY PRESENTATION

Bosch company was founded in Stuttgart, Germany by Robert Bosch in 1886. He soon realised that his magneto ignition devices for automobiles had a good chance of success everywhere, not only in Germany. By the year of 1898, he opened the first sales office of the company outside Germany, in London. By 1905, Bosch was already manufacturing in France, and by 1912 also in the United States. Today, the Bosch Group has some 300 manufacturing sites in over 60 countries (Bosch Group, 2014). Robert Bosch was a wise man who respected and followed his principles, such as the one it is presented below:

---

“I have always acted according to the principle that I would rather lose money than trust. The integrity of my promises, the belief in the value of my products and in my word of honour have always had a higher priority for me than a transitory profit.” (Robert Bosch, 1919)

---

The fundamentals of his thoughts and ideas are always present in everyday life at Bosch. All the processes and rules implemented in the companies are based on his convictions, which have been transmitted through generations and will continue to be passed along (Bosch S.A., 2011).

In figure 1, it can be seen the company Bosch Car Multimedia situated in Braga where most of the work for this dissertation was developed.

The Bosch Group is a leading global supplier of technology and services. The company employs approximately 360,000 associates worldwide (until April 1<sup>st</sup>, 2015), 45,700 of them are employed in the area of research and development. Its operations are divided into four business sectors: Mobility Solutions, Industrial Technology, Consumer Goods, and Energy and Building Technology.



**Figure 1** - Bosch Car Multimedia (Bosch S.A., 2011)

In terms of production and development of devices at Bosch Braga, they are related with system integration of complex, networked Car Multimedia systems and radio (in figure 2 (a)), entertainment, navigation, and telematics systems. More recently the company have been investing in products such as premium instrument clusters (in figure 2 (b)) and head-up displays (in figure 2 (c)) since they are the future of human machine interface (Bosch Group, 2014).

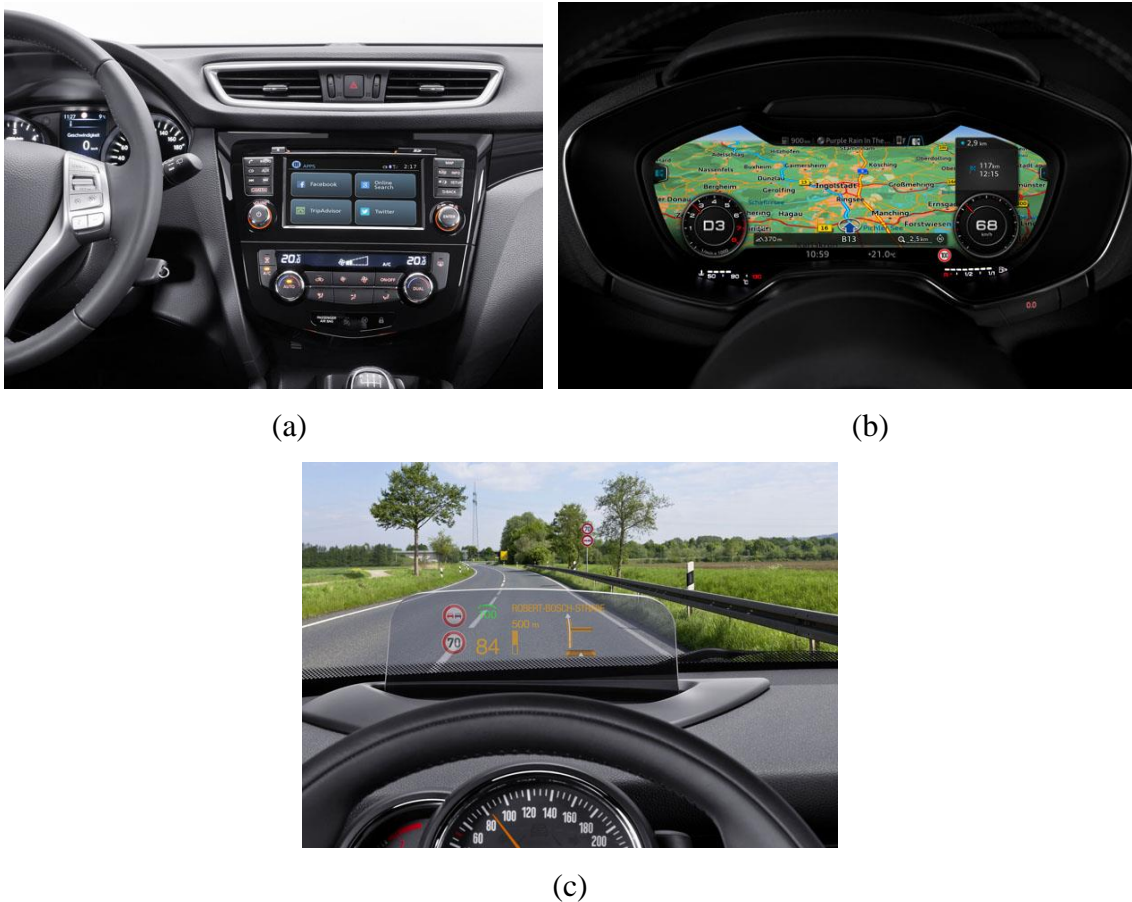


**Figure 2** - Types of products developed and produced at Bosch Braga (Bosch Group, 2014)

It is important to keep innovating and following the market demands, in order to be at the

forefront of technology.

The author of this dissertation was integrated in the mechanical development section (END), which was created in 2002, where the components are designed using softwares such as NX 7.5 and CATIA and structurally analysed with ANSYS. Nowadays, it is increasingly more important to simulate the processes to be aware of possible failures and, thus, saving money in prototypes. Along the fulfilling of their tasks, it is also important to communicate with the clients to ensure that all the requirements and standards are being followed.

This section has also the role of holding and moderating DFMA (design for manufacturing assembly) for all the projects in which it is discussed and decided the more suitable processes to produce and assemble the components. The DFMA coordinator has also the function of following the changes and progresses of the different activities. These are some of the roles that this section has to perform along with cost analysis and benchmarking tasks in every project.

In figure 3, it is presented an organisational chart of the engineering department.

In every section there are projects in course of the types of products previously referred. The main goal of department's head is that Bosch Braga becomes an independent company, in which, a product can be fully developed and produced in the same place. For that purpose, it is essential that Braga keeps investing in research of all areas with the view to possess knowledge in the various fields of product development, from the very beginning until the end of the whole process (Bosch Group, 2014).

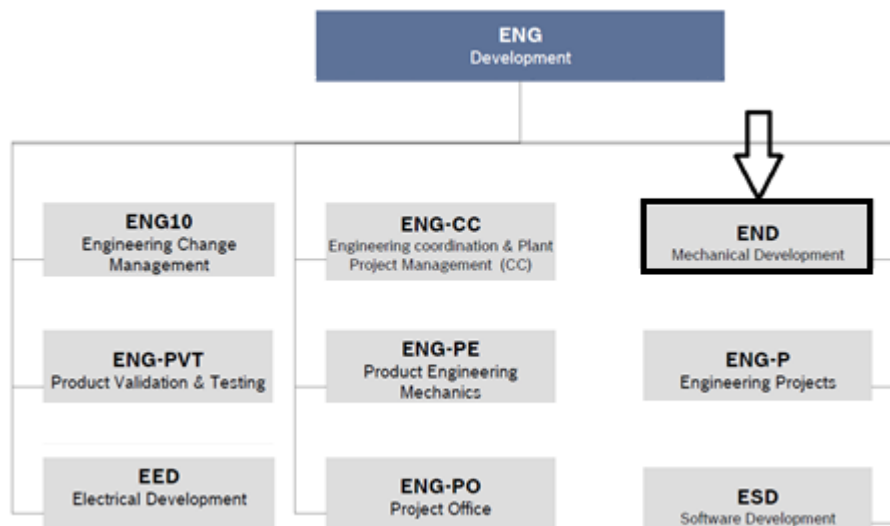


**Figure 3** - Organisational Chart (Bosch Group, 2014)

In conclusion, the strategic objective of Bosch Group is to create solutions for a connected world. Bosch improves quality of life worldwide with products and services that are innovative

and create enthusiasm. In short, Bosch creates technology that is “Invented for life”.

### 1.3. OBJECTIVES

There are several objectives expected to be accomplished by the end of this project which will be described in this part.

As it was referred in the previous section, there is a problem to be solved, a situation to be investigated which constitutes one of the primary goals to achieve. The interference of the components is a real possibility as, in certain circumstances, these pieces can reach high temperatures. Moreover, it is intended to analyse the behaviour of specific divisions of the elements, namely the contact of gear teeth and a path that must be followed by a pin of other component. If these features expand or contract, or continue working with some restrictions or limitations, it may threaten the correct function of the whole mechanism.

Another fundamental subject to study is the behaviour of polymeric materials, which constitutes a consequence of what was mentioned early. There are other types of materials to be examined, including some which could be alternatives to the ones being used. It is also intended to evaluate, based on the results of the simulations, if the tolerances applied to the gears are ranged between appropriate limits.

In the course of this project, it is expected for the author to develop skills regarding the software, its possibilities, and the types of analyses provided as well as enhance knowledge about the heat transfer field.

### 1.4. WORK METHODOLOGY

The work developed to this dissertation followed some methodologies which will be presented in this section. It is important to define strategies to achieve the proposed objectives and organise what needs to be done.

In the beginning of this work was performed some research of articles in order to understand the approaches of different people to thermal simulations as well as structural ones. The websites used was mainly Science Direct, Taylor and Francis and Springer. This inspection focused, mainly, on gears but also in other types of systems which are recurrently submitted to high temperatures and, because of that, their performance can be affected.

Next, the mechanisms it is intended to study were analysed in detail due to the importance of understanding how they function. To do so, they were examined some drawings of the components as well as the datasheets of the constitutive parts.



It was necessary to design the studied components and the chosen software was NX v7.5 (NX, 2015) as it is the one used for most of the employees of engineering section. Regarding the thermal and structural simulations, the adopted software was ANSYS v16.0 (ANSYS, 2015) due to its possibilities to implement the types of boundary conditions required in the problems and the diverse solvers it could be used to analyse the situations.

To perform the simulations it was mandatory to search for information about the possibilities of the software and how these features could be implemented. The website of ANSYS provides guides for the different modules including all the pertinent knowledge it is important to know including possible loads to be applied, diverse solvers and, most importantly, what types of solutions it is possible to obtain in each analysis. The tutorials available on this website are also very useful, whether in text or in video where it is explained every step of the studies.

There were consulted some books as well with the purpose of understanding and clarifying some definitions and processes about heat transfer, mechanical phenomena, gears and its operation, among other examples. It is crucial to support the work with the knowledge of books as they are, probably, the most reliable source of information there is.

## 1.5. OVERVIEW OF DISSERTATION CONTENT

This master dissertation is constituted by 6 chapters where will be detailed all the work and progresses which have been achieved for the last months. The background, the considerations, the decisions, the productions, the results will be described and explained for the next sections.

In the first chapter is presented introductory information related with generally instructions. The scope and motivation of the theme are explained as well as the company presentation where this dissertation was developed. Moreover, the objectives which are intended to reach are covered and the methodology followed to search for theory, to simulate, to conclude is also summarised in this section. Finally, it is focused on the structure of the dissertation in order to present the approached subjects.

The second segment deals with the background of the problem in which it is divided in 2 parts: technical and technological component. The first includes a brief history and some facts about gears as well as the reasons for the importance of having this type of mechanisms in our quotidian. It is also incorporated a few examples of applications of these systems in industry. The second portion summarises what has been performed on gears in the field of the thermal simulations and some cases of coupled analyses of thermal and structural studies produced on

components are displayed.

The third division covers the theoretical themes it is necessary to be intensely explained so that the reader can understand everything it is presented in the next parts. Firstly, there are the methods which the modules of ANSYS are based on and the details about how they are structured. Secondly, there are the descriptions of the heat and mechanical phenomena and of the physical features that constitute the outcomes of the simulations. Then, it is discussed the mesh, where the implemented methods and elements used are described. Consequently, the solvers of the different types of simulation are clearly explained with all the equations involved. Finally, some experimental technologies are described highlighting the one used to produce the experimental activities of this work.

The fourth part regards the presentation of the studied components, detailing its specifications and main characteristics. It is displayed the results of 2 analyses completed on the assembly of gears: a kinematic and a dynamic. It is important to investigate the mechanism in order to clarify under what conditions it functions. Consequently, there are the simulations performed on the pieces. Some are purely thermal and others are coupled, which means, a thermal and a structural study are joined in order to inspect the stresses of the gear teeth. At the end of this section, some results are compared highlighting the similarities and differences between them.

Regarding the fifth chapter, it is about the experimental activities which were executed at the metrology laboratory of Bosch. It starts with the description of what was done during the experiments and, then, the results are displayed for the various parts analysed. Consequently, the numerical and experimental results are compared and some conclusions are drawn. Finally, some recommendations are made considering the experimental results and the tolerances adopted for the diverse parts.

In the last section, it will be written some concluding remarks about the whole work as well as ideas will be presented for future work which could be developed having what is incorporated in these chapters as the basis.

Finally, there are some appendices which consists of documents used to check information used on parts and it is necessary to show them, although they are not truly essential to be included in the main segment of this report.

“You can never cross the ocean until you have the courage to lose sight of the shore.”

Cristóvão Colombo

## 2. BACKGROUND

This chapter congregates information about different types of transmission mechanisms although gears are the ones discussed more in detail since it is the crucial system of this work. It is fundamental to describe certain aspects for the readers to have the appropriate background in order to understand the decisions drawn during the project. The general characteristics, the main advantages and disadvantages of these systems are explained in which shafts, couplings, chain and belt drives are approached.

The strength of a shaft is only one of the considerations for its design. It must also be rigid enough to minimise deflection and must have sufficient angular and torsional stiffness to avoid vibratory movement. There are several different types of shafting. Power transmission shafting is usually round, either solid or tubular. For some small equipment, the shafting may be square or rectangular. This type of shafting is used to facilitate connecting; a mating part with a square or rectangle bore is used. This type of shaft is also used where length compensation may be required (International Organisation for Standardisation, 1988; South & Mancuso, 1994).

The basic function of a coupling is to transmit torque from the driver to the driven piece

of rotating equipment. There are two basic classes of couplings: rigid and flexible. Rigid couplings should only be used when the connecting structures and equipment are rigid enough so that very little misalignment can occur and the equipment is strong enough to accept the generated moments and forces. There are hundreds of types of flexible couplings, in which the most common are gear couplings, grid couplings, chain couplings, elastomeric shear couplings, elastomeric compression couplings, disk couplings, diaphragm couplings. Flexible couplings expand the basic function by accommodating misalignment and end movement. During the initial assembly and installation of rotating equipment, precise alignment of the equipment shaft axes is difficult to achieve. In operation, this can be caused by flexure of structures under load, settling of foundations, thermal expansion of equipment and their supporting structures, piping expansion or contraction, and many other factors. A flexible coupling is used to compensate for or minimise the effects of misalignment. (South & Mancuso, 1994; Chironis & Sclater, 1996)

Chains are manufactured to various degrees of precision ranging from unfinished castings or forgings to chains having certain accurately machined parts. It may be stated that a chain, composed of a series of links pinned together, is a form of flexible gear connecting two toothed sprocket wheels mounted on parallel shafts. Their main advantages are having the same flexibility as belts, the excellent design flexibility they provide as well as convenience, and resistance to shock loading. Also, they operate satisfactorily in adverse surroundings, they can be manufactured in various special steels to resist specific environments, and they have unlimited shelf life, simplicity of installation and general economy. Mechanical efficiency, in comparison to gear and belt drives, is favourable. In other words, chains operating under ideal conditions can have efficiencies as high as 97 to 99 %. There are 3 principal types of chains: roller, silent, and engineering steel. In terms of applications, their major uses are: power transmission drives, conveyors, bucket elevators and tension linkages. (International Organisation for Standardisation, 1988)

Belts have many advantages over other power transmission mechanisms. One of the most important is overall economics. The efficiency and reliability of belts as a power transmission method is well recognised. Belts are clean and require no lubrication. They can transmit power between shafts spaced widely apart with a wide selection of speed ratios. Belts can be used for special design purposes such as clutching, speed variation and transmitting power in more than one plane. They are also capable of handling large load fluctuations and have excellent shock-absorbing abilities. Belts have an extremely broad application range (torque, speed, ambient conditions, etc.) that make them ideal for virtually any application. They have gained wide usage mainly due to lack of lubrication requirements, and very high power density of modern

curvilinear belts. (South & Mancuso, 1994)

Gears are used to transmit power positively from one shaft to another by means of successfully engaging teeth (in two gears). They are preferred over other alternatives when exact speed ratios and power transmission must be maintained. Gears may also be used to increase or decrease the speed of the driven shaft, thus decreasing or increasing the torque of the driven number. There are several types of gears such as spur, bevel, helical, worms, rack and pinion among others and, some of them, can be internal or external.

Gears and gear systems have been fundamental machine components which contributed to an evolution of machinery efficiency and capability. Technological evolution of gear systems has been supported also by a constant research developed throughout the years which resulted in the publication of many books. Some of them are enumerated as they contribute, somehow, to the development of this dissertation. Regarding the history of gears and the major contributions to this field, the books *A History of the Machine* by Strandh (1979) and *A Gear Chronology: Significant Events and Dates Affecting Gear Development* by Crosher (2014) were published. Concerning the design, the kinematic and dynamic movements of gears, the number of existing books is enormous. In 1903 it was published the *Kinematics of Machines* (Durley) and the French Henriot wrote *The Theoretical and Practical Treaty of Gears* (1979). These books are very helpful to clarify some singularities about gears which are important to analyse. There is also the *Mechanisms and Dynamics of Machinery* by Mabie and Reinholtz (1987), followed by the publication of the book *Fundamentals of Gear Design* by Drago (1988) and in 1989 the compilation *Mechanical Engineering Design* by Shigley and Mischke (1989) emerged which is considered as one of the most outstanding books to learn about gears.

In the 20th century several publication appeared namely, *Kinematics and Dynamics of Machinery* by Wilson and Sadler (1993), *Theory of Machines and Mechanisms* by Shigley and Uicker (1995) and *Design of Machine Elements* by Spotts and Shoup (1998). These books are essential to study and investigate the movement as well as the forces involved in the mechanism in study.

More recently, the book *Fundamentals of Machine Component Design* was published in 2006 (Juvinall & Marshek), along with *The Kinematic of Mechanisms* by Flores and Claro (2007) and *Applied Mechanics – A Practical Approach* published in 2012 (Antunes) was also publicised. All these manuals are important to be consulted when some doubt appears related to gears.

As gears are a type of mechanism usually used in several contexts, they present much diversified applications. There are examples of automotive industry (Hwang & Huang, 2011;

Kadmiri et al., 2012; Haj-Fraj & Pfeiffer, 2001; Meng et al., 2015; Lingamanaik & Chen, 2012), aeronautical industry (Wen et al., 2009; Savaria et al., 2015; Heyns et al., 2012; Stander et al., 2002), the aviation industry (Wang et al., 2008; Gualdi et al., 2008; Ossa, 2006; Lee et al., 2003; Bagnoli et al., 2008; Khapane, 2006) and the wind turbines (Qiu et al., 2015; Nejad et al., 2014; Fernandes et al., 2015; Fernandes et al., 2014). In these fields, the systems are mostly responsible for the transmission of movement which, consequently, causes the displacement of the parts and the locomotion. However, it is also crucial to investigate alternative materials, maintaining the same characteristics, which could be used in these applications and some examples can be found in the following articles (Zhou et al., 2013; Mao et al., 2009; Kurokawa et al., 2003; Düzçükoglu, 2009; Yakut et al., 2009; Hoskins et al., 2014).

There are various softwares in the market which are capable to perform simulations of assorted types since static, dynamic, and thermal analysis across the linear and nonlinear domains. Some examples are ANSYS (ANSYS, 2015), Abaqus (Abaqus, 2015), Nastran (MSC Nastran, 2015), Algor (Algor, 2011) and SolidWorks (SolidWorks, 2015). They present different levels of accuracy for the individual modules although they are able to execute all kinds of simulations. Then, there is the software DEFORM (DEFORM, 2015) which is used to analyse metal forming, heat treatment, machining and mechanical joining processes. This programme has proven itself to be extremely effective in a wide range of research and industrial applications. Lastly, there is the FloTHERM (FloTHERM, 2015) which is a software to perform thermal analyses, create virtual models and test design modifications of electronic equipment mostly before physical prototyping. It is capable of considering different situations and applications, dimensions and materials as well as optimising the processes.

### 2.1. TECHNICAL COMPONENT

This section is constituted by the description of the history about gears, highlighting the most important aspects, which happened along time. It also explains why it is fundamental to have gears in our society and what the advantages of their incorporation in other systems are. Then, it is detailed various types of transmissions as well as some types of gears. Finally, there are some examples of applications in industry referring the reasons why engineers should, from now on, adopt more polymeric gears in their applications.

#### 2.1.1. The History of Gears and Its Importance in the Quotidian

It is long the history associated to the genesis and evolution of gears (Crosher, 2014).

Around the year of 1700 b.C. it emerges, in poems of literature Hindu, references of cars and wheels. Gears are also mentioned in the work of Aristoteles (384-322) as well as of Arquimedes (287-212).

The primitive gears were initially used by the Chinese people in the 3<sup>rd</sup> century b.C. and it is represented an example of one in figure 4. Nowadays this type of wheel is still being incorporated in systems of water lifting, which are commonly called of “norias” (Branco et al., 2009). Wheels of this kind are also being used on mills.



**Figure 4** - Primitive Gear (Branco et al., 2009)

The primitive gears were very rudimentary as they were constituted by pieces of wood which were inserted in a disc or in a wheel. The important fact is that they had to be consisted of some material easily workable so it could be possible to draw the shape of the teeth. Later, around the 15<sup>th</sup> century, the Italian Leonardo da Vinci presents several illustrations where it could be identified gear arrangements, which can be seen in figure 5.

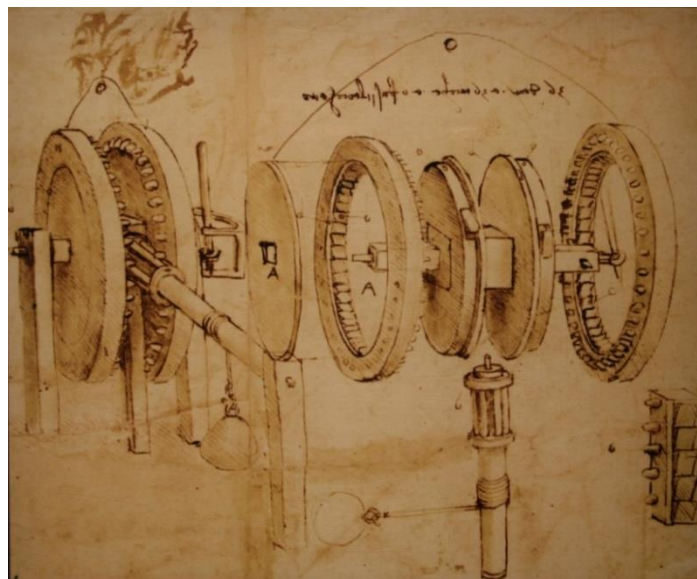


**Figure 5** - Gear Illustrations of Leonardo da Vinci (Drago, 1988)

Nowadays, the most frequent materials used to construct gears are low carbon steel, stainless steel, and nodular cast iron, bronze and polymeric materials.

Until the 16<sup>th</sup> century, gears were manually fabricated and its final shape was obtained more by accident than as a result of a study or intensive planning. The first machine able to manufacture gears was developed by the Spanish Juanelo Turriano (1501-1585), which was specially fabricated to facilitate the construction of a mechanical watch to the king Carlos V of Spain (Vera, 1996). The watch included approximately 2000 gears. In fact, the field which more significantly contribute to the development of gears was horology. The Italian Giovanni Dondi (1348-1364) was responsible for designing the first mechanical watch, for which there are only some basic design layouts known. Gears are, therefore, the type of mechanical transmission with greater practical application as they are pieces of machines which guide movement from a shaft to a driven shaft, through the use of teeth which successively contact with each other.

The industrial revolution, which happened around the century XVIII, changed the way gears were manufactured at that time as they started to be fabricated with metallic materials. Due to this development, gears presented higher durability and load capacity. In the beginning of the 19<sup>th</sup> century, the industry of gear production was already as we know it nowadays, in which the profiles of the teeth obeyed to curves previously defined such as the cycloid or the involute (Flores, 2009). Among the most important names of people who significantly contribute to the study and development of gears, it could be highlighted Girolamo Cardano, Robert Willis and Wilfred Lewis. Other authors could be included, however, the ones mentioned above summarise the most essential improvements (Drago, 1988). Girolamo Cardano established the first mathematical models for gears in 1525 while Robert Willis leaded several studies related to gears as well as trains of gears.

Presently, the new progresses in the scientific and technical area of gears are associated with new materials, new manufacturing techniques and the advanced methodologies of design, simulation and optimisation of gears in addition to the extensive use of electronics (Li et al., 2014; Denkena et al., 2014; Simon, 2014).

Although people think they had invented gears, in 2013 Malcolm Burrows and Gregory Sutton performed a study which discovered that it was nature the first to create and implement gears on animals. Until recent times, it was assumed that the mechanical gear was invented around 300 B.C. by Greek mechanics who lived in Alexandria. The fact is that it might not be true, as a small hopping insect called *Issus Coleoptratus*, whose existence dates before that, uses toothed gears to precisely synchronize the impulses of its hind legs in order to jump forward.

This team of biologists from the University of Cambridge in United Kingdom studied the



anatomic structure of the three-millimetre long insect and revealed that only the juveniles of the species possess a complex system, located in the posterior part of its body, similar to a gearing system which allows them to jump forward. This mechanism is extremely important for the insect to move straight forward as the legs are locked together and they rotate at the exact same time. In order to prevent being off course, the existence of this system of gears is fundamental or otherwise, there is the possibility of one leg be extended a fraction of second earlier than the other.

This discovery is believed to be the first functional gearing system ever discovered in nature, although there have been previously found another systems resembled with gears in other animals. However, these mechanisms did not contribute for the animal's life in any way which proved they did not have any function.

It is important to refer that this is the primal natural system that mechanically functions like gears as we know them. They represent the highest level of machinery which evolved in animal structure to be possible its synchronisation of movement (Mechanical Gears Seen for the First Time in Nature, 2013).

The animal called *Issus Coleoptratus* as well as the gearing system are presented in figure 6.



**Figure 6** - *Issus Coleoptratus* (Mechanical Gears Seen for the First Time in Nature, 2013)

### 2.1.2. The Application of Gears in Industry

In mechanisms, the transmission or transformation of movement can be executed in 2 distinct ways, namely by direct contact (figure 7) or by an intermediate connection (figure 8) (Flores & Claro, 2007). In the first case, the movement is promoted through the contact between surfaces of the driver and driven organs. Gears can be included in the first group, such as the ones it can be seen in figure 7.

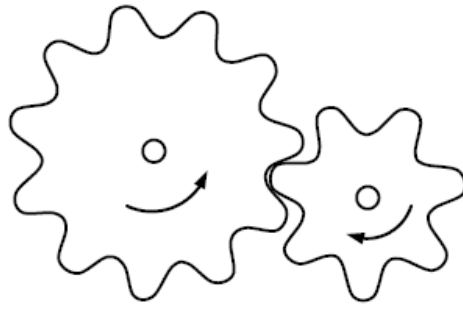


**Figure 7** - Example of Gears (Flores & Claro, 2007)

On the other hand, the second group is constituted by systems in which the transmission of movement between the motor and the moved components is promoted by a medium body. When there is a third body involved, the connection can be rigid, as in the case of a 4 bar mechanism, or flexible, such as in belts and chains.

Figure 8 illustrates these 3 types of transmission using an intermediate connection, which were previously explained (Flores & Claro, 2007).

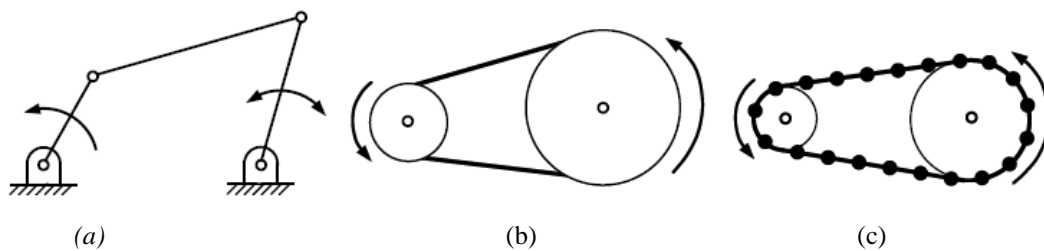


**Figure 8** - Movement Transmission Systems by Intermediate Connection: (a) four bar mechanism; (b) transmission by belt; (c) transmission by chain; (Flores & Claro, 2007)

The principal characteristic of gears is the fact they allow the transmission of movement between bodies with a constant relation. In addition, the transmission ratio can be defined as the quotient of the rotation velocities of 2 bodies where there is a progression of mobility from one to the other. Furthermore, a gearing system is a mechanism composed by 2 rigid wheels with teeth which conduct locomotion between distant axes, or they could also be used when there is the need of reducing or increasing the velocity or the moment of the motor shaft. In these mechanical organs, the movement is transferred by the driver's gear teeth, which roll without slipping, over the teeth of the driven gear. The smallest wheel, and consequently the one with a lower number of teeth is called of pinion. On the other hand, the wheel of bigger dimensions is simply denominated of gear. These designations have nothing to do with the fact that they are the driver or the driven body, the only important aspect is the dimensions of the gears (Henriot, 1979).

Gears are used to transform the rotating movement of a shaft into rotation or translation

of other body, as it is shown in figure 9.



**Figure 9** - (a) Rotating movement transmission for rotation; (b) Rotating movement transmission for translation  
(Flores & Gomes, 2015)

Among the several systems of transmission of rotating movement, gears are very versatile bodies. In fact, the use of gears enables the transmission of movement between parallel or non-parallel shafts. Moreover, these components are also adaptable in cases it is necessary to operate mechanical systems of low and high number of rotations. In general, gears present an efficiency considerably large (until 99 %), except worms which manifest efficiencies relatively low (about 45-70 %) due to the elevated slipping that happen in this type of gear (Niemann, 1971).

There are other particularities which turn gears into such a useful and unique type of transmission, such as:

- The extensive capacity of resistance to overloads;
- The high precision in transmitting movement;
- The constant ratio of transmission and independent from the applied charges;
- The good reliability and durability;
- The ability of conducting movement from low to high powers;
- The possibility for the components to have small dimensions.

One of the most significant examples related to the compactness of gears can be observed in mechanical watches, in which, in a very small space, it is possible to obtain very large ratios of transmission. It is also important to refer the excellent performance of gears, where it should be highlighted the quantity of thousands of kilometres that the automobile differentials provide without having the necessity of being repaired or substituted (Wilson & Sadler, 1993).

Apart from all these relevant aspects, gears can be manufactured using diverse materials, such as metals and polymers. However, as gears are constituted by rigid bodies, they do not absorb shocks and need to be lubricated. In addition, they are relatively expensive and noisy

and, can be affected, in their performance, by the environmental conditions such as humidity and dirt. Finally, it is essential to mention that gears can be used to transmit movement between parallel shafts, concurrent or non-coplanar, as it is exemplified in figure 10.

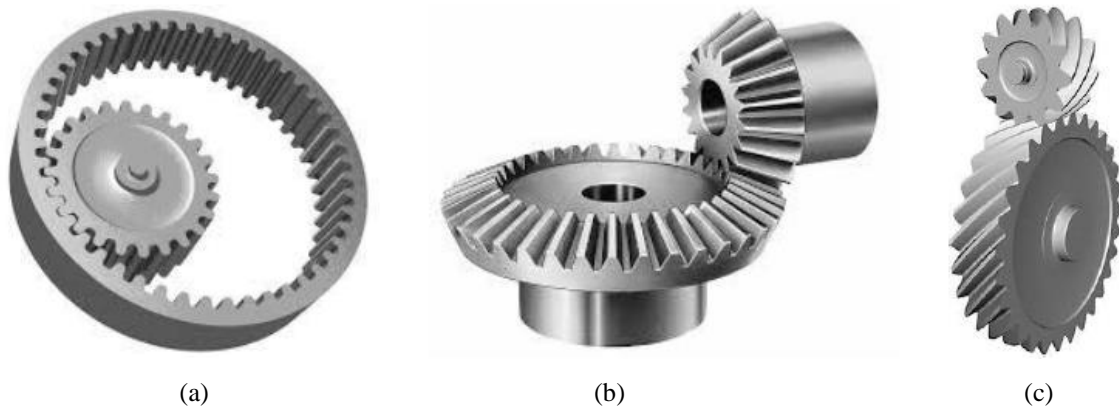


**Figure 10** - (a) Gearing with Parallel Shafts; (b) Gearing with Concurrent Shafts; (c) Gearing with Non-Coplanar Shafts (Flores & Gomes, 2015)

The principal manufacturing processes of metallic gears are machining, sintering, casting and forming. In general, these procedures require posterior superficial finishes. In contrast, polymeric gears are obtained through the process of injection. This type of gears present several advantages, namely the low weight and its reduced cost. This last aspect is particularly significant when it comes to large series of production. Polymeric gears have, however, a lower load capacity and they are mainly used in smaller mechanical systems, such as, home appliances and toys. Figure 11 shows this type of gears being used in the referred applications.

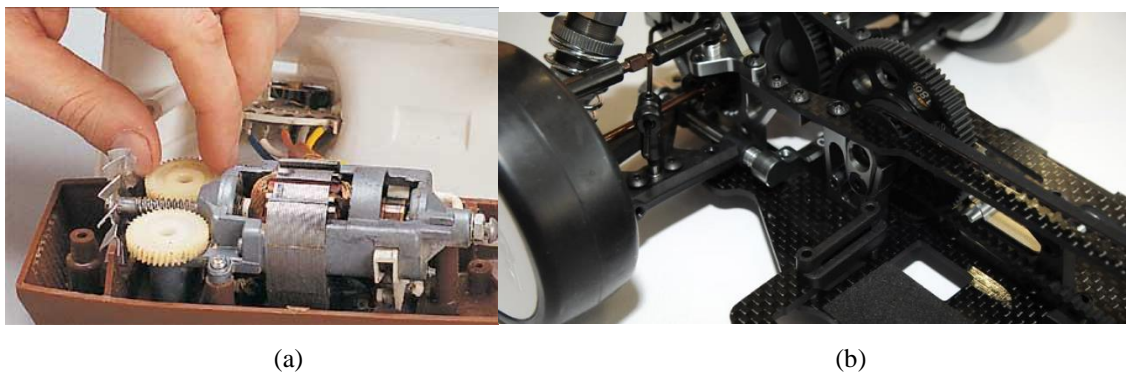


**Figure 11** - (a) Gears of a mixer; (b) Gears of a toy (Flores & Gomes, 2015)

It is vast and very diversified the field of application of gears. In figure 12, there are various examples, such as, a mechanical watch, an automobile differential, a pinion-rack used in mountain trains, a gear used in a large machine (applied, for example, in the cement industry), a counter, a reduction gear, an industrial mixer and a manual reduction gear used in a car.

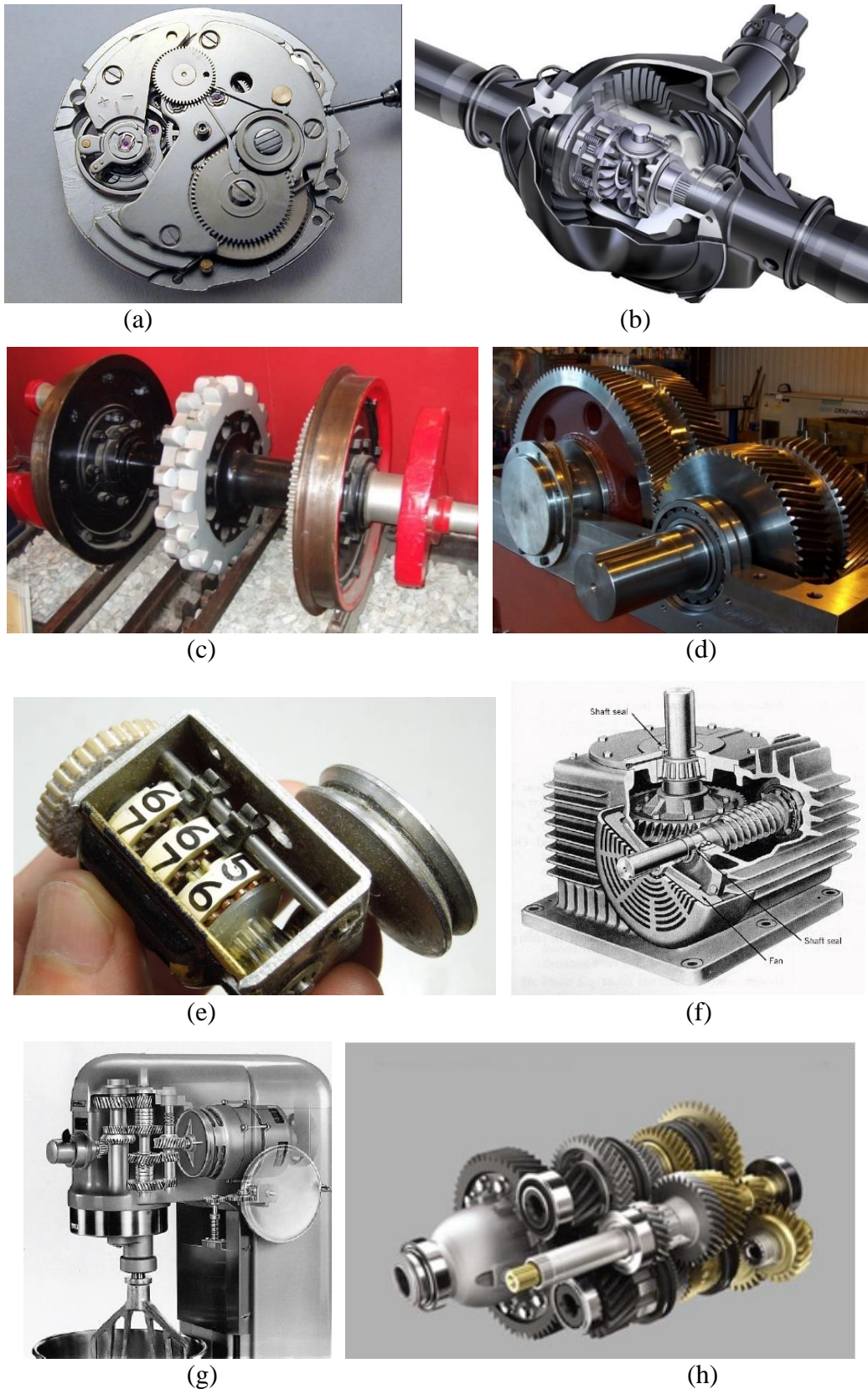


**Figure 12** - (a) Mechanical Watch; (b) Automobile Differential; (c) Pinion-Rack; (d) Large gear; (e) Counter; (f) Reduction Gear; (g) Industrial Mixer; (h) Manual Reduction Gear of a Car (Flores & Gomes, 2015)

As it has been referred throughout this section, metal gears present several advantages

over the polymeric materials. However, this last field is being developed everyday which means there is so much that can be discovered about the capabilities of polymers and their abilities to attend what society need. Plastic suppliers offer numerous plastic gear with a low coefficient of friction and the strength, stiffness, fatigue, and wear–resistance characteristics that designers can take advantage of to optimize their gear tooth geometry. Designers have developed gears for many applications, such as:

- Automotive actuators (power seats, window lifts, mirrors, ignition, parking brakes, latches, closures);
- Large and small appliances (vacuum cleaners, washing machine transmissions, food processors);
- Industrial (power tools, conveying line rollers, water and gas meters);
- Electronics (printers, copiers, scanners, audio and video equipment);
- Medical dispensing devices;
- Garden (irrigation sprinklers, mowers, sweepers, blowers, fertilizer spreaders, swimming pool equipment).

The design freedom inherent in moulding plastic allows more–efficient gear geometries than it is possible using metal. Moulding can create shapes that are hard to form at a reasonable price in metal, such as internal, cluster, and worm gears. Plastic gears can have a wider aspect ratio than the ones of metal, thus increasing their load–bearing capacity and power density. Plastics have also become essential in the ongoing demand for quieter drives, which requires for high precision, new tooth shapes or flexible materials.

Gears made of plastic typically permit a 50 to 90 % cost reduction in comparison with machined metal gears, as they are usually produced in large quantities, depending on their precision requirements, and they usually expect no superficial finishing. They weigh less than metal gears, and their relative inertness means they can be used in situations that cause metal gears to corrode or degrade.

Plastic is a more compliant material than metal which makes it simpler to work with in certain situations. Not only do they deflect easier, which allows them to absorb impact loads and better distribute localized loads caused by misalignment, they have lower hardness that helps disguise certain tooth errors. The inherent lubricity of many plastics makes them ideal for computer printers, toys, and other low–load situations where external lubricants are excluded. In addition to use in dry gears, plastics can be lubricated by grease or oil.

Dimensional stability, however, is a complex factor. Polymers that absorb water or chemicals will have more dimensional variation. Temperature changes will also have an effect on

part dimensions. If they are moulded in an incorrect manner, geometry can change as the gear cools after moulding and be deformed by the working environment and friction. That is why it is so important to study the behaviour of plastics when they are in the presence of heat, humidity and other external factors. The more people know about this type of materials, the more it can be predicted during the production of pieces. If the engineers are aware of the time where failure can happen, measures can be implemented or the processes can be changed in order to avoid problems. Besides these negative aspects, polymers have been increasingly used in a variety of products as they present various advantages in comparison to metallic materials (Childs, 2013).

## 2.2. TECHNOLOGICAL COMPONENT

In this segment there are some examples of articles which were written having gears as the component of study. The first part deals only with thermal simulations and the outcomes are related to temperatures or heat. The second part summarises coupled thermal-structural simulations applied to different components and the objectives of the studies are diversified.

It is crucial to investigate what has been done in this field as this can help establish some conditions in the analysis and by reading this type of publications, some errors can be avoided. Other important aspect is to detail the capabilities of this type of analysis.

### 2.2.1. Thermal Simulations Performed on Gears

To introduce this section, it is important to refer that some articles cover analyses performed on softwares while others develop their own numerical studies and other researchers even take an existing model and simplify it or adapt to other situations. It is quite often to compare the obtained results to the outcomes of experiments or of a previous analytical or numerical model in order to validate what has been executed.

Some researchers built a model with a deforming mesh, which means the mesh is being replaced along the simulation, to study a turbulent flow in the section chamber of a gear pump, using ANSYS Fluent (Castilla et al., 2010). The mesh replacement strategy is adopted in order to avoid skewed meshes and allow for simulation of solid contact between gears. Several models were tested and all of them failed in some respect although the solvers RSM and RNG k-epsilon were the best choices. This data was, consequently, compared with experimental results.

Other investigators studied the distortions of bevel gears due to heat treatment using a software named DEFORM (Cho et al., 2004). The distortions of forged and machined gears are measured and compared. This analysis is used to simulate the complete heat treatment process

for the machined gears and the results showed good agreement with the experimental measurements. The analysis concluded that the deviations are larger in the forged gears, specifically in the outer diameter and in the tooth width were almost doubled.

Stark and his colleagues (2013) used the software DEFORM to perform their study of heat flux and temperature distribution in gear hobbing operations. Firstly, they evaluated the generated heat during chip formation and, then, used these results to perform a heat flow simulation. The objective is to calculate the heat flow of the process and the thermal deviations. The results showed a good agreement between the measured and calculated temperature fields in chip formation and heat flow.

Other authors have decided to present equations for calculating bulk temperature as well as critical temperature of a lubricant/steel combination based on gear scuffing results obtained on a high speed gear teste rig (Jiang & Barber, 2000). Critical scuffing temperature, previously thought to be independent of operating conditions, is found to be greatly influenced by gear speed and oil type. Experiments show that synthetic oils increase the value of critical temperature dramatically in comparison with base mineral oils, and speed also alters this temperature. This paper presents a modified equation for converting scuffing load limit between simulated and practically used gears.

One other article describes a numerical method of the flash temperature for polymer composite gears and the heat partition between gear teeth (Mao, 2007). The problem is treated as an unsteady one where the intensity distribution and velocity of heat source changes as meshing proceeds. A numerical approximation is adopted using finite difference method and the results are shown to be similar of those found using semi-analytical method. Moreover, it is shown that the solution of Blok (1937) can be used to provide a quasi-steady approximation that is for mean flash temperature estimation. However, in other circumstances, the Blok's solution is inaccurate and the current approach should be used.

Atan with a co-author (2005) simplified a model (Seireg & Atan, 2002) and, consequently, executed a comparison between the interpretation they had developed and the previous formulation. These researchers used existing data to establish an artificial intelligence model where a multi layer feedforward neural network has been employed. The model accepts surface roughness, gear ratio, horsepower and the number of teeth as input variables, and as outputs the calculated pinion surface asperity temperatures. The aim of this work is to provide a straightforward and simple way to compute the asperity temperature rise for a given set of variables. The analytical method requires many iterations between the viscosity and the temperature, and though the iterations, many data has to be entered by hand. In the more recent method, none of



these difficulties exist.

A group of researchers investigated the thermal deformation of large-scale computer numerical control gear hobbing machines on the purpose of obtaining the law of thermal deformation to improve machining precision (Shilong et al., 2013). This article presents a novel computing model based on the theory of thermal expansion deformation, the extensional beam theory, non-uniform temperature distribution of the Euler-Bernoulli beam and the Kirchhoff theory of plane-section assumption. The curves for overall displacement error of cutting points and teeth trace error are obtained. Comparing deformation theory and experimental data, the relative error is lower than 5 %, which verifies the computing model proposed by this paper.

Other author has developed a numerical model himself to test a method on scoring of cylindrical spur and helical gear mechanisms, based on the mean tooth profile heat (Tevruz, 1997). Basically, it consists of a comparison between the profile heat during meshing with the critical profile heat. In order to check the method, experiments were executed and, then, with this data a correction factor for the method was determined.

The same investigator produced another similar paper about scoring of cylindrical spur and helical gears and calculation by a temperature method (Tevruz, 1998). According to the experiments, which were performed to validate the model, it is apparent that scoring increases with time. This situation can be interpreted as scoring roughens the surface, which in turn increases the amount of scoring.

Barglik et al. (2014) created a model for induction hardening for gear wheels. The model consists of two nonlinear partial differential equations describing the distributions of magnetic and temperature fields in the system, with respect to the temperature dependences of all material parameters. The results were in very good accordance with the existing practical experience, even when the uncertainties in the material parameter lead to their variances. Numerous computations showed that the most distinct is the influence of specific heat capacity. The difference in the temperatures at the end of heating reached about 50°C.

A team of researchers have decided to present a novel modelling approach and supporting theoretical analysis for predicting the unsteady thermo-fluids of geared systems that experience periods of constant gear speed operation (Yazdani & Soteriou, 2014). A set of numerical and mathematical approximations are established to reduce this separation based on physical motivations. In addition, a novel solution approach and associated mathematical derivation are presented which explores the separation of time-scales and solves for the time-dependent stationary state of the system with modest computational cost. The numerical approach is successfully verified against a traditional simulation using both methods.

Then, there is an adaption of the previous numerical model (Yazdani et al., 2015). In general, the revision demonstrates the application of the recently developed modelling methodology, on a set of three interlocking gears that serve as a validation vehicle. Along with the modelling approach, a novel gridding methodology is presented for simulating interlocking gears with substantially improved accuracy. The long-term temperature distribution within the gearbox is obtained through the proposed simulation method and compared to the experimental measurements. In addition, the model is shown to be capable of reproducing the temporally cyclic temperature oscillations once the system reaches the stationary-state condition.

A group of investigators developed a model for calculating transient, three-dimensional, thermal elastohydrodynamic tooth flank contacts in spur gears with involute gearing (Bobach et al., 2012). The calculation model is based on the combined numerical solutions of the generalised Reynolds, energy and Fourier heat equations. States of mixed friction and microhydrodynamic effects are ascertained integrally based on real-measured surface topographies. The results clearly demonstrated that the form of the tooth trace correction has considerable influence on the load capacity of the tooth surface contact. A tooth trace correction which was designed as a fillet proved to be good, but only if significant misalignment of the gear wheels can be neglected.

In conclusion, this part presented a succinct description of the most recent contributions to the thermal study of different types of gears (spur, bevel, helical, etc.). The proposed problems analyse how diverse parameters influence the distribution of gear temperature such as, wear, lubricants, speed, and applied loads, among others. The main focus of the analyses is the local where the teeth establish contact as it is the place which presents more details in the geometry. It is also through this contact that the power is transmitted, which means it is where most problems occur.

### 2.2.2. Coupled Simulations Performed on Diverse Components

After discussing the thermal simulations performed on gears, it is appropriate to explain some coupled analysis executed on diverse components. There are studies which join temperature with mechanical phenomena in order to study a variety of effects and occurrences. Other researchers include factors such as wear, spatial variations, and temperature rise, among others. Different outcomes are studied namely, damage/failure effects, residual stresses and thermo-mechanical behaviours.

Some authors investigated a bi-metallic conformal cooling channel design with high thermal conductive copper tube insert for injection moulds, using ANSYS Workbench (Saifullah

et al., 2012). This performance is compared with a mould with conventional straight cooling channel and, both simulation and experimental results, led to the conclusion that the first approach gives better cycle time. Fratila and Radu (2010) considered the thermal processes in gear machining being focused on comparing several cooling and lubricant techniques used at gear milling, using the software Algor. Research results confirms that minimal lubrication and cooling techniques are favourable alternatives, the strains and thermal stresses have intermediate values to both dry cutting and flood lubrication approaches. As thermal analysis is one of the first steps towards developing a CAD system for injection moulds, Kansal et al. (2001) investigate the temperatures at different points inside the cavity of a cooling channel in order to optimise it. The main objective is to determine the temperature distribution and thermal residual stresses which are developed due to non-uniform cooling of the molten plastic inside the mould cavity.

A team of analysts evaluated the performance of a disc rotor when it is under severe braking conditions, using the software ANSYS (Nathi et al., 2012). To do so, they attempted to study the effect of stiffness, strength and variations in disc brake rotor design on the predicted stress and temperature distributions. By identifying the true design features, the extended service life and long term stability are assured. Belhocine and Bouchetara (2013) analysed the same subject, more specifically, the thermomechanical behaviour of the dry contact between the brake disc and pads during the brake phase, using ANSYS. The main goal is to determine the deformation and the Von Mises stress established in the disc, i.e., the contact pressure distribution in pads. One other analysis introduces two micromechanical modelling approaches to examine spatial variations of temperatures, stresses and displacements in particulate composites during transient heat conduction (Khan et al., 2011). Li and his co-authors (2015) considered the dual-coolant lithium-lead blanket, and developed a model based on finite- volume method which is employed to investigate mechanical behaviours and heat transfer in the component under nuclear reaction. Temperature distribution, thermal deformation and thermal stresses are calculated in this work, and the effects of thermal conductivity, convection heat transfer coefficient and flow velocity are analysed. The next part to be studied by Wu and his colleagues (2014) is a thermoelectric power generator, in which a numerical analysis on the thermodynamics and thermal stress performance of the element is performed, considering the variation of the thickness of materials. The influence of high heat flux on thermal efficiency, power output, and thermal stresses are examined. It can also be mentioned the investigation completed by a team of researchers on fibre reinforced composites (Jeon et al., 2014). Basically, the study consists of an analysis of the time-dependent response of this material undergoing heat conduction and

mechanical loading. It is also established a comparison between several studies with different arrangements of fibres. The effects of thermal stresses and stress discontinuities are examined using a finite-element method. Finally, there is a contribution written by Behnke and Kaliske (2015) where it was considered a numerical framework for the efficient thermo-mechanical analysis of 3D tire structures in steady-state motion. The results of rolling resistance and surface temperature distribution are compared with experimental ones.

The next articles introduce a new subject: fracture. A group of investigators developed a numerical model in order to evaluate the fracture characterisation parameters to a fractured gear tooth (Sfakiotakis et al., 1997). The influence of heat convection characteristics and mechanical loading conditions are examined. Stress intensity factors are evaluated for a wide range of operating parameters useful for design purposes. Another paper was written by Hu and his colleagues (2009) about a transient coupled finite element model which is developed to compute the temperature and stress field in cast billets, so as to predict the defects of the I-type billets made from magnesium alloy. It is also intended to find the causes and solutions for surface cracks and shrinkages during the casting process. The simulation is performed in the software ANSYS and the main goal is to optimise the parameters. The next study was completed by a group of researchers who modelled a thermo-mechanical interface for failure analysis of concrete subjected to high temperature (Caggiano & Etse, 2015). This model is an extension of a fracture energy-based interface formulation which now includes thermal damage induced by high temperature and/or fire. It is also suggested by some analysts a model similar to the previous for thermally-induced rock damage based on the particle simulation method (Xia, 2015). The mechanism of surface failure due to temperature rise is a very important problem in gear design. So, the author Atan (2005) considered that this subject is not fully analysed and considered also the mechanisms of thermal stresses and the thermal cycling in contact zone, during the gear mesh. The point is to predict the design criteria for modifying the contact stresses due to thermal stresses. The effect of the material, oil film thickness, surface roughness and geometric operating parameters are illustrated. Also the effects of a load on the temperature rise and the modification parameters are evaluated.

A team of investigators concentrated on the study of acetal gear wear behaviour and its performance prediction based on the extensive inspections on the gear thermal mechanical contact (Mao et al., 2010). An approach for acetal gear transition torque prediction is proposed and this method is based on the link between polymer gear wear rate and its surface temperature. This is crucial in cases where the gear operating temperature reaches the material melting point due to a sudden increase of wear rate, under the critical load condition. Still in the same theme,

another project was implemented on gears of the same material (Mao et al., 2015). The main point is to establish a comparison between machine cut and injection moulded gears. Extensive experimental tests are executed to investigate the wear performance of this type of components. Finally, a group of analysts proposed a thermal–structural coupled finite element analysis method for wear prediction of seal (Xin et al., 2014). To perform finite element simulation of wear process, a novel mesh reconstruction strategy to reflect the evolution of geometry caused by the wear is presented. As the sealing force is important for seals to evaluate the sealing capability, the effect of wear is reflected through the change of sealing force.

It is also important to study the variations which occur when some condition is altered. For example, Kim and her colleagues (2013) evaluated the thermal effects of a stratified flow in 2 different safety injection piping systems in order to examine structural integrity of the components, using a coupled CFD-FE method. There has not been a study where a stratified flow was considered. A team of researchers investigated a tooth surface temperature rise during meshing spur gear pair due to frictional heat (Taburdagitan & Akkok, 2006). A coupled thermo-elastic analysis is executed considering the elastic deformation of teeth and corresponding load shearing between the contacting tooth pairs and heat generation in the contact. Another group predicted the influence of the ambient temperature on the stress, deformation and temperature of a dump truck tire with the virtual tire model established in this work by employing the finite element method and Algor software (Li et al., 2012). The analysis of heat transfer is steady-state and the mechanical event simulation is nonlinear material model.

Welding procedure is complex and there are several aspects it can be studied. That is why some authors developed a 3D element model to simulate a coupled thermal-mechanical fields in ultrasonic welding of aluminium foils (Zhang & Li, 2009). Transient distributions and evolution of some variables of the process, including normal stress, shear stress, slide distance, heat generation, temperature, and plastic deformation on the contact interface, and their interactions are studied in detail. A group of researchers performed an analysis on the material flow and thermal-mechanical phenomena happening during Friction Stir Welding of polymers (Simões & Rodrigues, 2014). The results expressed a weld morphologic analysis, the residual stresses and the temperature measurements during welding.

There is an article of Kadashevich et al. (2015) which documents the compensation of thermal deviations necessary to achieve high gear quality during dry gear hobbing. The main goal is to predict temperature distributions in work pieces during dry gear hobbing, which enables the avoidance of lubricants.

In conclusion, to couple several types of simulations namely, thermal and structural allows different analyses. The examination of processes, materials, prediction of behaviours and modification of parameters are some of the most usual themes. The inexistence of lubricants is also an important aspect as it allows operations more clean, although it is fundamental to assure that the conditions of function are the same. The studies are focused on diverse parts such as, disc rotors, all types of gears and sets of it, cooling channels, piping systems, and tires among others. When it is necessary to assess conditions or procedures, it is beneficial to perform simulations like the ones demonstrated in this section in order to understand better what is or may happen in certain circumstances.

“Never throughout history has a man who lived a life of ease left a name worth remembering.”

Theodore Roosevelt (1858-1919), 26th president of the U.S.

### 3. THEORETICAL INTRODUCTION

In this chapter will be presented and explained all the themes, subjects and topics necessary to understand what will be displayed in the following 2 sections.

The first describes the finite element method which is the basis for some types of numerical simulations. The steps of this approach are reviewed and detailed, praising the most important aspects. The second division deals with the finite volume method, which is similar to the anterior, although presents some differences in the sort of analysis it performs.

Next, the clarifications are focused on the heat transfer phenomena in which it is covered what circumstances are necessary for conduction and convection to occur. Consequently, it is detailed the mechanical phenomena, the types of simulations available and the kinds of loads possible to be applied on the bodies. Therefore, the deformation and stress measures are clarified as well as how to determine it.

The fifth section summarises the methods used on the mesh in order to obtain the best structure possible which will be employed to get the most accurate results. In addition, it is described the type of elements constituting the mesh. Lastly, it is presented the parameters available to evaluate the quality of the mesh.

In addition, the next section deals with the models used to perform the simulations in the

3 modules: steady-state thermal, Fluent and static structural. There are diversified approaches adopted by the software depending on the type of analysis it is being performed and that is what is intended to explain.

Finally, the last segment deals with the experimental methodologies that exist and some concepts about this theme are detailed. The technique of triangulation is explained since it is the one applied by the machine in order to obtain the 3D model of the mechanism.

#### 3.1. FINITE ELEMENT ANALYSIS

Finite element analysis (FEA) is a computerized method for numerical solutions of field problems. This method is used to predict how a product reacts to physical effects such as real-world forces, vibration, heat, fluid flow, among others. In addition, in a field problem it is supposed to determine the spatial distribution of one or more dependent variables. With that said, finite element analysis shows whether a product will break, wear out, or work the way it was designed. The mathematical form of describing a field problem is using differential equations or by an integral expression (Cook et al., 2002).

The component in study is divided into individual finite elements which will be the basis of the FE analysis. In opposition, in calculus it is used infinitesimal elements and that constitutes the principal difference between both methods. In each finite element, it is allowed for a field quantity to have only a simple spatial variation, perhaps described by polynomial terms up to  $x^2$ ,  $xy$  and  $y^2$ . It is important to mention that, in reality, the variation of a region measured by an element is almost certainly more complicated, which means that FEA provides an approximate solution. The particular arrangement of elements in a body or region is called of mesh, and the connections at points of that structure are denominated of nodes. An FE mesh is numerically represented by a system of algebraic equations which have to be solved for the unknown values at nodes. Nodal unknowns are values of the field quantity and, depending on element type, perhaps also its first derivatives. The solution for nodal quantities, when combined with the assumed field in any given element, completely determines the spatial variation of the field in that element. Although an FEA solution is not exact, it can be improved by using more elements to represent the structure, which means refining the mesh.

Finite element analysis, which can also be called as finite element method (FEM), presents several advantages over most other numerical analysis methods, and it can be applied in any application field namely heat transfer, stress analysis, magnetic fields and others (Murashov & Panin, 2015; Coda et al., 2015; Nakano et al., 2014; Elhosni et al., 2014). For this type of



study there is no geometric restriction, which means the body or region may have any shape. In figure 13, it is displayed the 2D model of a gear tooth where all nodes elements are contained in the plane of the figure. The supports of the tooth are not included in this representation (Cook et al., 2001).

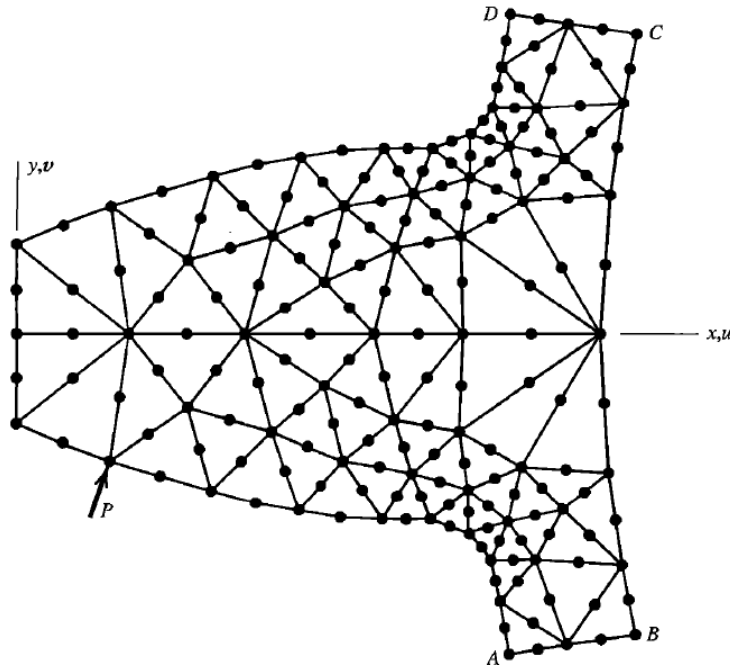


**Figure 13** - A two-dimensional model of a gear tooth (Cook et al., 2002)

In terms of boundary conditions and loadings, there are also no limits. For example, in a stress analysis, it is possible to support a part of a body while applying distributed or concentrated forces to another segment. Regarding the materials, different elements of the mesh can have various behaviours or even within an element. Components which have different natures, and distinctive mathematical descriptions, can be combined. Therefore, a single FE model might contain bar, beam, plate, cable and friction elements.

A structure used in a finite element analysis closely resembles the body or region to be examined. When the study does not produce the expected results, the approximation can be simply improved by grading the mesh so that more elements appear where field gradients are high and more resolution is required.

### 3.1.1. Problem Classification

The first step in solving a problem is to identify it. Then, there are some important aspects necessary to be examined. To understand the physical phenomena involved, to know if the problem is time-independent or time-dependent (using another terminology, if the problem is

static or dynamic), or even, if there is any factor that turns the analysis nonlinear, so that iterative solution is necessary, are just some of them. Regarding the solution, it is essential to define what type of results is intended to obtain as well as the required accuracy for them. Answers to such questions influence how much information must be gathered to perform the analysis, how the problem is modelled, and what method of solution should be adopted.

A complicated problem is usually not related with only one category. An example of this statement is a fluid-structure interaction problem, such as earthquake excitation of a storage tank which contains liquid. The motion of the liquid causes the tank to deflect, and, as a result, the deflection modifies the liquid motion. Therefore, both structural displacement and fluid motion fields cannot be considered separately; calculations must take their interaction into account. This situation, in which each field influences the other, is an example involving what may be called of direct or mutual coupling. In opposition, if one considers an analysis for thermal stresses, where temperature influences stresses but these have negligible influence on temperature, then this is an example of what may be called indirect or sequential coupling (Hutton, 2004).

#### 3.1.2. Modelling

An analytical method is applied to a model problem rather than to an actual physical problem. A model for analysis can be idealised after the physical nature of the understanding of the problem.

In modelling, the analyst attempts to exclude useless details, so that the study of the model is not unnecessarily complicated, although includes all essential features in order to provide results which describe the real problem with sufficient accuracy.

A geometric model becomes a mathematical model when the behaviour of the body is described by selecting differential equations and boundary conditions. It is important to recognise that a finite element analysis is a simulation, not a real situation. In addition, an FEA is applied to the mathematical model which means that if it is created an inappropriate or inadequate formulation, the study will not be in agreement with physical reality, even if it is very accurate.

A mathematical model is an idealisation, in which, it must be included geometry, material properties, loads, and/or boundary conditions are simplified based on the engineer understanding of what features are important in obtaining the required results (Moaveni, 1999).

### 3.1.3. Discretisation

A mathematical model is discretised by dividing it into a mesh of finite elements. Therefore, a fully continuous field is represented by a piecewise<sup>1</sup> continuous field defined by a finite number of nodal quantities and simple interpolation within each element. Software can automatically prepare most of the mesh, although the analyst must provide some direction as to the type and size of the element as well as the mesh density desired in what portions of the body. With that in mind, it is simple to claim that discretisation introduces another approximation. Relative to reality, two sources of error are included in the study: modelling and discretisation errors. The first one can be reduced by improving the model, while the second can be reduced by using more elements. Even if discretisation error would be eliminated, the physical reality would not be perfectly represented as modelling error is also part of the simulation. Besides, an analysis performed by a computer introduces numerical error by using numbers of finite precision to represent data and the results of manipulation. Poor discretisation as well as other physical situations can contribute to a large numerical error, although it is usually small (Cook et al., 2002; Huebner et al., 2001).

### 3.1.4. Solving a Problem

#### **Preliminary Analysis**

It is quite important to obtain a preliminary solution before going from a mathematical problem to a finite element analysis. In order to obtain this result, it should be used any means available whether it is simple analytical calculations, handbook formulas, trusted previous solutions, or experimental activities. It is expected that this initial exercise may conduct to a better mathematical model which will, later, be used to establish a comparison with numerical results.

If this work is done before the finite element study rather than after, the tendency to find answers that support whatever computed results have already been obtained is greatly reduced. It is simple to make mistakes in supplying data to software and, for that reason, it is fundamental to execute a preliminary analysis (Moaveni, 1999).

---

<sup>1</sup> In mathematics, a piecewise function is one which is defined by multiple sub functions, each of them applying to a certain interval of the main function's domain (a sub-domain).

#### **Finite Element Analysis**

In order to perform a numerical analysis, the software automatically generates matrices which describe the behaviour of each cell of the mesh and, consequently, combines them into a large matrix equation. The software takes this latter system, which represents the finite structure, and solves this equation to determine values of field quantities at nodes. It is claimed by Fallah et al. (2000) that the accuracy of the finite volume solution is comparable to the finite element method. This means that the FV method can be considered as an equally appropriate candidate as the FE involving problems related to deformations and stresses. Hence, this provides the opportunity to solve multiphysics phenomena (i.e., fluid-structure interaction) using a single modelling formulation.

Significant additional calculations are performed if the behaviour of the simulation is nonlinear or time-dependent. Regarding the postprocessing, it is important to inspect the solution and the quantities derived from it, displayed by the software. This information is generated automatically, the analyst only has to choose the data to be exhibited.

In a study of stress, typical displays include deformations and stresses of various types on diverse planes. In a thermal analysis, it is regular to ask for results of temperature distribution and heat fluxes. The studies executed in the modules of ANSYS called Steady-State Thermal and Static Structural are based on this type of elements (Cook et al., 2002; Moaveni, 1999).

#### **Check/Revise the Results**

Firstly, it must be performed a qualitative examination to inspect if the results contain obvious errors. Secondly, the analyst should evaluate if the problem solved was the intended one, if the boundary conditions were not misrepresented or even, if there are any displacements where there should not be any. It is necessary to study the results having a critical view over them. If these questions are satisfactorily answered, then, the numerical results can be compared to any data previously obtained or other useful information available.

Seldom has the first analysis produced satisfactory results. If there are large divergences between what is expected and what is computed, it is necessary to find an explanation for that occurrence. Physical understanding might be not exactly the correct one which means the mathematical model should be adapted. Also, the finite element model might have some inaccuracy which could be contributing for the unacceptable results. After running the analysis cycle again, the discretisation may be judged inadequate, perhaps being too coarse in some places. Next, it is required a mesh revision before performing a new study.

When a problem is being investigated, it is appropriate to begin with a simple finite element model and, then, it is added details as the analyst learns more. Each revision is an expected step on the way to an adequate solution, not a punishment for failure in the preceding attempt (Hutton, 2004).

### 3.2. FINITE VOLUME METHOD

Finite-volume methods (FVM) are mainly applied for the numerical solution of problems in fluid mechanics, although the employment of the FVM is not limited to flow problems.

The finite volume methodology is a discretisation method for the approximation of one or multiple partial differential equations stating the conservation or balance, of one or more, quantities. This characteristic is the principal advantage of this type of analysis over the others, especially in areas involving heat transfer. For this reason, this method is used as the basis for the thermal module of ANSYS named Fluent where are simulated the behaviour of fluid-structures interfaces (Versteeg & Malalasekera, 2007; Moukalled et al., 2015).

These partial differential equations (PDE) are often denominated as conservation laws; they may be of different nature, e.g. elliptic, parabolic or hyperbolic, and they are used as models in a wide number of fields, including physics, biophysics, chemistry, image processing, finance, dynamic reliability. They define the relations between partial derivatives of unknown fields (such as temperature, pressure, and molar fraction, etc.) with respect to variables within the domain (space, time...) under consideration.

As in the finite element method, a mesh is constructed, which consists in a division of the domain in finite elements where the space variable is included. The cells of the mesh are called control volumes. The integration of the PDE over each control volume results in a balance equation. Consequently, the set of balance equations is then discretised with respect to a set of discrete unknowns. The main issue is the discretisation of the fluxes at the boundaries of each control volume: in order for the FVM to be efficient, the numerical fluxes are generally conservative and consistent. The first characteristic means that the flux entering in a control volume from its neighbour must be on the opposite side of the one entering the neighbour from the control volume. To be consistent represents that the numerical fluxes of a regular function interpolation tends to the continuous flux as the mesh size approximates of zero.

The finite volume method is preferred over other types of approaches. In addition, finite volume structures takes full advantage of arbitrary meshes to approximate complex geometries. With that said, experience shows that non-conservative schemes are generally less accurate than

conservative ones, particularly in the presence of large gradients (Hirsch, 2007).

In conclusion, the general methodology of the finite volume method includes some steps starting with the generation of the mesh, which means decomposing the problem domain into a set of discrete control volumes. Next, it is established the formulation of integral balance equations for each control volume. The following phase is the determination of integrals by numerical integration. Consequently, there is the calculation of function values and derivatives by interpolation with nodal values. Finally, the discrete algebraic system is solved, after the values are all assembled (Versteeg & Malalasekera, 2007; Moukalled et al., 2015).

This explanation shows the differences between the finite element analysis and the finite volume method. Therefore, it can be concluded that it is in the discretisation process as well as the approach of solving the problem where they are more distinct.

#### 3.2.1. Discretisation

As the discretisation step is the one where more differences are verified between both methods, it will be explained in detail.

The finite volume method is able to operate with any type of mesh, whether it is structured or unstructured, and, therefore, has the same flexibility of finite element method. Unstructured meshes are consisted by arbitrary combinations of tetrahedrons, hexahedra or pyramids in a 3D problem. They offer a large flexibility for complex geometric configurations which is their main advantage and the reason why they have to be employed.

In general, there are two types of discretisation in which it is distinguished between cell-centred and cell-vertex methods. In cell-centred FVM, the variables are attached to a cell where the averaged values over the cell coincides with the ones of the control volume (figure 14 (a)). In the cell-vertex FVM, the variables are associated with a mesh point called node (figure 14 (b)) (Versteeg & Malalasekera, 2007; Moukalled et al., 2015). The module Fluent employs finite elements (cell-centred numerics) to discretise the domain (ANSYS I. , 2010). This approach is more suitable and achieves more accurate results for unstructured meshes (Wang et al., 2010) which justifies the adoption of this method over other options provided by ANSYS. There was also the possibility to simulate this situation with Steady-State Thermal which discretises its domain with a finite element method where the determination of the unknowns occurs on the nodes. These methodologies were tested by Frisani & Hassan (2015) on fluid flow problems with complex geometries. Computations were performed using FEM and FVM approaches for the three-dimensional flow past a sphere domain. It was concluded that the finite

element approach is numerically more accurate than the finite volume discretisation. In contrast, the latter is computationally more efficient than the former which is an aspect less important in this simulation.

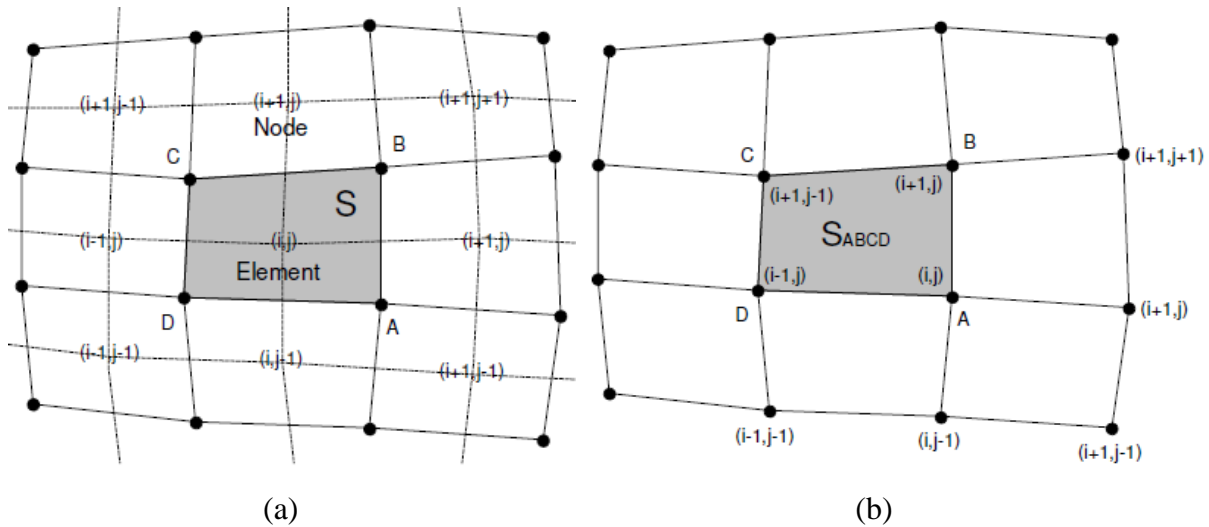


**Figure 14** - Mesh for finite volumes: (a) cell-centred; (b) cell-vertex (Moukalled et al., 2015)

### 3.3. HEAT TRANSFER PHENOMENA

To perform a thermal simulation, the software ANSYS supports on the principle of conservation of energy which states that in a system, energy cannot be generated or destroyed. This principle is described by a heat balance equation. The solution obtained in the finite element analysis calculates nodal temperatures and, consequently, these values are used to determine other thermal unknowns.

It is possible to operate in ANSYS with all three fundamental modes of heat transfer: conduction, convection and radiation.

The objective of a steady-state thermal study is to investigate the response of a component or system to steady thermal loads, which means that do not vary over time. This type of analysis can be applied in order to determine temperature distributions, thermal gradients, thermal fluxes as well as the quantity of heat which entered or exited in the system. Moreover, it is possible to implement diverse types of loads which include phenomena such as convection and radiation, heat flow rates, heat fluxes (heat flow per unit area), heat generation rates (heat flow per unit volume) and constant temperature boundaries.

The simulation can be considered as nonlinear, if the material properties differ with temperature or linear for constant values of properties. If the radiation effects are included in an analysis, then it becomes nonlinear.

Thermal simulations play an important role in the design of many engineering applications where it could be inserted examples of internal combustion engines, turbines, pistons, heat exchangers, brakes, electronic components, among others. It is quite usual to perform a thermal analysis followed by a stress study with the purpose of verifying the thermal stresses, which means the stresses resulting from thermal expansions or contractions (ANSYS Inc., 2009a; ANSYS Inc., 2009c; Incropera et al., 2013).

#### 3.3.1. Conduction

When there is a difference of temperature between 2 bodies included in the same system, occurs a phenomenon in which the component with higher temperature transfers heat to the colder one. This process ends when it is reached an equilibrium of temperatures in the system. Therefore, the flux of heat should be a function of both body temperatures incorporated in the previous frame. This thermal characteristic is, usually, dependent of temperature which turns the calculations nonlinear. However, sometimes, the situation is simplified when small temperature variations are involved. That is what happens for practical situations such as when the sun rays heat to our bodies, in optical experiments with low intensity laser beams, among others.

More specifically, steady-state conduction is a phenomenon which is developed when the difference of temperatures is constant, which means that, its spatial distribution in the conducting object does not suffer any variation. In conclusion, in steady-state conduction, the portion of heat exiting the system is equal to the amount which is entering (ANSYS Inc., 2009a; ANSYS Inc., 2009c; Rohsenow et al., 1998).

#### 3.3.2. Convection

Convection is a phenomenon which occurs at the surface of solid or shell elements. The basis of this mechanism is the transfer of heat by mass motion of a fluid. What happens is that the heated fluid tends to deviate from the origin of heat and transports energy during this process. As the temperature of the fluid increases, it becomes less dense and rises, which, consequently, creates convection currents.

This thermal phenomenon is included in simulations with the objective of determining specific aspects fluid velocities, local values of film coefficient and heat flux, and temperature distributions. It is possible to examine these details whether to the fluid included in the study or to the body in question by using the appropriate CFD elements.

It is necessary to define parameters to the surfaces in order to apply this phenomenon in a simulation which are the convection film coefficient and the bulk temperature. If the first is



dependent of the temperature, the analyst must specify a value of this coefficient to the individual temperatures. The second is a convenient reference point for evaluating properties related to convective heat transfer (ANSYS Inc., 2009a; ANSYS Inc., 2009c; Rohsenow et al., 1998; Holman, 2009).

### Heat Transfer Coefficient

In free convection fluid motion is due to buoyancy forces<sup>2</sup> within the fluid, while in forced convection it is externally imposed. Buoyancy is due to the combined presence of a fluid density gradient and a body force that is proportional to density. In practice, the body force is usually gravitational, although it may be a centrifugal force in rotating fluid machinery or others. There are also several ways in which a mass density gradient may arise in a fluid. However, for the most common situation it is due to the presence of a temperature gradient. The density of gases and liquids depends on temperature, generally decreasing (due to fluid expansion) with increasing temperature.

If it is considered a laminar boundary layer development adjacent to a heated vertical plate (which is, in this case, the kinematic system), an empirical correlation for free convection in a complex geometry might be used, such as:

$$\overline{Nu}_L = 0.68 + \frac{0.67 Ra_L^{1/4}}{[1 + (0.492/Pr)^{9/16}]^{4/9}} \quad (3.1)$$

where  $Nu$  represents the Nusselt number,  $Ra$  characterises the Rayleigh number and  $Pr$  is the Prandtl number of this situation.

This correlation had been developed for common immersed (external flow) geometries which are suitable for many engineering calculations where it is important to obtain a slightly better accuracy. The adopted exponents are also the most appropriate considering the situation which means they also enable to reach the most precise values (Incropera et al., 2013).

Equation 3.2 shows the expression that allows to determine the Rayleigh number based on the characteristic length where  $Gr$  describes the Grashof number. For a laminar flow this number should be placed in the range  $10^4 \leq Ra_L \leq 10^9$ .

$$Ra_L = Gr \times Pr \quad (3.2)$$

After calculating the values of Grashof, Prandtl and, consequently, Rayleigh numbers, these values are inserted in equation 3.1 and it is estimated a result for Nusselt number. In order

---

<sup>2</sup> In science, buoyancy is an upward force exerted by a fluid that opposes the weight of an immersed object.

to determine Grashof number, it is required to know the value of the gravitational acceleration  $g$ , the volumetric thermal expansion coefficient  $\beta_v$ , the surface and bulk temperature  $T_S$  and  $T_\infty$  respectively, the characteristic length  $L_C$  and the kinematic viscosity  $\nu$ . The Prandalt number is obtained by dividing the latter variable to the coefficient of thermal expansion  $\alpha$ .

Then, equation 3.4 is equalled to that number and, it is found an average value for the heat transfer coefficient ( $\bar{h}$ ) through the characteristic length  $L_C$  and the thermal conductivity of the fluid  $k_T$ .

Table 1 summarises the definition and equations for the aforementioned parameters involved in the determination of this coefficient.

**Table 1** - Parameters to determine h

Name	Definition		Interpretation
Grashof Number (Gr)	$\frac{g\beta_v(T_S - T_\infty)L_C^3}{\nu^2}$	(3.3)	Measure of the ratio of buoyancy forces to viscous forces
Nusselt Number (Nu)	$\frac{\bar{h} \times L_C}{k_T}$	(3.4)	Ratio of convection to pure conduction heat transfer
Prandalt Number (Pr)	$\frac{\nu}{\alpha}$	(3.5)	Ratio of the momentum and thermal diffusivities

### 3.4. MECHANICAL PHENOMENA

The structures used in this type of study are part of a wide group in which there are not only bridges and buildings, but also naval, aeronautical, and mechanical components such as machine housings, pistons, tools and others.

A static analysis investigates the outcome of a structure under steady loading conditions. This type of study can only include steady inertia loads, like gravity and rotational velocity. In addition, it is also possible to incorporate loads that do vary in time which can be approximated as static equivalent loads, for example, wind and seismic forces.

As it was previously referred, several loads can be applied of different natures namely, external forces and pressures, steady-state forces, but also, imposed displacements and temperatures. With this sort of examination, it can be determined displacements, stresses, strains and forces in structures, and the analysis can be considered whether linear or nonlinear.

Regarding the results, it is important to mention that the fundamental unknowns (nodal degrees of freedom) obtained from a structural analysis are displacements. Consequently, other variables, such as, strains, stresses and reaction forces are then calculated from the nodal displacements.

It is possible to perform 7 types of structural analysis in ANSYS which are static, modal, harmonic, transient dynamic, spectrum, buckling and explicit dynamic (ANSYS Inc., 2009b).

### 3.4.1. Deformation

Deformation estimates the response of a structure under loading conditions. With that said, this characteristic is the variation of a body from a reference to a current configuration.

There are several types of deformation, depending on the nature of the load which causes it. Axial solicitations result in axial deformations while temperature causes expansions or contractions. The equations 3.6 and 3.7 are used to determine deformation for a uniform member which is subjected to an axial loading and to temperature, respectively (ANSYS Inc., 2009c).

Axial deformation

$$\delta_P = \frac{P_A L}{AE} \quad (3.6)$$

where  $P$  is the axial load,  $L$  describes the length of the bar,  $A$  expresses the cross-sectional area and  $E$  characterises the Young's modulus.

Temperature

$$\delta_T = \alpha (\Delta T)L \quad (3.7)$$

where  $\alpha$  is the coefficient of thermal expansion,  $\Delta T$  describes the difference of temperatures presented in the analysis and  $L$  represents the length of the component.

In a continuous body, a deformation field results from a stress induced by applied forces or due to changes in the temperature field. For linear elastic materials, the relation between stresses and strains is described by constitutive equations, for example, the Hooke's Law.

There are 2 different sorts of deformation: elastic and plastic. The first is applied when deformations are recovered after the stress field has been removed, in which the component returns to its original configuration. The second occurs when irreversible deformations remain after stresses have been removed, which means that the elastic limit, also called of yield stress, was exceeded (ANSYS Inc., 2009a; Rohsenow et al., 1998).

### 3.4.2. Stress

The word stress ( $\sigma$ ) is used to describe the loading in terms of force applied ( $F$ ) to a certain cross-sectional area ( $A$ ) of an object as it follows in figure 15. The equation 3.8 expresses that definition.

$$\text{Stress} = \frac{\text{Force}}{\text{Cross - Sectional Area}} \Leftrightarrow \sigma = \frac{F}{A} \quad (3.8)$$

Regarding the loading, stress is designated as the applied force (or system of forces) which tends to deform a body. Concerning what happens within the material, stress is the internal distribution of forces which react and balance to the solicitations employed in it. The stress dispersion could be uniform, for example, a bar loaded in pure tension, while a bar loaded in bending will have a stress distribution which changes with distance perpendicular to the normal axis.

For many engineering calculations as well as for material property determination, it is generally used simplifying assumptions to represent stress as a vector quantity. The term vector regularly indicates a quantity that has a magnitude and a direction. An example of that is the fact that the stress in an axially loaded bar is simply described as the applied force divided by the cross-sectional area of the bar (Moaveni, 1999; ANSYS Inc., 2009b).

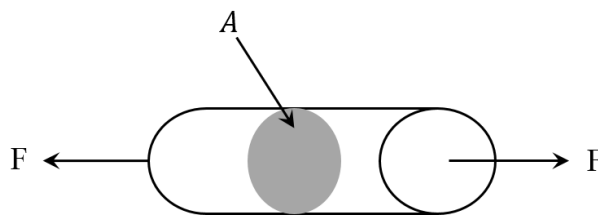


**Figure 15** - Axial Forces applied in a Bar (Moaveni, 1999)

### 3.5. METHODS AND TYPES OF ELEMENTS USED ON THE MESH

In ANSYS, it is possible to generate a mesh automatically to a part or multibody part. To do so, it is used a default element size determined by the software, depending on the geometry of the components and its complexity. Generally, the adopted element dimension is the smallest measure it is necessary to mesh all the parts concerning the proximity of different topologies, body curvature, among others. However, if the user is not satisfied with the mesh created, there are several possibilities to improve it. The fineness of the mesh can be adjusted up to four times (eight times for an assembly) to achieve a successful mesh changing the options established for the assembly or, more specifically, to one of the parts.

On the other hand, the engineer can manage the mesh the most convenient way by using the control tools, provided by the software. Both global and local mesh commands are available. The principal objective of meshing with ANSYS Workbench is to provide robust, intuitive and uncomplicated meshing tools which will simplify the process of creating a mesh. These tools have the benefit of being highly automated along with having a moderate to high degree of user

control.

Once the structure of the mesh is completed, it is possible to evaluate its quality using several different parameters. The mesh metric option allows to view information and thereby concluding about the necessity of refining the mesh. The criteria available to be displayed are: element quality, aspect ratio for triangles or quadrilaterals, jacobian ratio, warping factor, parallel deviation, maximum corner angle, skewness, and orthogonal quality.

### 3.5.1. Global Mesh Controls

There are diverse options in ANSYS Workbench to manage the parameters of the mesh and they are divided in groups which are: defaults, sizing, inflation, assembly meshing, patch conforming, patch independent, advanced and defeaturing. Only the first 2 will be explained in detail as they were the ones used to refine the meshes.

The set of default options is constituted by physics preference, solver preference and relevance. These should be defined early and it regards all the parts which constitute the model. The physics preference option allows to establish how Workbench will perform meshing based on the physics of the analysis type it is specified. Available options are: mechanical, electromagnetic, CFD and explicit. Choosing CFD as physics preference causes a solver preference option to appear which can be CFX, Fluent, or polyflow. Based on what is adopted, the meshing application sets certain defaults that will result in a mesh that is more favourable to the CFX, Fluent, or polyflow solver, respectively. Within the mechanical application, choosing mechanical as the physics preference conducts to the creation of a mesh more appropriate to a structural study. The relevance command enables to control the fineness of the mesh for the entire model. The value of -100 indicates a preference toward high speed, while +100 expresses an inclination to high accuracy solutions. It is important to refer that the finer the mesh, the more accurate the results. However, a finer mesh uses more elements, more time, and consequently, more system resources.

The sizing group consists of several options, such as, advanced size function, relevance centre, element size, smoothing, transition, span angle centre and minimum edge length which will, next, be specified.

The advanced size function command provides greater control over sizing functions, in which the user can choose one of these options: curvature, proximity, the combination of both and fixed. The applied preference determines which refinement mechanisms are activated in the advanced size function. The curvature size function examines curvature on edges and faces

and computes element sizes on these entities such that the dimension will not violate the maximum size or the curvature normal angle. These values can be specified automatically by the software or by the user. The proximity size function enables to specify the minimum number of element layers created in regions that constitute “gaps” in the model. For the purposes of specifying a proximity size function, a “gap” is defined as an internal volumetric zone between 2 faces or an area between 2 opposing boundary edges of a face. There are controls which are common to all types of advanced size function including minimum size/proximity minimum size, maximum size, maximum face size, and growth rate. The first 2 specifications represent, respectively, the global minimum and maximum allowable element size regarding the volume. The option maximum face size expresses the global maximum allowable size of the element surfaces created by these methods. The growth rate describes the increase in element edge length with each succeeding layer of elements from the edge or face.

With respect to the relevance centre, this characteristic sets the gauge of the relevance control in the defaults group. The options available are coarse, medium, and fine.

The command element size allows to specify the cell dimension used for the entire model. This size will be used for all edge, face, and body meshing.

In regard to smoothing, it attempts to improve element quality by moving locations of nodes with respect to surrounding nodes and elements. The low, medium, or high option controls the number of smoothing iterations along with the threshold metric from which the mesh generator will start smoothing.

Transition affects the rate at which adjacent elements will grow, where slow produces smooth transitions while fast results in more abrupt progress between cells.

Concerning the span angle centre, it establishes the reference value for curvature based refinement. The mesh will subdivide in curved regions until the individual elements span this angle. The options available include coarse (from 60° to 91°), medium (from 24° to 75°) and fine (from 12° to 36°).

Finally, the minimum edge length provides a read-only indication of the smallest edge length in the model (ANSYS Inc., 2013).

#### 3.5.2. Local Mesh Controls

In ANSYS there are diverse commands to implement on the mesh with the purpose of refining it locally. The accessible controls are: method, mesh grouping, sizing, contact sizing, refinement, mapped face meshing, match, pinch, inflation, sharp angle, and gap. Only the method and sizing options will be thoroughly described as they are the ones implemented in

meshes.

The method control is valid only for a body. Within this command there are several controls to construct a successful mesh, such as, automatic, tetrahedrons, sweep and multizone.

The default option (automatic method) employs meshing methods that provide a successful automated mesh, which attempts to use hexahedra for solid models and quadrilateral element generation for surface body models. The quadrilateral elements provide a simpler analysis which is why they are the preferable.

If the option tetrahedrons is selected, an all tetrahedral mesh is created. This control is used to force a mesh to be constituted by tetrahedral elements in which, by default, it would be composed of other type of elements.

If the user selects the sweep method, a swept mesh is forced on sweepable bodies, which are symmetric bodies with respect to an axis, using hexahedral elements. The mesh will not be constructed if the geometry contain errors or the body is not perfectly symmetric.

Concerning the multizone mesh method, it provides an automatic decomposition of geometry into mapped (sweepable) regions and free regions. When the multizone mesh approach is selected, all regions are structured with a pure hexahedral mesh if possible. To handle cases in which a pure hexahedral mesh will not be possible, the user can adjust the settings so that a swept mesh will be generated in structured regions and a free mesh will be constructed in unstructured regions. The advantage of this method is that it is not necessary to slice the components while in the sweep method it is due to the demand of separating the structured of the unstructured segments.

The sizing control sets the element size for a selected body, face or edge as well as the number of divisions along an edge and, even, the element size within a user-defined “sphere of influence” which can include a selected body, face, edge, or vertex. It is also possible to define a finite minimum mesh sizing to be used for a selected body, face, or edge. This setting overrides the default global sizing. Summarising, the sizing command include the options element size, sphere of influence, body of influence or number of divisions.

To refine a body or a face locally, there is the possibility of specifying an element size or a sphere of influence. To define the first it is necessary to mention the type of behaviour wanted, where by using the hard option, these values override the global dimensions of the mesh while the soft option does not. Moreover, the local element size, the growth rate, the curvature normal angle and the local minimum size must be detailed. For the sphere of influence, it is necessary to indicate the centre of the sphere, its radius and the length of the elements which will be part of it (ANSYS Inc., 2013).

#### **Elements used on the Mesh**

There are diverse types of elements which can be used to construct meshes. In ANSYS Workbench the software adopts the most appropriate type of cell concerning the analysis it will be performed. They can vary in shape, size, number of degrees of freedom, among other aspects.

The first to be presented is a tetrahedron called SOLID72 which is a 3D element well suited to model irregular meshes. The element is defined by 4 nodes having 6 degrees of freedom at each node: translations in the nodal x, y, and z directions and rotations about the nodal x, y, and z directions. The element also has stress stiffening capability. The SOLID72 element can often be used in place of others to reduce the wavefront<sup>3</sup> and solution time (since it does not have midside nodes). Although the element has additional degrees of freedom per node, it is not as accurate as the ones which have more nodes.

Other 3D element used to construct meshes is the tetrahedron named SOLID92 which has a quadratic displacement behaviour and is also well suited to model irregular meshes. The element is defined by 10 nodes having 3 degrees of freedom at each node: translations in the nodal x, y, and z directions. The element also has plasticity, creep, swelling, stress stiffening, large deflection, and large strain capabilities.

Next, there is the hexahedron element denominated as SOLID95 which is a higher order version of the 3D 8-node solid element (SOLID45). It can tolerate irregular shapes without as much loss of accuracy. It can also be highlighted that it has compatible displacement shapes and is well suited to model curved boundaries. The element is defined by 20 nodes having three degrees of freedom per node: translations in the nodal x, y, and z directions. Moreover, the element may have any spatial orientation and has plasticity, creep, stress stiffening, large deflection, and large strain capabilities.

For similar meshes, SOLID72 will be significantly less accurate than the 10-node tetrahedral solid element SOLID92. SOLID72 models, however, have the advantage of fewer degrees of freedom, a lower wavefront, and smaller file sizes. This makes SOLID72 most useful for the initial analyses of models that are easily meshed with tetrahedrons. A detailed analysis of the specific regions of interest should be redone, if necessary, using submodelling techniques with higher order elements, such as SOLID92. When the element SOLID92 is preferred over the SOLID95, less random access memory is required per element and when the PCG solver is employed, it is gained a modest speed advantage (ANSYS Inc., 2009b; ANSYS Inc., 2009c;

---

<sup>3</sup> A surface associated with a propagating wave and passing through all points contained in it, which are in the same phase.



ANSYS Inc., 2013).

In figure 16 are displayed the aforementioned elements where the differences between them can be observed.

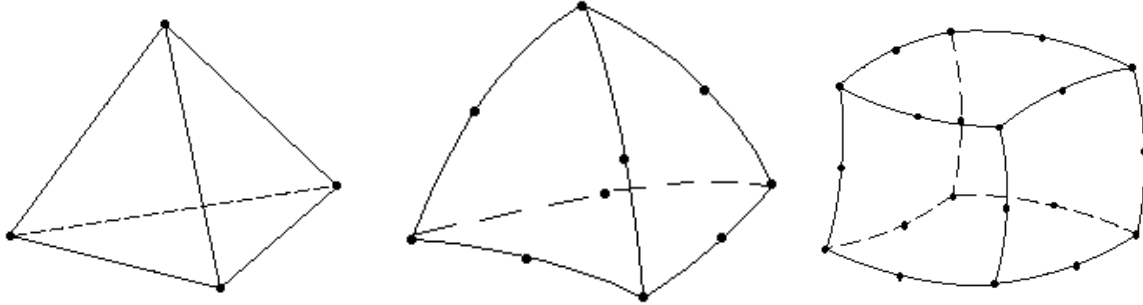


**Figure 16** – Tetrahedron with 4 nodes (left) and 10 nodes (centre); Hexahedron with 20 nodes (right) (ANSYS Inc., 2013)

### 3.5.3. Evaluation of Mesh Quality

There are diverse guidelines, which were previously referred, to assess a mesh. Next, the most relevant will be explained in detail being element quality, aspect ratio calculation for triangles, maximum corner angle and skewness.

Regarding the element quality, this option provides a composite quality metric that ranges between 0 and 1. This metric relates area and edge lengths for 2D elements while it is associated with the volume of the elements and its edge lengths for 3D elements. A value of 1 indicates a perfect cube or square while a value of 0 indicates that the element has a zero or negative volume.

Concerning the aspect ratio for a triangle, it is computed using only the corner nodes of the element. First, a line is constructed from one node of the element to the midpoint of the opposite edge, and another through the midpoints of the other 2 edges. In general, these lines are not perpendicular to each other or to any of the element edges. Then, rectangles are drawn with these lines as it can be seen in figure 17.

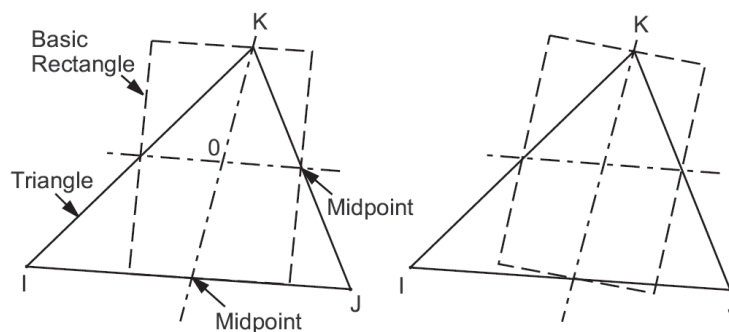


**Figure 17** - Triangle Aspect Ratio Calculation (ANSYS Inc., 2013)

The best possible triangle aspect ratio, for an equilateral triangle, is 1. Various triangles having different aspect ratios are displayed in figure 18.



**Figure 18** - Aspect Ratios for Triangles (ANSYS Inc., 2013)

The next aspect is the maximum corner angle which is the maximum angle between adjacent edges and it is computed using corner node positions in 3D space. The best possible maximum angle, for an equilateral triangle, is  $60^\circ$ . In figure 19 it is possible to see an example of that as well as a triangle having a maximum corner angle of  $165^\circ$ .



**Figure 19** - Maximum Corner Angles for Triangles (ANSYS Inc., 2013)

On the other hand, skewness is one of the primary quality measures for a mesh. Skewness determines how close to ideal a face or cell is. In figure 20, there are examples of an equilateral triangle and of a highly skewed triangle.

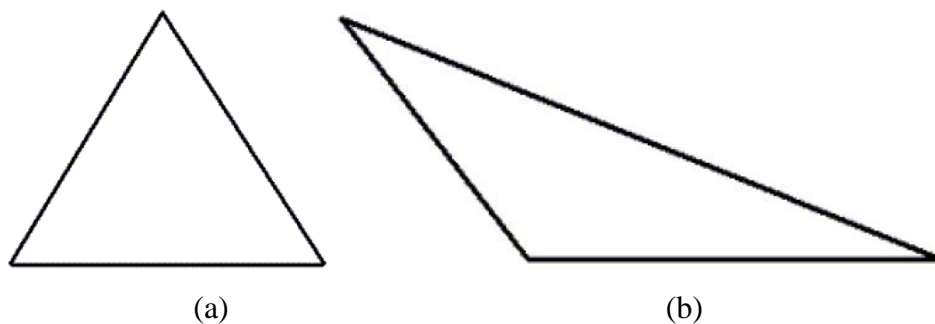


**Figure 20** - (a) Equilateral Triangle; (b) Highly Skewed Triangle (ANSYS Inc., 2013)

Table 2 lists the range of skewness values and the corresponding cell quality. According to the definition of skewness, a value of 0 indicates an equilateral cell (best) and a value of 1 expresses a completely degenerate cell (worst). Degenerate elements are characterized by nodes that are nearly coplanar. Highly skewed faces and cells are unacceptable because the equations

being solved assume that the cells are relatively equilateral/equiangular (ANSYS Inc., 2013).

**Table 2** - Evaluation of Mesh Quality

Value of Skewness	Cell Quality
1	Degenerate
0.9 — <1	Bad (sliver)
0.75 — 0.9	Poor
0.5 — 0.75	Fair
0.25 — 0.5	Good
>0 — 0.25	Excellent
0	Equilateral

### 3.6. MODELS USED IN SIMULATIONS

ANSYS provides different types of analysis which could be performed on the software namely steady-state thermal, fluid-structure interaction and static structural. All these studies are based on formulations which allow them to solve the proposed situations. The user must adopt the examination more suitable to what it is intended to be investigated.

Next, it will be presented and described the models behind the solutions, detailing the required equations and the basic definitions of them.

#### 3.6.1. Steady-State Thermal

The basic statement of a steady-state heat transfer simulation is based on the equation provided by Fourier's Law which is responsible for solving temperatures. Thus, they are determined using the expression 3.9:

$$[k]\{T\} = \{Q\} \quad (3.9)$$

where  $k$  is the heat flow,  $T$  describes the temperature and  $Q$  details the thermal conductance.

Through this expression it is possible to assume that no transient effects are considered in this type of analysis. Regarding the term  $k$ , it is important to refer that it can be constant or a function of temperature in which it is possible to apply a dependence to thermal conductivity for any material property. Likewise,  $Q$  can be constant or a function where temperature-dependent film coefficients are possible to be inserted for convective boundary conditions. (ANSYS, 2005)

A nonlinear solution will be required if temperature-dependent material properties or convection film coefficients are present. This means that several internal iterations will be run to

achieve heat equilibrium.

Two types of solvers are available in this simulation which are iterative and direct. The first can be efficient for solving large models while direct is a robust solver and could be employed in any situation. The specific solvers available to perform the studies are: the sparse, the Jacobi Conjugate Gradient (JCG), the JCG out-of-memory, the Incomplete Cholesky Conjugate Gradient (ICGG), the Preconditioned Conjugate Gradient (PCG), the PCG out-of-memory and an automatic iterative option.

It is employed the JCG solver in occasions when it is crucial to obtain results fast for single-field problems, such as, thermal, magnetics, acoustics and multiphysics. Similarly to the previous method, ICCG solver is used when solution velocity is needed but only for multiphysics applications. This solver deals with models which are more difficult to converge in other iterative solvers. Next, the PCG solver is applied for situations when solution speed is fundamental for linear analysis of large models. Moreover, it is especially well-suited for models of higher dimensions with solid models. Finally, there is the automatic iterative solver option which chooses the most appropriate solver based on the conditions of the problem being solved. To do that, it is necessary to define an accuracy level. It is specified as an integer of 1 until 5, being 1 the fastest settings (less number of iterations) and 5 the slowest (more accurate). This solver option is available only for linear static and linear full transient structural analysis.

Then, the sparse direct solver is explained in more detail as it is very important in the performed simulations. This solver is adopted when robustness and solution speed are necessary, in a nonlinear analysis, while it is applied in a linear study where iterative solvers are slow to converge. Basically, this solver is based on a direct elimination of equations as opposed to iterative solvers, where the solution is obtained through indirect means (that is, through iterative solution). Since the sparse direct solver is based on direct elimination, poorly conditioned matrices do not pose any difficulty in producing a solution (Moaveni, 1999; ANSYS Inc., 2009c).

#### 3.6.2. Static Structural

In ANSYS, a structural analysis is based on certain formulations in order to solve the problems. In addition, this section presents the principle of virtual work which is used to obtain formulas for the element stiffness matrix and for load vectors associated with initial strains, body forces, and surface tractions. These results apply to commonly used elements, which are based on interpolation of displacements from nodal DOF. The principle of virtual work, also known as the principle of virtual displacements, is described through the expression 3.10:

$$\int \{\delta\varepsilon\}^T \{\sigma\} dV = \int \{\delta u\}^T \{F_B\} dV + \int \{\delta u\}^T \{\Phi\} dS \quad (3.10)$$

where  $\delta\varepsilon$  represents the virtual strains,  $\sigma$  stands for stresses,  $\delta u$  describes the virtual displacements,  $F_B$  expresses the body forces and  $\Phi$  is the surface tractions on surface  $S$ .

This equation states that in an equilibrium configuration, the increment of strain energy stored (first integral) is equal to the increment of work done by body forces in volume  $V$  (second integral) and surface tractions on surface  $S$ . This approach makes plausible the assertion that displacement-based finite elements satisfy differential equations of equilibrium in an average or integral sense.

Consider the formula,

$$\{r_e\} = [K]\{d\} \quad (3.11)$$

where  $r_e$  represents the nodal loads applied on the element and  $K$  is the element stiffness matrix. Lastly,  $d$  lists the nodal displacements degrees of freedom of an element as well.

The expression of the element stiffness matrix is:

$$[K] = \int [B]^T [E_E] [B] dV \quad (3.12)$$

where  $B$  is the strain-displacement matrix and  $E_E$  is a constitutive matrix which contains elastic constants. With these equations it is possible to determine the displacements in a structural analysis.

The software provides several methods of solving the equations which define the model, being most of them common to the thermal solvers, and they are frontal solution, sparse direct solution, Jacobi Conjugate Gradient (JCG) solution, Incomplete Cholesky Conjugate Gradient (ICCG) solution, Preconditioned Conjugate Gradient (PCG) solution, and an automatic iterative solver option (ITER).

The frontal solution is used in situations when it is required robustness for a nonlinear analysis or when memory is limited. The other solvers were already mentioned in the previous section.

Next, the PCG solver will be described as it is the most important for the performed simulations. This solver starts with element matrix formulation and, then, assembles the full global matrix. Consequently, it calculates the degrees of freedom (DOF) solution by iterating to convergence (starting with an assumed zero value for all DOF). By itself, the conjugate gradient method provides a systematic procedure to reduce the error and improve the accuracy of the approximate solution. With the addition of an appropriate preconditioner matrix, however, the

iterative procedure progresses more quickly to a converged solution. Most computation resources for a PCG solver are used to form the preconditioner which is done once at the beginning of the iteration process and, at each iteration, by applying the preconditioner and multiplying by the system matrix. The PCG solver is best suited for structural analysis. It is valid for elements with symmetric, sparse, definite or indefinite matrices (Moaveni, 1999; ANSYS Inc., 2009b).

#### 3.6.3. Fluid-Structure Interaction

As for other types of simulations, the module Fluent, where they are performed fluid-structure interaction analysis, provides a diverse number of solvers. By modifying the solver settings it is possible to improve both the rate of convergence of the simulation as well as the accuracy of the computed result.

Firstly, it could be chosen to execute a pressure-based or a density-based solver. These approaches differ in the way that the continuity, momentum, energy and species equations are solved.

The pressure-based solver has been used for incompressible and mildly compressible flows. The density-based approach, on the other hand, was originally designed for high-speed compressible flows. Both methods can, nowadays, be applied to a wide range of flows. However, the origins of the density-based might give the analysis more accuracy for high-speed compressible flows. Moreover, two algorithms exist under the pressure-based solver in Fluent: a segregated and a coupled. In the first, the governing equations are solved sequentially, segregated from one another, while in the coupled algorithm the momentum equations and the pressure-based continuity expression are solved in a coupled manner. In general, the first improves the convergence speed and the second requires more memory.

ANSYS Fluent provides the option to choose among 4 pressure-velocity algorithms: SIMPLE, SIMPLEC, PISO for the pressure-based segregated algorithm, while coupled uses the pressure-based coupled solver. These preferences present several levels of complexity which could be used according to the problem.

It is also fundamental to refer the interpolation schemes for calculating cell-face pressures when using the pressure-based solver. In Fluent are available the options standard, PRESTO, Linear, Second Order and Body Force Weighted. The process standard reduces accuracy for flows exhibiting large surface-normal pressure gradients near boundaries although, in general, it is the most appropriate to use.

ANSYS Fluent provides comprehensive modelling capabilities for a wide range of incompressible and compressible, laminar and turbulent fluid flows. Steady-state or transient analysis can be performed. In this module, a broad range of mathematical models for transport phenomena (like heat transfer and chemical reactions) is combined with the ability to model complex geometries. It could be included several factors and to do that there are models of multiphase, energy, viscous, radiation, heat exchanger, species, discrete phase, solidification and melting, acoustics and eulerian wall film. Only the energy equation and a viscous model will be explained in detail.

Considering that Fluent is a thermal module, it is crucial to present the energy equation wherein the method is based.

$$\frac{\partial}{\partial t}(\rho E_{CV}) + \nabla \cdot (\vec{v}(\rho E_{CV} + p_S)) = \nabla \cdot \left( k_{eff} \nabla T - \sum_j h_j \vec{J}_j + (\bar{\tau}_{eff} \cdot \vec{v}) \right) + S_h \quad (3.13)$$

The term  $\rho$  represents the fluid density,  $E_{CV}$  is the energy in the control volume and  $\vec{v}$  characterises the flow velocity. The static pressure is  $p_S$  and  $k_{eff}$  expresses the effective conductivity, while  $T$  is the temperature. The term  $h_j$  represents the heat transfer of species  $j$  as well as  $J_j$  is the diffusion flux of species  $j$ . Finally,  $\bar{\tau}_{eff}$  expresses the effective stress tensor.  $S_h$  stands for the source of heat which includes the heat of chemical reaction and any other volumetric heat sources the user have defined. The first 3 terms on the right hand side represent energy transfer due to conduction, species diffusion, and viscous dissipation, respectively. The terms of the equation which represent phenomena not included in the simulation are null and are not part of the analysis. It is possible to consider energy in the study, if it is set as on or not consider if the option is not chosen.

The flows can be considered as laminar or turbulent according to their nature. In Fluent, it can be adopted the inviscid, laminar, Spalart-Allmaras, k-Epsilon, k-Omega, transition k-kl- $\omega$ , transition SST, Reynolds Stress, scale-adaptive simulation, detached eddy simulation and large eddy simulation models to characterise the flow. Only the laminar flow is detailed as it describes the proposed problem. In general, this type of flow is defined by the inexistence (or low level) of disturbances, low wall shear stress and heat transfer and, it is receptive to separation under weak pressure gradients.

For all flows, ANSYS Fluent solves conservation equations for mass and momentum. The equation for conservation of mass, or continuity equation, can be written as follows:

$$\frac{\partial \rho}{\partial t} + \nabla \cdot (\rho \vec{v}) = S_m \quad (3.14)$$

Equation 3.14 is the general form of the mass conservation equation and is valid for incompressible as well as compressible flows. The source of mass  $S_m$  is added to the continuous phase from the dispersed second phase and any user-defined sources. Conservation of momentum in an inertial (non-accelerating) reference frame is described by

$$\frac{\partial}{\partial t} (\rho \vec{v}) + \nabla \cdot (\rho \vec{v} \vec{v}) = -\nabla p_s + \nabla \cdot (\bar{\tau}) + \rho \vec{g}_F + \vec{F}_E \quad (3.15)$$

where  $p_s$  is the static pressure,  $\bar{\tau}$  is the stress tensor, and  $\rho \vec{g}_F$  and  $\vec{F}_E$  are the gravitational body force and external body forces, respectively. The term  $\vec{g}_F$  expresses the fluid acceleration vector and  $\vec{F}_E$  also contains other model-dependent source terms such as porous-media and user-defined sources.

The solvers available to process the equations of energy and momentum are first order upwind, second order upwind, power law, QUICK, and third order MUSCL. Basically, the field variables (stored at cell centres) must be interpolated to the faces of the control volumes. The value is computed at the centre of the cell but it must be estimated the value at each face so the flux can be processed. The preference to perform this is the second order upwind which may allow a slower convergence as it uses more data points to define the approximation of spatial derivative. On the other hand, it demonstrates a second order accuracy, essential with tetrahedral meshes (ANSYS Inc., 2009a).

### 3.7. EXPERIMENTAL TECHNOLOGY

In order to distinguish 2D from 3D systems, it could be said that 2D systems create digital images, while 3D systems create digital sculptures. Similar to comparing a common paper printer to a 3D printer, the main difference between them is how they interpret and reproduce data in real-world space. For a 2D system, depth is not considered which means that Z-axis information does not exist. A 3D system reproduces a complete 3D shape, including depth. The difference between 2D and 3D systems does not make them incompatible. Many of nowadays 3D scanning devices combine both technologies. For instance, there are 3D scanners that can produce colour digital 3D models by overlaying a 2D colour maps onto a 3D model.

3D scanning is the process of determining the shape of an object surface or its volume in three-dimensional space. By collecting information about the real-world object using a 3D scan-



ning device, this turns the measurement and visualization in three dimensions possible. Accurate 3D measurements derived from a scanned object are useful for material inspection and quality control. If a 3D scanning technology is capable of collecting a high quantity of 3D data from the scanned object, it has the ability to recreate a high resolution, accurate 3D digital model of the real object. (LMI Technologies, 2013)

In order to obtain a model with these characteristics it is required to use a 3D scanner which is a device for creating high resolution, accurate digital 3D models. The scanner is built around stereo-vision (normally two digital imagers) and structured light projection in order to generate 3D. The scanner is controlled by 3D scanning software that runs on a computer. A 3D scanner is also capable of capturing the colour map of an object. By merging the colour map onto the 3D model, a colour 3D digital model is created. The purpose of a 3D scanner is usually to create a point cloud of geometric samples on the surface of the subject. These points can then be used to extrapolate the shape of the subject which is a process called reconstruction.

A 3D sensor is a single device that uses fixed optics, a light source (typically laser) and at least one digital imager to acquire 3D data. Typically 3D sensors are pre-calibrated and operate in manufacturing facilities as part of an automated production line. The 3D sensor only gathers the functions of collecting and transmitting the data for processing. An external computer or controller takes in the data the 3D sensor generates and processes it to perform measurements, analysis, or visualisation.

There are a variety of technologies for digitally acquiring the shape of a 3D object which were developed over time. A well-established classification divides them into two types: contact and non-contact. The non-contact technologies are time-of-flight, triangulation, conoscopic holography, hand-held lasers, structured light, modulated light and volumetric techniques.

Contact 3D scanners probe the subject through physical touch, while the object is in contact with or resting on a precision flat surface plate, ground and polished to a specific maximum of surface roughness. When the object to be scanned is not flat or cannot rest stably on a flat surface, it is supported and held firmly in place by a fixture. The scanner of this mechanism may have different forms.

In the non-contact methodologies, it is integrated the triangulation in which a limited set of angles and lengths of a triangle are determined in order to, mathematically, find the values of the unknowns. This is the principle that enables 3D scanning technologies to determine the dimensions and geometry of the real components. Triangulation is used by both single camera and multiple camera (stereo-vision) devices. For 3D scanning technologies, the distance and angles between imagers and the projected light source (laser) creates a base of the triangle. The

angle of the projected light returning to the imager from the surface completes a triangle where a 3D coordinate can be calculated. By applying this principle of solving triangles repetitively, a 3D representation of an object is created, as it is presented in figure 21.

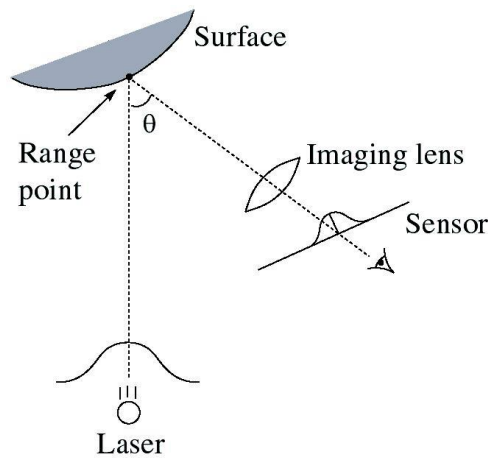


**Figure 21** - Principle of Triangulation Technology (LMI Technologies, 2013)

All these methods use 3D scanners to collect distance information about surfaces within its field of view. They differ somehow in the way they capture the position of the points which will constitute the final model of the part. The picture produced by the 3D scanner describes the distance to a surface at each point. This allows the three dimensional position of each point to be identified which enables the creation of the 3D model of the component.

For most situations, a single scan will not produce a complete model of the subject. Multiple scans, even hundreds, from many different directions are usually required to obtain information about all sides of the subject. These scans have to be brought into a common reference system, a process that is usually called alignment or registration, and then merged to create a complete model. This whole process, going from the single range map to the whole model, is usually known as the 3D scanning pipeline. (LMI Technologies, 2013)

“Science never solves a problem without creating ten more.”

George Bernard Shaw

## 4. INDUSTRIAL APPLICATION

The system which will be described and studied in this chapter entered into the market in a recent past. Due to the benefits it presents, its development and production have reached a rapid pace and, the industry is increasingly interested in investing in this type of navigation systems. There are a wide variety of these components being commercialised all over the world as they represent the newest and innovative structures being incorporated in cars.

The analysed components are constituted by different kinds of polymers and it is important to mention that their unique characteristics are also being improved with new advancements, whether in terms of materials or of processing. This is one of the reasons which is contributing so that plastic gears are continuously displacing metal gears in a widening arena of applications. The fact is that metallic materials and processes present a much higher level of development, contrary to what happens to the plastic ones.

This chapter is constituted by 2 sections being the first related to the presentation of the component, where will be described the different parts of it, the specifications it has to comply and the analyses executed on the elements. The second is about the numerical simulations performed during this dissertation, in which, initially it will be detailed some considerations, followed by the full description of the studies and, finally, there is the comparison of the results.

### 4.1. PRESENTATION AND STUDY

In the first subsection of chapter 4, it is presented the component it is being analysed. This product has been developed by Bosch and produced in Braga. Characteristics related to the device are exposed and some explanations are made in order to clarify the subject. It is also described the components that constitute the assembly and the specifications required by the client. Next, it is performed an kinematic and a dynamical analysis with the purpose of having some notion of the velocities involved and the forces applied in the system. Lastly, it is estimated the efficiency of the assembly of gears.

#### 4.1.1. Description of the Navigation System C-HUD

A head-up display (HUD) is any display of instrument readings in an aircraft or vehicle that can be seen without lowering the eyes, typically through being projected on to the wind-screen or on a particular component designed for this purpose.

The origin of the name comes from the fact that the pilot or the driver is able to view all the data he needs with the head positioned up and looking forward, instead of angled down looking at lower instruments, which means, it is not required for users to look away from their usual points of view.

Although they were initially developed for military aviation, this category of displays is presently being extensively used in commercial aircraft, automobile industry and others, mostly in professional applications. The head-up display allows the driver to visualise a variety of information such as current speed, fuel consumption, GPS directions, warnings, time and others without changing their frequent range of view.

Head-up displays are, nowadays, increasingly being included into more compact car models. This type of system can be fully integrated in the instrument panel in front of the driver.

As the information is projected directly in the driver's field of vision, the displayed instructions appear as if they were hanging in front of the vehicle. This has the advantage of soothing the driver's vision since the eyes have to refocus less frequently and the driver has the possibility of concerning only with what is happening on the road (BMW Technology Guide: Head-Up Display; England, 2014).

#### **Combiner Component**

There are essentially three types of head-up displays: AR-HUD (augmented reality), Box-HUD and, finally, C-HUD (figure 22). The latter is the only important within the theme, in

which the most important differences among them are related to how the image is shown to the driver. The system C-HUD stands for combiner head-up display which has been developed at Bosch. The image it generates, which offers quality and precision, is connected with the scenario outside the vehicle and it seems that they consolidate with one another at a distance of approximately two meters in front of the car.



**Figure 22** – Unit of Head-Up Display (Bosch Car Multimedia, 2014)

The system does not project the information onto the windshield but instead onto a small special plastic screen placed before it called combiner, as it is shown in figure 23. The new head-up system is therefore completely self-sufficient and can be fitted to various types of vehicle without any considerable technical modification necessary.



**Figure 23** – Representation of Combiner Head-Up Display (Bosch Car Multimedia, 2014)

One of the quality characteristics of this new system is that the displayed information remains sharp and distortion-free even when the driver changes his position. This is achieved through the sophisticated optical integration of all elements of the system. The aspheric surface of the plastic combiner screen is one of its technical highlights and there is also the possibility

to adjust the component by 3 degrees to both sides.

The tolerance specified for the front surface is extremely tight. The edge of the screen has been milled in a certain way to make it level with the driver's line of sight. Thus, as it becomes invisible to the driver, it causes the displayed information to merge with the background. The rear side has an anti-reflective coating and the surface is unusually scratch-resistant.

The plastic combiner screen is driven by a variable-speed electric motor to extend it out of the box when needed. When the system is switched off, the screen fully retracts into the box and the whole component becomes hidden inside the panel (Bosch Car Multimedia, 2014).

#### **More Safety and Comfort for the Passengers**

The new display comprises an imaging unit and a display unit. The imaging unit is equipped with a full-colour liquid crystal display (LCD) with a resolution of 480 by 240 pixels. Similar to a photographic slide, it is lit by a single light emitting diode with a high light intensity. The light signal bounces via folding mirrors to the display unit, whose key component is the combiner screen. This projects the image into the region in which the driver's eyes are situated, called eye box.

The angle of the combiner screen can be fine-tuned to suit the driver's height, and the brightness of the displayed information is adjustable by way of sensors or a dimmer wheel. The main goal of the new head-up display is to ease people's lives and so make car driving even safer and more comfortable (Bosch Car Multimedia, 2014; Technical Drawings of the Combiner Head-Up Display).

#### **Disassembly of the System**

The system Combiner Head-Up Display is constituted by several components which are shown in figure 24.

Firstly, there is the structure where the pieces are allocated called central carrier and the housing top unit is the part that covers all the others and enables closure. The format of the central carrier is complex as there are several components that will fit in it and also due to the necessity of fulfilling the requirements for the measures. Next, there is the combiner, which was explained previously, where the image is projected. The surface of this component is very important and requests delicacy when managed. This is caused by the fact that it is extremely sensitive and every small damage can lead to the malfunctioning of the device and, consequently, being rejected.

In terms of optics, there is the picture generator unit (PGU) which is responsible for creating the image and then, there is the light bezel unit whose narrowed shape guides the light to the combiner and prevents it from dispersing. These parts have to be mounted and assembled to the central carrier in a clean room because no particle of dust can incorporate in any of these pieces. Otherwise, there is the possibility of creating damage in the image such as distortion, rotation and changing of dimensions in length or height. Besides that, the projected image could be diverted from the place it is specified to be by the client which is, as the others, a situation to avoid.

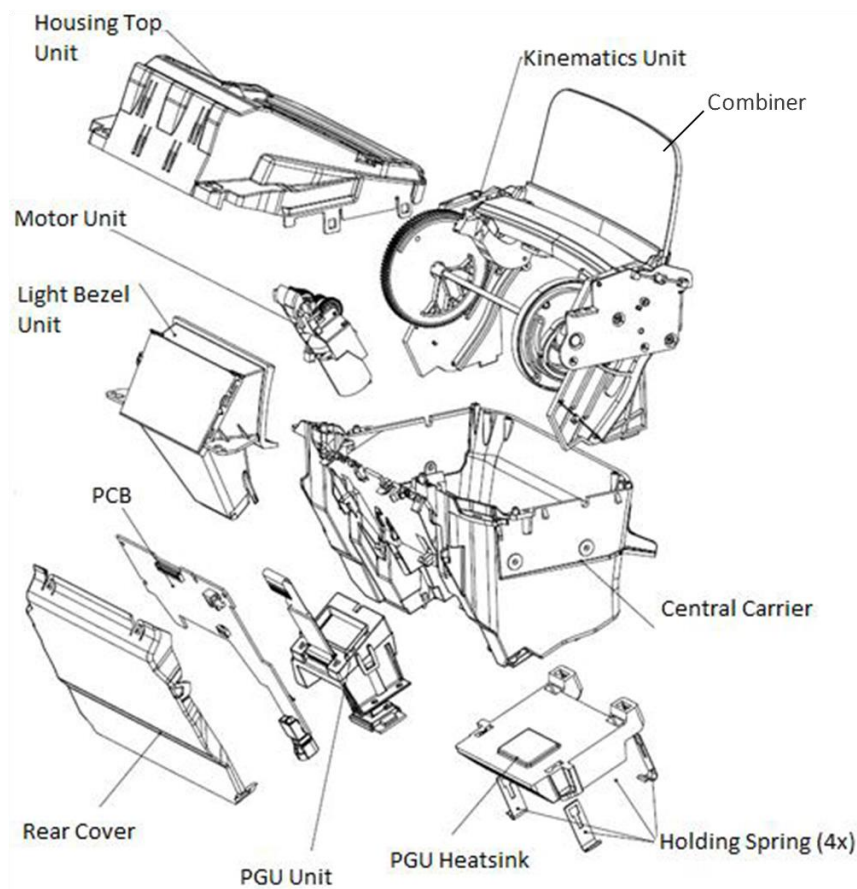


**Figure 24** - Components of C-HUD (Technical Drawings of the Combiner Head-Up Display)

Furthermore, there is a component called heatsink which is attached to the exterior part of the central carrier close to the PGU as this component reaches very high temperatures. Thus, it is necessary to dissipate the heat that comes from the PGU in order to decrease the temperature inside the central carrier. The heatsink is fixed to it using 4 holding springs.

In addition, the printed circuit board (PCB) mechanically supports and electrically connects components that will conduct the programmed information to the head-up display. This element has also to be assembled in the clean room due to the sensibility of the electrical components. It is also used a rear cover to protect all the parts from contamination.

Finally, it is essential to explain what the kinematics unit is, as this is the component it will be studied throughout this entire project. This set is constituted by various pieces but only the gears will be analysed in detail. This component will be described meticulously in the next subchapter. The motor unit is the responsible for promoting the movement of this system and it is connected to one of the gears (Bosch Car Multimedia, 2014; Technical Drawings of the Combiner Head-Up Display).

#### 4.1.2. Specifications of the Kinematics

This document describes the technical requirements for the kinematic module used in the automotive component Combiner Head-Up Display (C-HUD).

The kinematic module is part of C-HUD and consists of a frame unit, a combiner system (without the combiner) and a motor assemblage. The combiner system is fixed on the frame entity and both the motor and frame units are mounted in the central carrier (structure of the component). Kinematic module is driven by a DC motor which must be axially supported in order to control the axial forces and balance the axial play.

In figure 25 it can be seen the components that incorporate the kinematics module presented before.

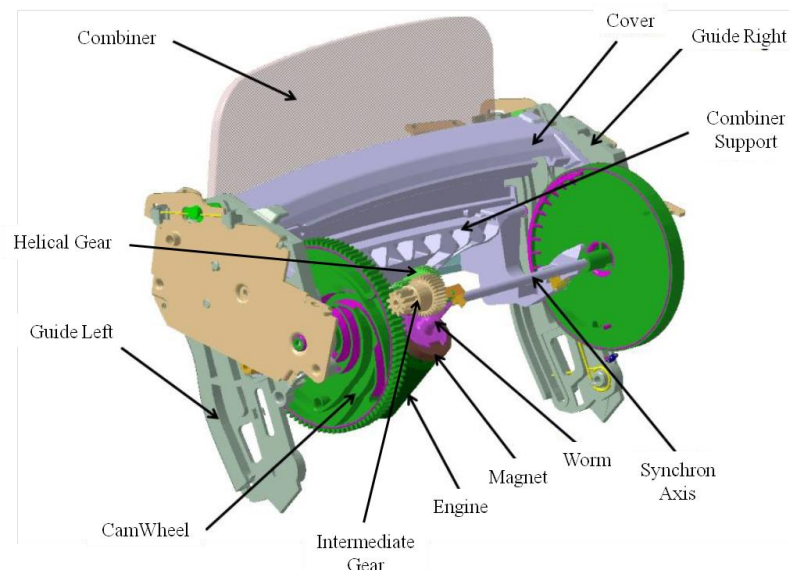


**Figure 25** - Components of the Kinematics Module

The main tasks of kinematic module are moving the combiner out from inside the structure to a service position and then, adjust the operating angle of the combiner. While the head-up display is functioning, the kinematic assembly must, also, hold the combiner in the operating position effectively. Afterwards, it should retract the combiner to a rest position and keep the unit there until the car is working again.



The angle of the combiner must be adjustable in the operating position to fulfil optical requirements. The adjustment around the rotation axis of the combiner unit is from  $-3^\circ$  to  $+3^\circ$  being the step of  $0.6^\circ$ . The specifications for this system indicate that it should function at a minimum temperature of  $-40^\circ$  and a maximum of  $90^\circ$  as well as that its lifetime is of 30000 cycles (Bosch Car Multimedia, 2014).

Although the kinematic module is incorporated by several components, only some will be analysed during this project. On the left side of the figure there is a system of 4 parts which is consisted by a camwheel, an intermediate gear, a wormwheel and a worm. This last element is connected to an engine which provides the movement necessary for the entire system to function. This train of gears can be classified of normal due to all the shafts that support the gears are fixed; it can also be called of compound, as there is more than one gear in, at least, one of the shafts. This mechanism is also a nonreverted system because the axes of the first and last gears are not co-axial which means that the input and output velocities do not share the same direction (Rao & Dukkupati, 1992; Flores & Gomes, 2015).

Next, it is displayed figure 26 in which it is possible to inspect closely the characteristics of this group of gears.

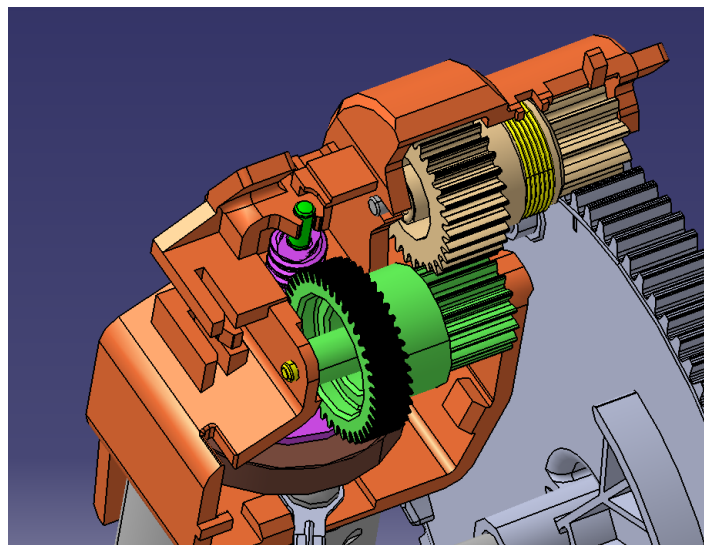


**Figure 26** - Kinematics System

The kinematics system includes 4 different pieces and more specifically 4 spur gears, a helical gear and a worm. Spur gears are the most common type used as they have high power transmission efficiency, they are compact and easy to install and they have the capability to transmit large quantities of power. However, when operated at higher speeds, they can produce much noise. As an alternative, there are helical gears which can be used in situations where it is necessary to transfer power between non parallel shafts although efficiency is compromised

in this case. In addition, they produce less noise as the teeth engage a little at a time rather than the entire face at once. Also, helical gears are able to endure more load than spur gears due to the helical gear tooth is effectively larger since it is diagonally positioned. At last, worm gears have the advantage of occupying less space, they operate silently and smoothly and they are suitable to increase torque or reduce speed. On the other hand, worm drives have high power losses and low transmission efficiency, their materials are expensive and they produce high quantities of heat during their operation (Childs, 2013; Budynas & Nisbett, 2014).

Next, there is figure 27 which presents gear characteristics in order to clarify the difference between them. As you can see, there are 4 types of diameters: external, pitch, internal and root.

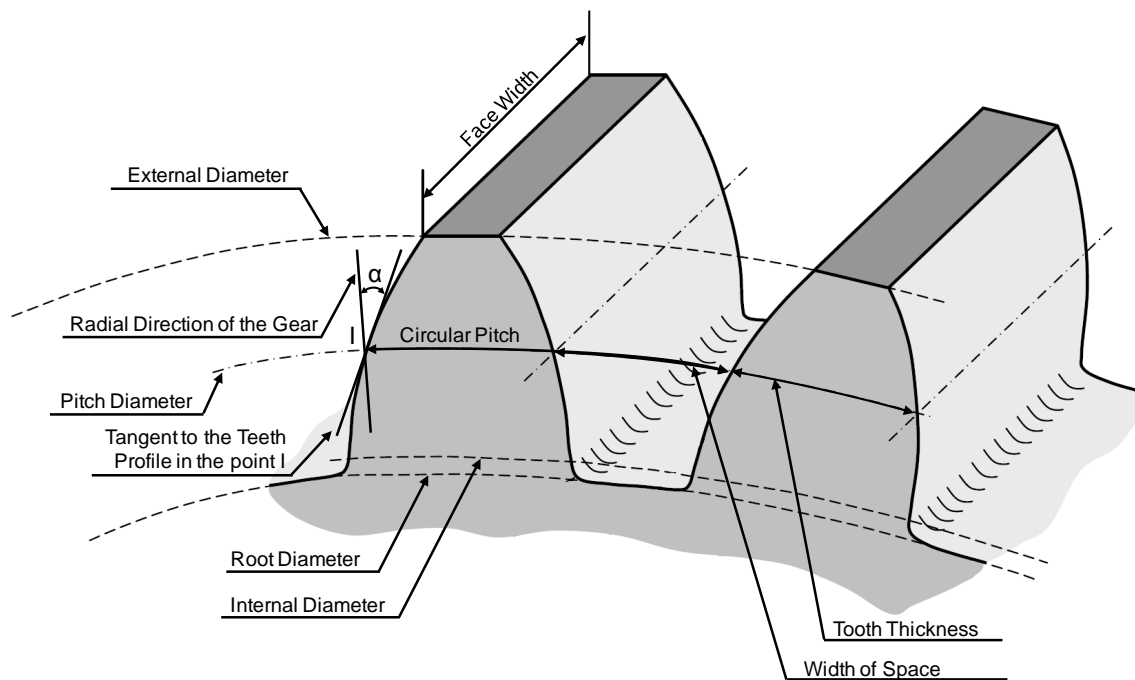


**Figure 27** - Nomenclature of Gears

These dimensions are used to draw the shape of the teeth according to the height and thickness the engineer wants them to have. In addition, the pitch diameter creates the pitch circle which is responsible for establishing the contact among the teeth of mating gears. The circular pitch is the sum of the tooth thickness and the width of space and can also be defined as the length measured along the pitch circle between two identical points on contiguous teeth. Next, there is the face width which is the dimension of the teeth in an axial direction. At last, the acute angle formed by the tangent to tooth profile in the primitive point (I) and by the radius of the gear in the same point is called the pressure angle. This angle defines the direction of the force that the driver gear practices over the driven one (Childs, 2013; Rao & Dukkipati, 1992).

In table 3 it is presented some important information related to the gears. These characteristics define the components which enable us to understand in a better way the type of elements that are part of the system which will be studied hereinafter.

**Table 3** - Characteristics of Gears

	Gear 1 (Worm)	Gear 2	Gear 3	Gear 4	Gear 5	Gear 6
Number of Teeth	2	41	18	31	10	95
Module (mm)	0.4	0.4	0.5	0.5	0.8	0.8
Pressure Angle (degree)	16	16	19	19	15	15
Root Diameter (mm)	2.39	15.11	7.80	13.80	6.56	73.12
Base Diameter (mm)	3.41	15.99	8.51	14.66	7.73	73.41
Pitch Diameter (mm)	4.61	16.65	9.00	15.50	8.00	76.00
Outside Diameter (mm)	5.57	17.28	10.40	16.40	10.40	76.96
Circular Pitch (mm)	1.26	1.26	1.57	1.57	2.51	2.51
Face Width (mm)	-	4.0	8.4	6.6	7.5	7.7
Width of Space (mm)	0.69	0.69	0.68	0.91	1.04	1.56
Tooth Thickness (mm)	0.57	0.57	0.89	0.66	1.47	0.95
Material	POM Asahikasei Z4520	PBT Poly- plastics 2002K	PBT Pol- yplastics 2002K	POM Mitsubishi engineer- ing plas- tics FX- 11JR1	POM Mitsubishi engineer- ing plas- tics FX- 11JR1	POM Asahikasei ZLV40

Through the analysis of the table, it is possible to conclude that there are 3 meshes in the system, as there are 3 different values of modules and pressure angles. It is important to refer that the normalised value for the pressure angle is  $20^\circ$ , whereas in these cases were used  $15^\circ$ ,  $16^\circ$  and  $19^\circ$ . This means that the base thickness of the tooth is small in proportion to the other tooth dimensions and, therefore, they do not have the strength to support heavy loads. This does not constitute a problem due to the fact that it was not one of the system specifications. In

addition, components with smaller pressure angles provide extensive uses and also higher contact ratio and consequent smoother and more silent operation (Engineering Information, s.d.).

#### 4.1.3. Kinematic and Dynamic Analysis

In this section it will be made 2 types of analysis to the mechanism in order to clarify how this system works. The first is related to the angular velocity at which the gears rotate and the second will analyse the forces applied in each part of the mechanism. The efficiencies of the 3 gearing system as well as the one of the total assembly will also be calculated.

#### Kinematic Analysis of the System

Through the analysis of the d. c. motor's datasheet (included in the appendix A), it is known that the maximum number of revolutions per minute is 4717. That means this is also the speed of gear 1 (worm) as it is the one connected to the motor. As it can be visualised in figure 28, the movement is transmitted from the right to the left since gear 1 until 6.

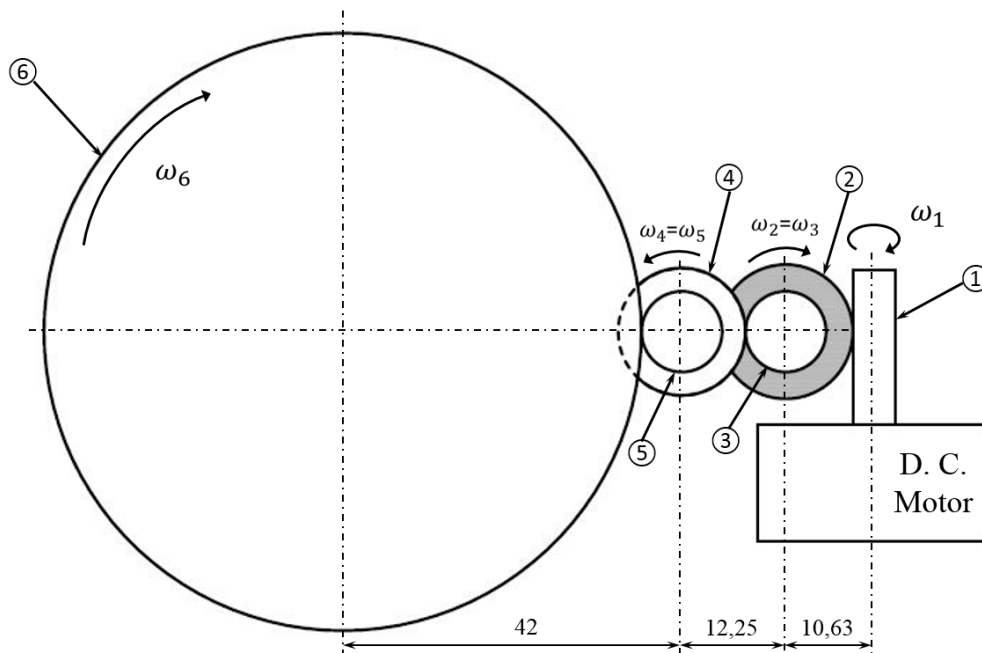


Figure 28 - Representation of the Train

With this information, it is possible to calculate the angular velocity of the exit gear ( $\omega_6$ ) of the system using the number of teeth ( $Z_n$ ) of all the components (Maitra, 2010). With that said:

$$\begin{aligned} \omega_6 &= \frac{\prod \text{number of teeth of the driven gears}}{\prod \text{number of teeth of the driver gears}} \times \omega_1 = \frac{Z_1 \times Z_3 \times Z_5}{Z_2 \times Z_4 \times Z_6} \times \omega_1 \\ &= \frac{2 \times 18 \times 10}{41 \times 31 \times 95} \times 4717 = 17 \text{ rpm} \end{aligned} \quad (4.1)$$

Next, it is possible to calculate the transmission ratio ( $i$ ) of the mechanism with the information obtained previously (Maitra, 2010). So:

$$i = \frac{\omega_1}{-\omega_2} \times \frac{-\omega_2}{-\omega_3} \times \frac{-\omega_3}{\omega_4} \times \frac{\omega_4}{\omega_5} \times \frac{\omega_5}{-\omega_6} = (-) \frac{\omega_1}{\omega_6} = (-) \frac{4717}{17} \cong (-)278 \quad (4.2)$$

The transmission ratio of this assembly of gears presents a high value due to the difference of size between the entrance and exit gears. The minus sign only represents that the considered gears have different directions of rotation.

In order to perform a more complete analysis, the angular velocities of gears 2 and 4 are calculated knowing that the product of the angular velocity by its number of teeth is equal in mating gears, which means that:

$$\omega_2 \times Z_2 = \omega_1 \times Z_1 \quad (4.3)$$

Hereupon:

$$\omega_2 = \frac{Z_1}{Z_2} \times \omega_1 \Leftrightarrow \omega_2 = \frac{2}{41} \times 4717 \Leftrightarrow \omega_2 = 230 \text{ rpm} \quad (4.4)$$

and

$$\omega_4 = \frac{Z_3}{Z_4} \times \omega_3 \Leftrightarrow \omega_4 = \frac{18}{31} \times 230 \Leftrightarrow \omega_4 = 113.5 \text{ rpm} \quad (4.5)$$

To conclude this section, it is presented all the velocities in table 4 with the values calculated before.

**Table 4 - Gear Speed**

Gear	Speed
1	$\omega_1 = 4717 \text{ rpm}$
2	$\omega_2 = 230 \text{ rpm}$
3	$\omega_3 = \omega_2$
4	$\omega_4 = 113.5 \text{ rpm}$
5	$\omega_5 = \omega_4$
6	$\omega_6 = 17 \text{ rpm}$

Through the analysis of the table, it is important to refer that the speed is decreasing as you progress along the mechanism. This can be explained by the fact that the number of teeth increases in all engagements as well as the size of the components.

### Dynamic Analysis of the System

To analyse dynamically the system, it is necessary to study the 3 gearing systems that constitutes it. The first is established between gears 1 and 2, which is the worm and a helical gear. The second mating system is represented by gears 3 and 4 while the third gear aggregation is compound by gears 5 and 6, all of those are spur gears. Next, these explanations will be presented in this order.

To calculate the forces applied on the worm as well as on the helical gear, it is required to know the pressure angle  $\alpha_n$  of the assemblage, which is  $16^\circ$ , the worm pitch diameter of value 4.61 mm, and the lead angle  $\beta$  of the worm teeth (Flores & Gomes, 2015; Maitra, 2010). To discover this value, consider figure 29:

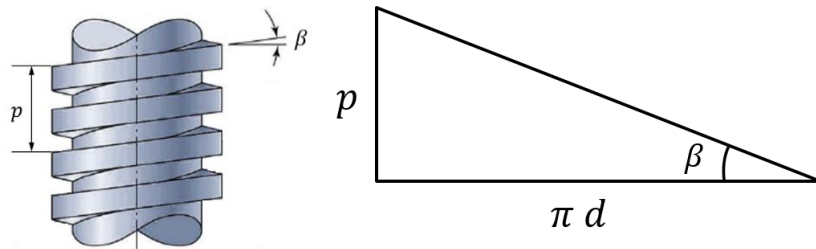


Figure 29 - Lead Angle of a Worm

The triangle shows that the pitch ( $p$ ) is the length the worm travels on a turn between 2 similar and consecutive points, which is 2.52 mm. The other cathetus represents the perimeter of a circle ( $\pi \times$  diameter of gear 1) which is the space between the same points. In order to know the angle ( $\beta$ ), and after analysing the presented geometry, it is said that:

$$\beta = \tan^{-1}\left(\frac{p}{\pi \times d_1}\right) = 9.87^\circ \cong 10^\circ \quad (4.6)$$

In figure 30, it is presented the forces which act on a worm. There is the total force and the 3 components on the 3 axes which it is constituted by. The angles previously referred are also represented.

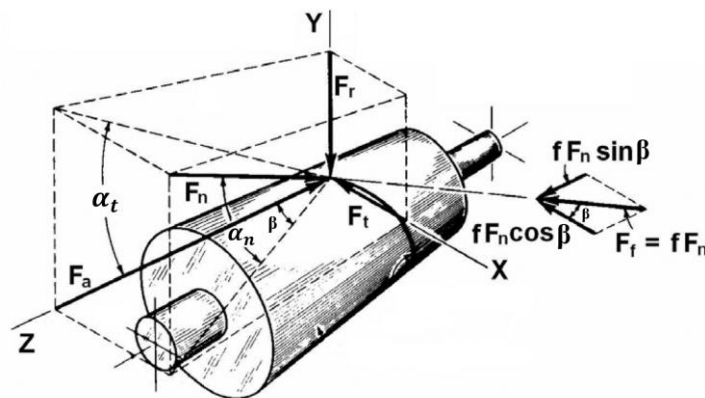


Figure 30 - Forces Applied on a Worm Gear (Gopinath & Mayuram)

According to the motor datasheet, which can be inspected on appendix A, the power transmitted from it to the worm (P) takes the value of 0.81 W. The angular velocity of gear 1 was studied before and it is 4717 rpm. With that said, it is possible to determine the tangential component of the force ( $F^t$ ) which is the one responsible for transmitting power (Flores & Gomes, 2015; Maitra, 2010).

$$F^t = \frac{60 P}{\pi \times d_1 \times \omega_1} = 0.71 \text{ N} \quad (4.7)$$

Next, it is presented the equation to estimate the total force ( $F$ ), using the value obtained in the expression 4.7. It is important to refer that these calculations are taking into consideration the friction existing between the components. Therefore, the coefficient used for the interface of gears 1 and 2 ( $f_{12}$ ) which are constituted by the materials POM and PBT, respectively is 0.18. The term  $\alpha_n$  represents the pressure angle and assumes the value of  $16^\circ$ .

$$F^t = 0.71 \Leftrightarrow F(\cos \alpha_n \times \sin \beta + f_{12} \cos \alpha_n) = 0.71 \Leftrightarrow F = 2.06 \text{ N} \quad (4.8)$$

With all the known values, achieved through the preceding expressions, it is simple to calculate the radial ( $F^r$ ) and axial ( $F^a$ ) components of the force.

$$F^r = F \sin \alpha_n = 0.57 \text{ N} \quad (4.9)$$

$$F^a = F(\cos \alpha_n \times \cos \beta - f_{12} \sin \beta) = 1.89 \text{ N} \quad (4.10)$$

Finally, it is essential to understand the efficiency of the worm gear ( $\eta_{12}$ ) whereby it is used the formula 4.11 to determine it.

$$\eta_{12} = \frac{\cos \alpha_n - f_{12} \tan \beta}{\cos \alpha_n + f_{12} \cotan \beta} \times 100 = 46.9 \% \quad (4.11)$$

As it was said before, worms present worse performances than spur gears when it comes to transmit power, due to the slipping it occurs during the process, as it can be concluded by the low percentage of 46.9 (Childs, 2013).

In the next case, the gearing system is constituted by spur gears and, therefore, the applied forces are presented in figure 31. This figure is used to clarify the components it will be calculated and the variables it is being considered (Flores & Gomes, 2015; Maitra, 2010).

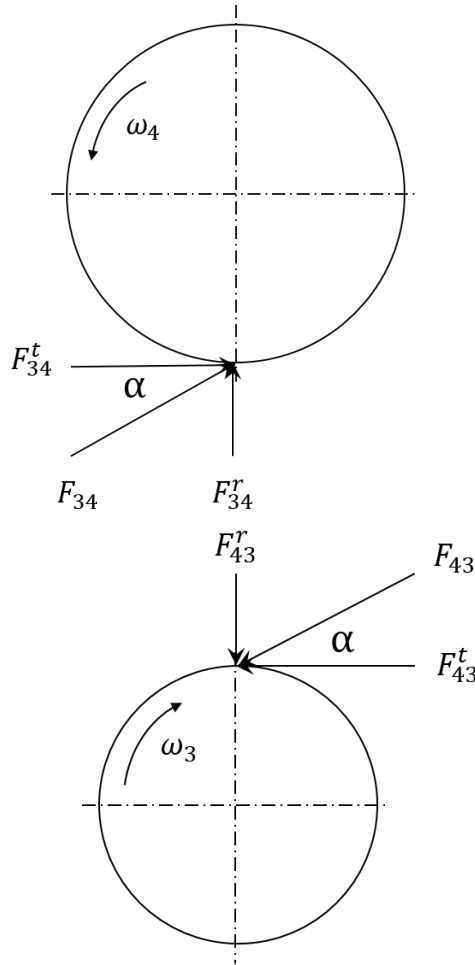


**Figure 31** - Forces Applied on Spur Gears

From the previous result, it can be calculated the power that gear 3 receives from the worm, named  $P_1$ . For that, the efficiency and the last known value for power are substituted in the expression 4.12.

$$P_1 = \eta_{12} \times P = 0.38 \text{ W} \quad (4.12)$$

Like the preceding case, the tangential component of the force is the first to be determined for gear 3 ( $F_{34}^t$ ), knowing that its pitch diameter ( $d_3$ ) is 9 mm and the angular velocity ( $\omega_3$ ) is 230 rpm.

$$F^t = F_{34}^t = \frac{60 P_1}{\pi \times d_3 \times \omega_3} = 3.51 \text{ N} \quad (4.13)$$

From the geometry of the figure, it can be deduced the expression for the radial component of the total force. It is important to mention that, in this case, the pressure angle ( $\alpha_n$ ) assumes the value of  $19^\circ$ .

$$F_{34}^r = F_{34}^t \times \tan \alpha_n = 1.21 \text{ N} \quad (4.14)$$

To know the magnitude of the total force, it has to be calculated the root of the sum of



both squared components which result in 3.71 N.

$$F_{34} = \sqrt{(F_{34}^t)^2 + (F_{34}^r)^2} = 3.71 \text{ N} \quad (4.15)$$

The efficiency of this contact ( $\eta_{34}$ ) is estimated using the expression 4.16. For that, it is used the coefficient of friction for the interface POM-PBT ( $f_{34}$ ) which is 0.18 and the pitch diameter of gear 4 which is 15.5 mm.

$$\eta_{34} = 1 - \frac{f_{34}}{\cos \alpha_n} \times \left( \frac{1}{d_3} + \frac{1}{d_4} \right) \times \frac{l_a^2 + l_r^2}{l_a + l_r} \times 100 \quad (4.16)$$

For this calculation, it is necessary to determine the length of approach ( $l_a$ ) using the addendum of gear 4 ( $h_{a4}$ ) which is the radial distance between the pitch diameter and the outside diameter and assumes the value of 0.45 mm.

$$l_a = \sqrt{(r_4 + h_{a4})^2 - r_4^2 (\cos \alpha_n)^2} - r_4 \times \sin \alpha_n = 1.16 \text{ mm} \quad (4.17)$$

In the same way, it is estimated the length of recess ( $l_r$ ) using the addendum of gear 3 ( $h_{a3}$ ) which is 0.7 mm.

$$l_r = \sqrt{(r_3 + h_{a3})^2 - r_3^2 (\cos \alpha_n)^2} - r_3 \times \sin \alpha_n \quad (4.18)$$

With this information, it is possible to discover the efficiency value which is, approximately, 96.41 %. That level of performance is normal in spur gears, which usually present high values of efficiency (Flores & Gomes, 2015).

The next case is also related with spur gears whereby the same procedure is followed. The representation of forces previously shown is also admitted in this situation. With that said, the new value of power ( $P_2$ ) is calculated.

$$P_2 = \eta_{34} \times P_1 = 0.37 \text{ W} \quad (4.19)$$

The pitch diameter of gear 5 is 8 mm and the angular velocity  $\omega_5$  takes the value of 113.5 rpm.

$$F^t = F_{56}^t = \frac{60 P_2}{\pi \times d_5 \times \omega_5} = 7.71 \text{ N} \quad (4.20)$$

The radial component of the force can be determined through equation 4.21, having the knowledge that the pressure angle for this case is  $15^\circ$ .

$$F_{56}^r = F_{56}^t \times \tan \alpha_n = 2.07 \text{ N} \quad (4.21)$$

Therefore, the magnitude of the total force can be calculated as before.

$$F_{56} = \sqrt{(F_{56}^t)^2 + (F_{56}^r)^2} = 7.98 \text{ N} \quad (4.22)$$

The efficiency of the connection can be estimated using the coefficient of friction between materials POM-POM ( $f_{56}$ ) which is 0.28. It is important to refer that the pitch diameter of gear 6 is 76 mm.

$$\eta_{56} = 1 - \frac{f_{56}}{\cos \alpha_n} \times \left( \frac{1}{d_5} + \frac{1}{d_6} \right) \times \frac{l_a^2 + l_r^2}{l_a + l_r} \times 100 \quad (4.23)$$

Similarly to the previous situation, it is necessary to calculate the lengths of approach and recess using expressions 4.24 and 4.25. For that, it is required to know  $h_{a5}$  and  $h_{a6}$  which is 1.2 mm and 0.48 mm, respectively.

$$l_a = \sqrt{(r_6 + h_{a6})^2 - r_6^2 (\cos \alpha_n)^2} - r_6 \times \sin \alpha_n = 1.72 \text{ mm} \quad (4.24)$$

$$l_r = \sqrt{(r_5 + h_{a5})^2 - r_5^2 (\cos \alpha_n)^2} - r_5 \times \sin \alpha_n = 2.44 \text{ mm} \quad (4.25)$$

With these values, the efficiency  $\eta_{56}$  can be calculated and it is, approximately, 91.41 %. This number is considerably high as the gear teeth are parallel to its axis. Hence, spur gear train does not produce axial thrust (Maitra, 2010).

Finally, it is possible to determine the efficiency of the whole assembly ( $\eta_T$ ). For that, it will be used an expression where the 3 efficiencies previously calculated will be multiplied. The result of that is:

$$\eta_T = \eta_{12} \times \eta_{34} \times \eta_{56} = 0.4133 = 41.33 \% \quad (4.26)$$

Facing this value, it is simple to conclude that most of the power transmitted by the engine is lost in the first stage due to the low performance of the worm gear.

## 4.2. NUMERICAL SIMULATIONS

In this subsection of chapter 4 it will be presented the total procedure followed in order to perform the simulations of this dissertation. Initially, there are some considerations to be defined and explained such as the assembly used in the work, the materials and contacts, among others. Then, the second issue is related to the validation of the software where some simple experiments are executed on ANSYS in order to conclude the influence that material properties have on the results. Consequently, it will be taken into consideration the total assembly with the purpose of performing thermal simulations using Steady-State Thermal module of ANSYS. Next, it is performed an intensive study on the bigger gear, using both fluid-structure interface

and thermal-stress simulations, using 2 different processes of heating the component. It is also tested how this piece would behave if it was constituted of another material. Thereupon, the study includes the 6 gears to execute thermal-stress simulations with the view to inspect how the components behave when facing very high temperatures. Finally, these results of the simulations are compared and analysed. All the outcomes are evaluated according with the objectives of the simulations.

#### 4.2.1. Initial Considerations

##### **Assembly in Study**

In the previous subsection were presented the real components which will be studied and analysed along this dissertation. The company responsible for producing and supplying these parts to Bosch is Pioneer Corporation. They provided the 3D models, however, there was no possibility to change them which obliged to perform an intensive and prolonged work of drawing the components from the beginning. Using the software NX 7.5. (NX, 2015), the gears were modelled one by one having those which were delivered as a basis. With that said, the required measures to design as lengths, depths, angles, among others were consulted on the provided files. Next, the assembly was created with the designed pieces employing all the constraints necessary to position them correctly with respect to each other.

Moving to the software ANSYS, it was detected that the elements are very complex, containing several peculiarities which turned the model very heavy and, in these conditions, it would be difficult to simulate regarding the size of the files as well as the processing time. Consequently, after realising that some features of the gears are not important for what it is being investigated, they were simplified using the ANSYS DesignModeler software. It provides unique modelling functions for simulation which includes several tools to geometry repairing, CAD geometry modification and diverse custom tools designed for fluid flow, structural and other types of analyses. With these means, some errors resultant from the modelling were detected and corrected for example, discontinuities, deformed shapes, lacks of material, etc. The components were sliced in order to apply different meshes to the gear teeth and the remaining piece, which means that it was used different element sizes on the portions according to the required refinement. In addition, some other changes were made having in mind these could not influence the results in any way. The main concern was to keep the format and size of the components intact. Next, the simplified components are presented and some details are inspected.

In figure 32, it can be seen the outsider part of the assembly where there is the central

carrier and the heatsink. These components were included in the ensemble as the box is important to limit the area of influence of the air and encloses it. In terms of the dissipator, it helps the heat to come outside of the central carrier and turns the simulation more realistic. The measures of central carrier are 218×167×152 mm and the ones for heatsink are 98×75×22 mm, which is constituted by 17 fins.

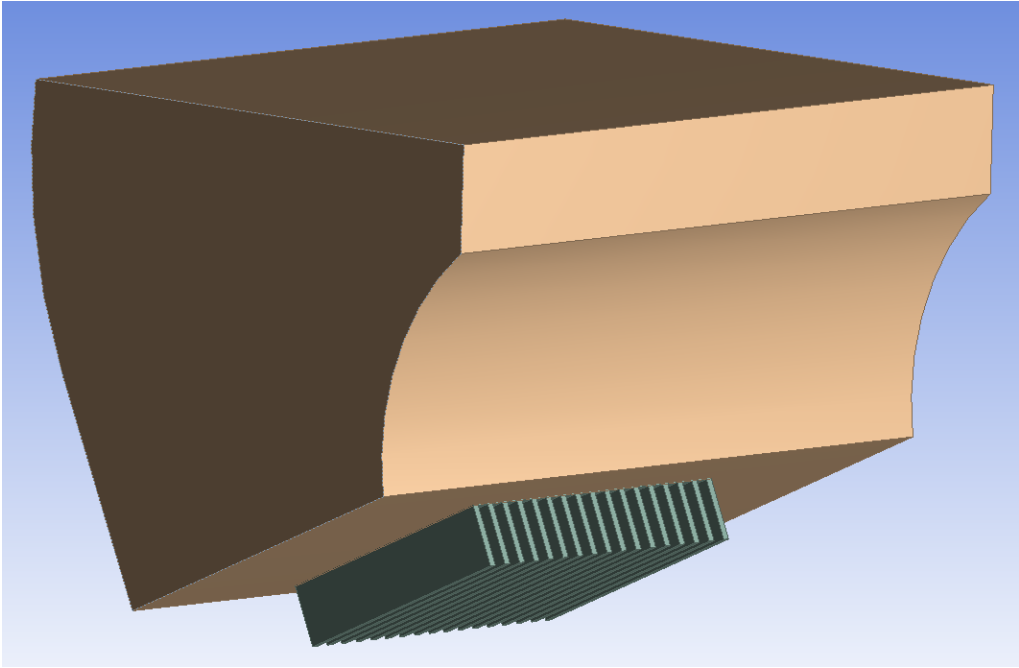


Figure 32 - Assembly in Study

In figure 33 the central carrier was removed and the inside can be inspected. The heatsink is in contact with a PCB (printed circuit board) which, in turn, establishes a connection with PGU (picture generator unit). The dimensions of the PCB are 45.5×28×1 mm and the PGU is defined by the general measures of 47.5×30×44 mm.

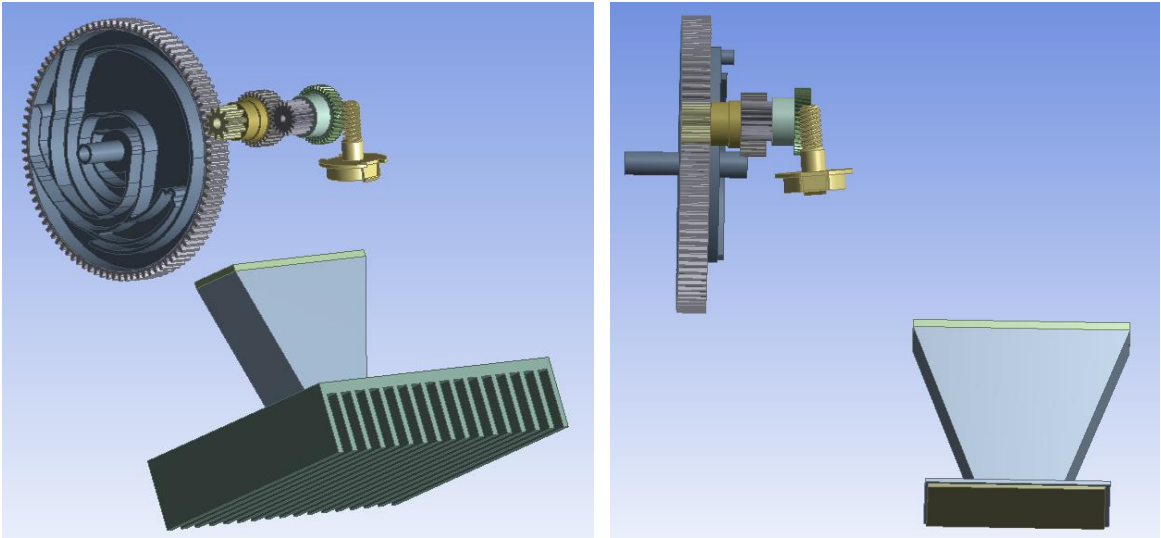
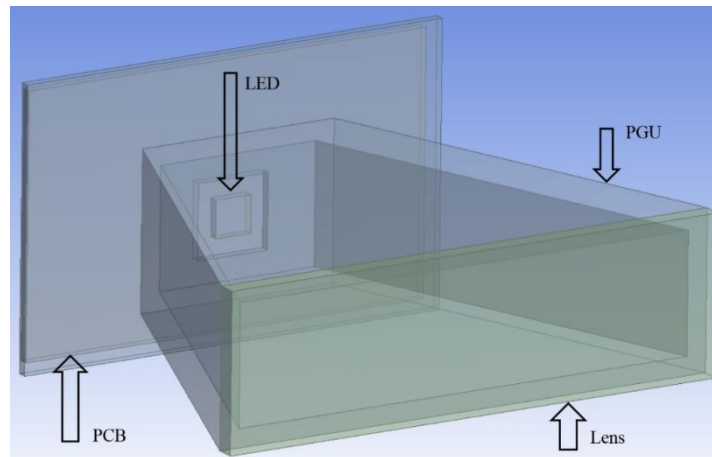


Figure 33 - Parts of the Assembly

As it can be understood from the figures, gears are suspended in the box. From the point of view of the simulations, this fact does not influence the results as the transfer of heat remains the same whether they are fixed or not. Figure on the right is used to clarify the distance between parts as well as the orientation of the components in space.

Next, it is shown more in detail a representation of several pieces with the purpose of clarifying how the system works and how they are all connected (figure 34). The PCB, which is attached to PGU, contains a LED in its middle of dimensions  $4 \times 4 \times 1$  mm. Therefore, this unit is constituted by a board with a hole in its middle, where the LED fits, and a piece with the shape of a funnel. This portion is responsible for transmitting the image from the display until the combiner, where it is reflected. Finally, there is a lens of dimensions  $46.5 \times 17 \times 2$  mm which covers the picture generator unit.



**Figure 34** - View in Detail about Picture Generator Unit

In figure 35, it is displayed a closer view of gears which are 6, but only 4 pieces. There are 2 axes which have 2 gears in it and the number of teeth as well as its dimensions are variable. As it was showed before, the movement is transmitted from the worm (gear 1) until the bigger one (gear 6).

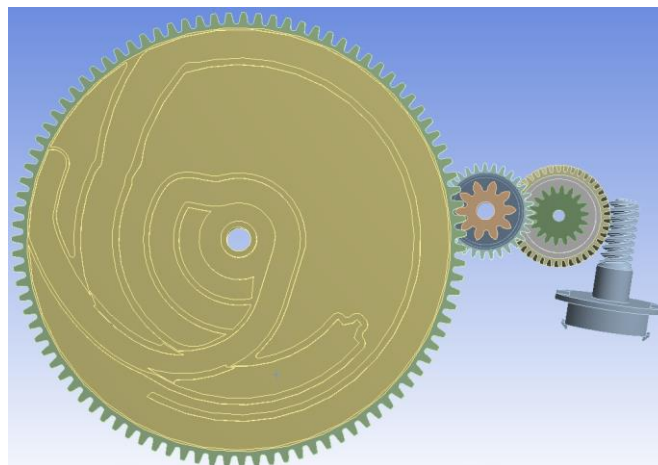


**Figure 35** - Gears of the Assembly

### Materials Presentation

After presenting the components, it is of paramount importance to describe the materials that constitute them. Table 6 contains the materials of all the parts of the assembly which were used to perform the simulations. This information was provided by the material producers in order to use the most accurate data. The density, the thermal conductivity and the specific heat are used in the thermal simulations while the remaining properties are used in the structural simulations in order to estimate the displacements for high temperatures. The properties of air are also important to have in consideration as they will be used in thermal simulations, which will be presented in a following subsection. The viscosity of the air takes the value of  $1.79 \times 10^{-5}$  kg/m.s. For the density, it was used a piecewise-linear model in order to account for the different values of density at different temperatures. As the thermodynamic properties of materials vary with temperature (Yang & Li, 2015; Butaud et al., 2015; Xiao & Nguyen, 2015), it is important to account for temperature variation because in this analysis this effect cannot be disregarded. In table 5 it is presented the adopted values for the density at distinct temperatures.

The last line of table 6 stands for the material PP which is a polypropylene filled with carbon and stainless steel fibres. It will be used in simulations to examine what is its behaviour when facing high temperatures. With that said, it is important to document its properties as well.

**Table 5** - Values for Air Density at Different Temperatures

Temperature (°C)	Density (kg/m <sup>3</sup> )
0	1.293
20	1.205
40	1.127
60	1.067
80	0.999
100	0.946
120	0.898
140	0.854
160	0.815
180	0.779
200	0.746

**Table 6** - Materials Properties

Material	Density (kg/m <sup>3</sup> )	Thermal Conductivity (W/m.k)	Specific Heat (J/kg.K)	Tensile Modulus (MPa)	Poisson's Ratio	Coefficient of Linear Thermal Expansion (K <sup>-1</sup> )	Part
PBT+PE T GF30	1550	0.28	1100	11000	0.35	2.5×10 <sup>-5</sup>	Central Carrier
Aluminium Si9Cu3	2750	115	963	71000	0.33	2.1×10 <sup>-5</sup>	Heatsink
Aluminium 5052	2680	138	880	69300	0.33	2.4×10 <sup>-5</sup>	PCB
Epoxy	1255	0.19	1210	13000	0.40	1.1×10 <sup>-4</sup>	LED
PBT 2002-2	1310	0.38	2083	2550	0.40	1×10 <sup>-4</sup>	PGU
PC HF1130R	1200	0.20	1029	2350	0.37	7×10 <sup>-5</sup>	Lens
POM ZLV40	1410	0.23	1465	2700	0.35	1×10 <sup>-4</sup>	Gear 6
POM FX-11JR1	1390	0.35	1700	2700	0.35	1.1×10 <sup>-4</sup>	Gears 4-5
PBT 2002K	1360	0.34	1220	3100	0.35	9×10 <sup>-5</sup>	Gears 2-3
POM Z4520	1410	0.23	1470	2700	0.35	1×10 <sup>-4</sup>	Worm
Air	Piece-wise-linear	0.02	1006.43	NA	NA	NA	NA
PP	1210	0.28	1700	9450	0.41	6.1×10 <sup>-5</sup>	Gears

### Deduction of the Coefficient of Convection $h$

In the thermal simulations performed in this dissertation, the heat phenomenon of convection will be considered. To do that, it was necessary to estimate a coefficient of convection ( $h$ ) in order to use it in the study. After an intensive analysis, it was chosen to adopt an empirical correlation that have been developed for common immersed (external flow) geometries. This correlation is suitable for many engineering calculations and a slightly better accuracy may be obtained for laminar flow using the expression 4.27. This correlation was applied considering it was a vertical plate, surrounding by a constant temperature, which means it is an isothermal plate. With that said, the Nusselt number can be defined as:

$$\overline{Nu}_L = 0.68 + \frac{0.67 Ra_L^{1/4}}{[1 + (0.492/Pr)^{9/16}]^{4/9}} \quad (4.27)$$

where  $Nu$  represents the Nusselt number,  $Ra$  characterises the Rayleigh number and  $Pr$  is the

Prandalt number of this situation.

The Grashof number ( $Gr$ ) frequently arises in the study of situations involving natural convection. For this calculation, it is demanded to know the value of gravitational acceleration ( $g = 9.8 \text{ m/s}^2$ ), the surface temperature ( $T_S = 90^\circ\text{C}$ ), the bulk temperature ( $T_\infty = 20^\circ\text{C}$ ), and the characteristic length  $L_C$  (which was defined to be the diameter of the bigger gear that takes the value of 0.076 m). Then,  $\beta_v$  stands for the volumetric thermal expansion coefficient which is, approximately, equal to  $1/T_S$  for ideal gases (in absolute temperature) and gives the value of 0.03 and, at last, there is the kinematic viscosity of the fluid ( $\nu$ ) at  $90^\circ\text{C}$ , which is  $16.2 \times 10^{-5} \text{ m}^2/\text{s}$ . The expression 4.28 denotes the Grashof number for a situation of a vertical flat plate.

$$Gr_L = \frac{g\beta_v(T_S - T_\infty)L_C^3}{\nu^2} = 2.95 \times 10^6 \quad (4.28)$$

The next step is to calculate the Rayleigh number, which is, defined as the product of the Grashof number, previously determined, and the Prandtl number, which describes the relationship between momentum diffusivity and thermal diffusivity. The Prandtl number is established to be 0.695 for gases at  $90^\circ\text{C}$ .

$$Ra_L = Gr \times Pr = 2.05 \times 10^6 \quad (4.29)$$

According to Incropera et al (2013), the correlation expressed in equation 4.29 is appropriated for the situation when the Rayleigh number is between the range  $10^4 \leq Ra_L \leq 10^9$ , which turned to be correct in this case.

With the values previously obtained, it is possible to determine the average value of the heat transfer coefficient ( $\bar{h}$ ) using the formula 4.30. The term  $L_C$  is the characteristic length, in metres, and  $k_T$  is the thermal conductivity of the fluid, in  $\text{W/m.K}$ .

$$\overline{Nu}_L = \frac{\bar{h} \times L_C}{k_T} = 20.1 \Leftrightarrow \bar{h} \cong 8 \text{ W/m}^2\text{K} \quad (4.30)$$

Given that, the final result for the heat transfer coefficient is  $8 \text{ W/m}^2\text{K}$  which is considered to be a normal value, since the range between 5 and 20 is acceptable (Incropera et al., 2013).

#### 4.2.2. Software Validation

To execute a coupled investigation, it is necessary to use two modules which, in this case, are steady-state thermal and static structural. When they are joined, they look like figure 36, where they share engineering data and geometry.



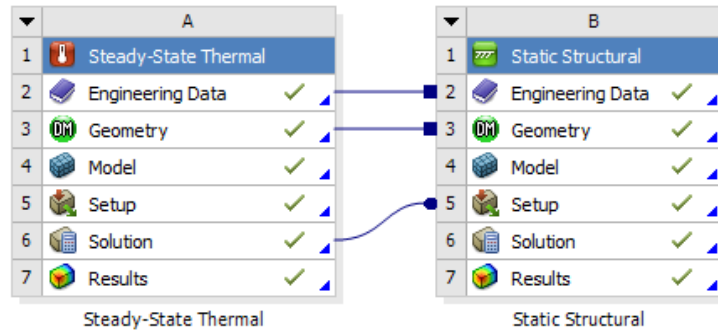


**Figure 36** - Coupled Simulation Steady-State Thermal and Static Structural

The model could be also the same if there was only one mesh, which does not happen in this situation. Next, the solution of the first simulation is introduced in the setup of the second, which means that, these results are used as input data of the following analysis.

Every project involving finite element methods should conduct a validation of the software which is, in this case, ANSYS. To do so, it will be considered a simpler geometry of a bar where the analytical calculations are practicable. Then, it is used the software to simulate the same situation and it is established the comparison between both results. Another important aspect related to this work is that the materials in study are polymers and, in order to analyse the difference in behaviour between plastics and metals, the calculations will be made using the polymer POM, and 2 metals, an aluminium alloy and steel. Three situations will be investigated: a cantilever beam<sup>4</sup>, a bar fixed at both ends and, finally, a component fixed in 2 holes which are located near the ends. Finally, it will also be done simulations of a bar with different dimensions with the purpose of understanding the influence of the geometry on errors.

To perform the analytical calculations, it is important to start by referring that a part can suffer a variation in its dimensions due to heat transfer or external solicitations. A thermal change in a body conducts to a modification in its geometry, which, usually, turns the component longer if the difference of temperatures is positive, otherwise, it contracts the segment. Similarly, if it is applied an external force to a body, there is the tendency of getting smaller due to a compressive force and the opposite occurs as a result of a traction force. The displacements previously referred can be estimated through the expressions 4.31 and 4.32:

$$\delta_T = \alpha (\Delta T)L \quad (4.31)$$

$$\delta_P = \frac{PL}{AE} \quad (4.32)$$

<sup>4</sup> A cantilever is a rigid structural element which is anchored at only one end to a support, usually vertical, from which it is protruding.

where  $\alpha$  is the coefficient of thermal expansion,  $\Delta T$  describes the difference of temperatures presented in the analysis,  $L$  represents the length of the component,  $P$  expresses the applied load,  $A$  characterises the cross-sectional area and, finally,  $E$  describes the tensile modulus of the material.

Hereupon, knowing that the thermal deformation ( $\delta_T$ ) and the deformation caused by the applied force ( $\delta_P$ ) must be compatible, it is possible to determine the necessary force to counter the effects of a temperature variation. Therefore, the result should present a null displacement of the beam. If equations 4.31 and 4.32 are substituted in the next formula, it gets to:

$$\delta = \delta_T + \delta_P = 0 \Leftrightarrow \alpha \times (\Delta T) \times L + \frac{PL}{AE} = 0 \Leftrightarrow P = -A E \alpha (\Delta T) \quad (4.33)$$

The component in study is a bar with 1000 mm of length and 100×100 mm (bar 1) of cross section. It suffers a temperature increase from 20 to 90 °C. The properties of the used materials are presented in table 7.

**Table 7** - Properties of Materials

Material	Coefficient of Thermal Expansion, $\alpha$ (K <sup>-1</sup> )	Tensile Modulus, E (MPa)
POM Z4520	$1 \times 10^{-4}$	2700
Aluminium	$2.3 \times 10^{-5}$	71000
Steel	$1.2 \times 10^{-5}$	200000

The forces for the 3 materials will be, posteriorly, calculated using this information and presented later in this section.

The second part of validation started by drawing the same bar and applying the correct material. Then, it was employed a mechanical mesh constituted by elements of the type SOLID95 (hexahedron of 20 nodes) with a size of 5 mm, which resulted in a mesh of 80000 elements and 345681 nodes. Figure 37 shows the meshed bar with all the elements being very well defined squares.

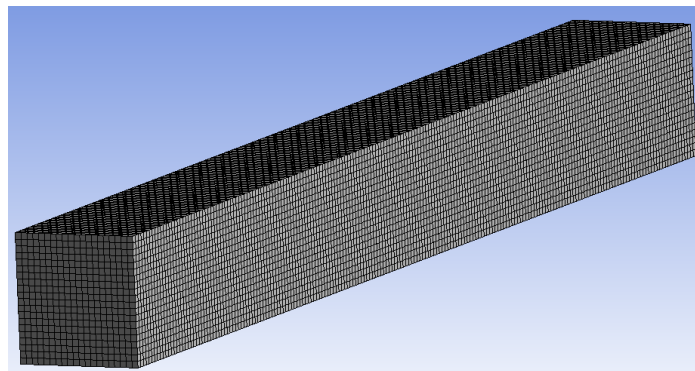


**Figure 37** - Geometry and Mesh of the Bar

The element quality of the cells is very close to 1 and the skewness is 0 for all meshes which means that they present an excellent quality (see section 3.5.3). The decision of establishing a finer mesh, with more elements than it was necessary to solve the problem, was taken in order to achieve more accurate results. For the component with holes, it was fundamental to pay attention to the voids. It was adopted the same dimension for the cells of the mesh, otherwise, it would not be possible to compare the results. When it is defined a length for the element, the software begins by meshing the edges with this size initially, and then they are refined for curvature and 2D proximity, which is the reason why the discontinuities presented a refined mesh as well, with 78939 elements and 342850 nodes, as it can be seen in figure 38.

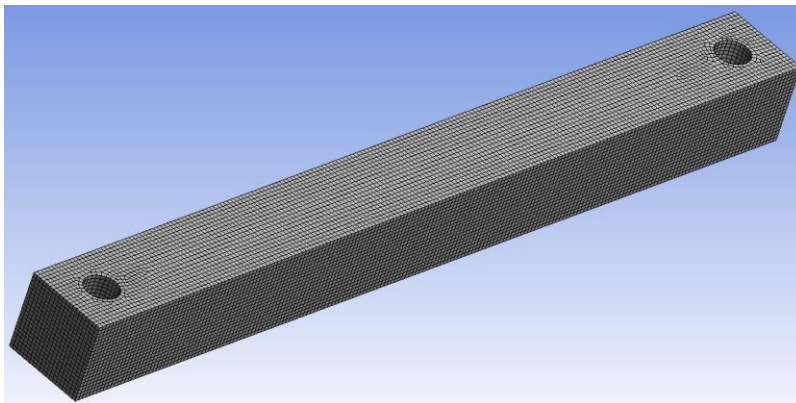


**Figure 38** - Geometry and Mesh of the Bar with Holes

To reproduce a similar situation to what was considered analytically, the bar was submitted to a temperature increase from 20 °C to 90 °C for the 3 cases. In terms of mechanical boundary conditions, it was defined 3 different scenarios.

Firstly, the component was fixed in just one end and applied a compressive force on the other extremity, of equal value of the theoretical forces. The second situation considered both ends of the bar fixed (figure 39) and, finally, in the third scenario both holes were locked, as it is represented in figure 40.

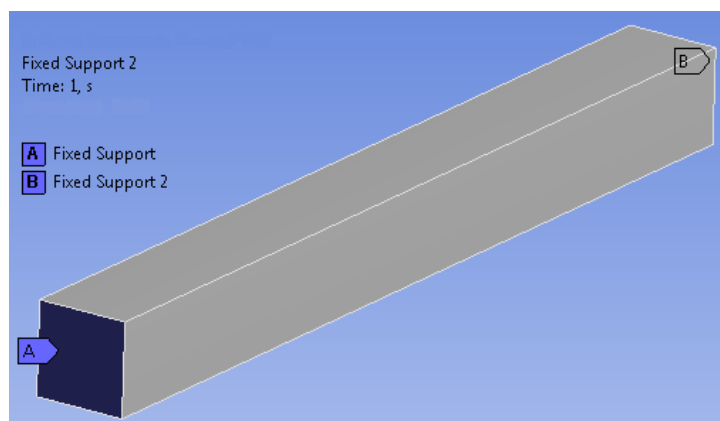


**Figure 39** - Fixed Bar at both Ends

The orifices have 40 mm of diameter and they are placed in the middle of the bar, at 5 mm of distance from the extremities.

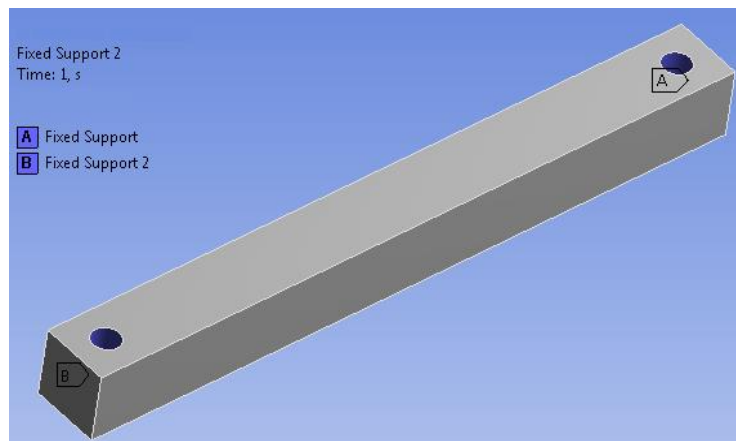


**Figure 40** - Fixed Bar at both Holes

Another set of simulations was produced with the same boundary conditions and were also used the 3 materials. For this situation, the bar had a length of 1000 mm and 10×10 mm of cross-sectional area (bar 2), which means the length of the sides of the cross section is 10 times smaller. In this case, the element of the mesh had a dimension of 0.5 mm and the element type, the size of the holes as well as its placement maintained the same proportions. The quality of the meshes is the same of the previous ones which means that they present an excellent quality.

In figure 41, it is displayed a sectional view of the element middle plane for bar 1. On the left there is the bar fixed at both ends and, on the right, the bar fixed on the holes. It is not presented the results for the situation of having the bar fixed at only one end as it is very similar to the figure on the left.

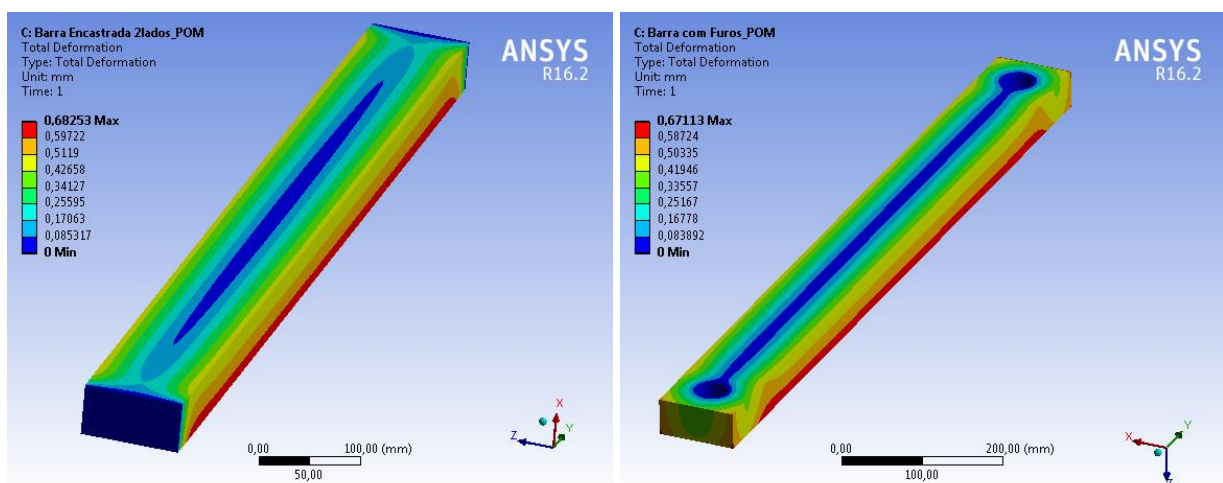


**Figure 41** - Results for Bar 1

The three cases were analysed and it was verified that in the central axis of the beam the

total displacements are null as it was expected according to the analytical calculations. For this reason it can be concluded that the behaviour of the beam, resultant from simulation, agrees with what was performed analytically. The total deformation considers all 3 directions which means these results show the total component of the displacements. These displacements are for material POM although the others have also been tested and the conclusions to be drawn are the same.

The simulations were repeated for bar 2 which has different dimensions and, the results for material POM are presented in figure 42. The maximum values of displacements are significantly inferior in comparison to the ones on figure 41. However, the most important conclusion of these figures is that in the central axis of the beam, the deformation assumes the value 0, as it was expected.

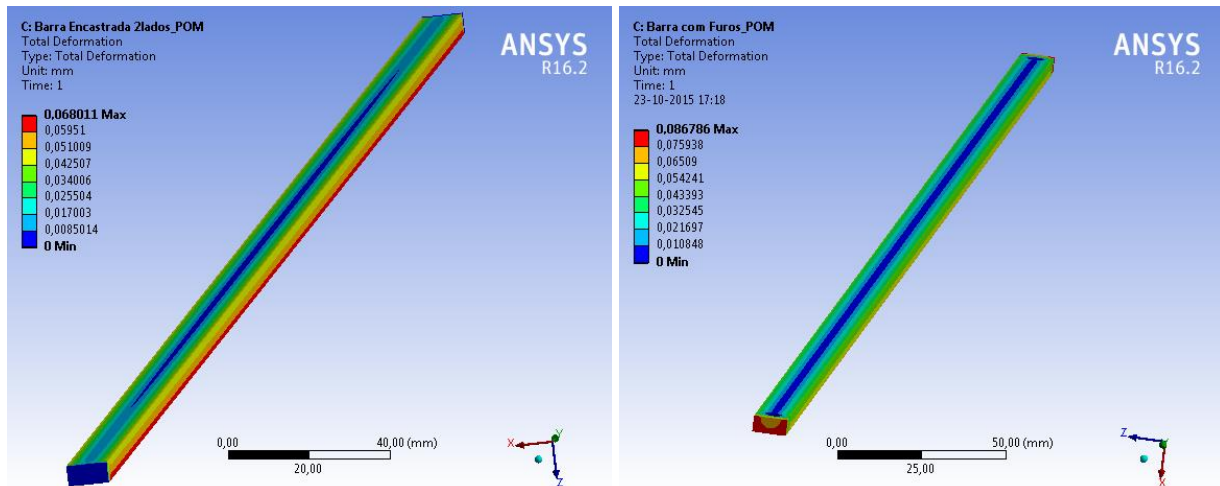


Figure 42 - Results for Bar 2

In table 8, it is presented the results for the theoretical forces (T) and the outcomes of the reaction forces measured on the centre of the fixed supports of the simulations (N). Consequently, it is calculated the error (E) which separates them for both geometries and different materials.

After a thorough inspection of the table, it is possible to verify that all the numerical values are superior to the theoretical in the case of the fixed bar at both ends. Still on this scenario, the error decreases from the material POM to steel, which means this happens as it is moving down in the table. Similarly, the results reduced from bar 1 to 2 and it is important to refer that the dimensions of the element were lowered 10 times and the error is, approximately, smaller in the same proportion. This occurrence allows to conclude about the influence of the element size on the results.

**Table 8** - Comparison between Theoretical and Numerical Results

		Beam fixed at both ends		Beam fixed in both holes	
		Bar 1	Bar 2	Bar 1	Bar 2
POM	T	189000 N	1890 N	189000 N	1890 N
	N	195140 N	1896.1 N	187600 N	1889 N
	E	<b>+ 3.20 %</b>	<b>+ 0.32 %</b>	<b>- 0.74 %</b>	<b>- 0.053 %</b>
Aluminium	T	1143100 N	11431 N	1143100 N	11431 N
	N	1177200 N	11465 N	1133600 N	11424 N
	E	<b>+ 2.94 %</b>	<b>+ 0.30 %</b>	<b>- 0.83 %</b>	<b>- 0.061 %</b>
Steel	T	1680000 N	16800 N	1680000 N	16800 N
	N	1723700 N	16843 N	1664200 N	16788 N
	E	<b>+ 2.57 %</b>	<b>+ 0.26 %</b>	<b>- 0.94 %</b>	<b>- 0.071 %</b>

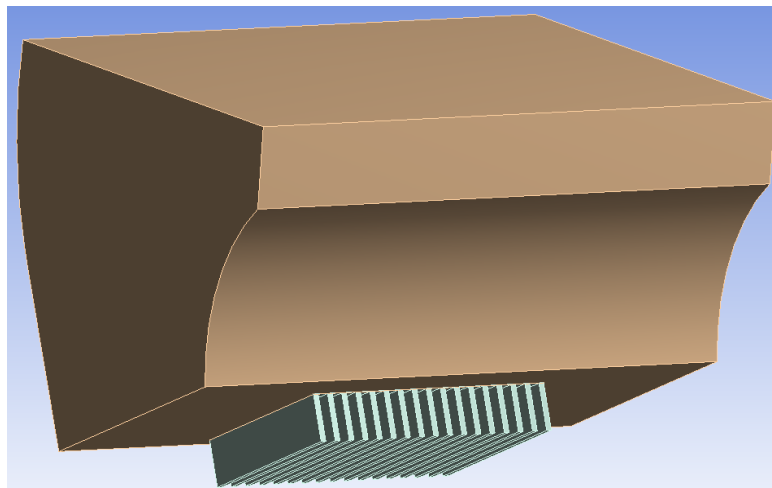
On the other hand, for the situation of the beam fixed on the holes, the numerical values are inferior to the analytical ones. Contrary to the previous case, the error increases from POM to steel, although, it follows the same tendency in terms of geometry as before, since the errors decrease with the size reduction (more than 10 times). With that said, it is likely to be concluded that the geometry and the boundary conditions it has been considered have influence on the outcomes. In addition, it should be noted that the tensile modulus increase from POM to steel, in opposition to the coefficient of thermal expansion which decreases. With these facts it can, certainly, be assumed that material properties contribute to the error between theoretical and numerical results.

The differences found among the outcomes can be explained by some aspects which are not completely the same in both analysis. Firstly, the analytical study was performed considering only 1 dimension while the numerical one was defined using 3 dimensions. Secondly, the calculation of the theoretical forces handled with just 1 element described as a bar element and the software formulation uses various cells (which constitute the mesh) characterised differently, which means the considerations are not equal. At last, it is essential to mention that a restrained end is defined with only one reaction force in the analytical study, in contrast with the numerical where the fixed extremity is defined with 3 components of a force plus 3 of a momentum. Therefore, these explanations can justify the existence of small differences between the results.

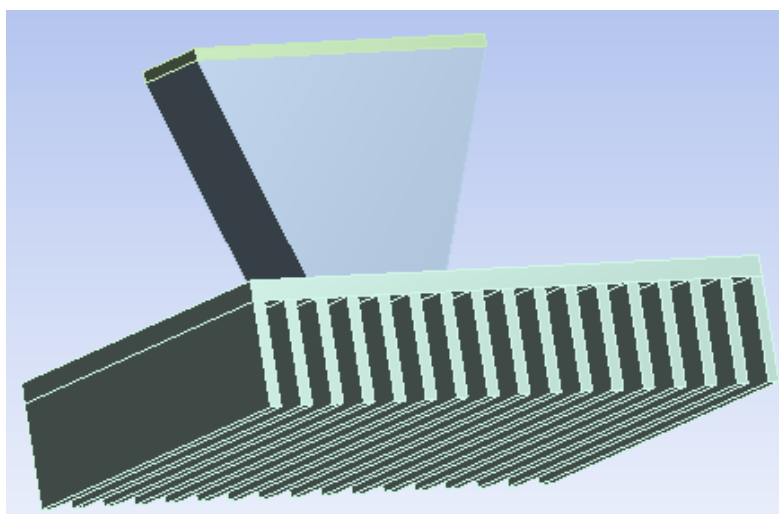
In general, the principal conclusion it can be drawn from this table is that the values of the errors are low, being the highest of 3.2 %, which means that the validation of the software was successfully executed.

#### 4.2.3. Simulations on the Total Assembly

The simulations performed on the assembly previously presented in section 4.2.1 were executed using the module Steady-State Thermal of ANSYS. The principal objective of this study is to investigate what is the temperature distribution that the LED creates on the surrounding components. In order to simplify the analysis, gears were not considered since it would be possible to execute a preliminary examination without them. Then, if it was considered necessary, the study could be repeated with all the elements. In figure 43 (a), it is visible the central carrier which encloses the heat and turns the simulation more realistic, and in figure 43 (b) there is the contact between the PCB (which includes the LED) and the heatsink which has the responsibility of dissipating from the heat source. This connection was defined as bonded since the components are fixed among them.



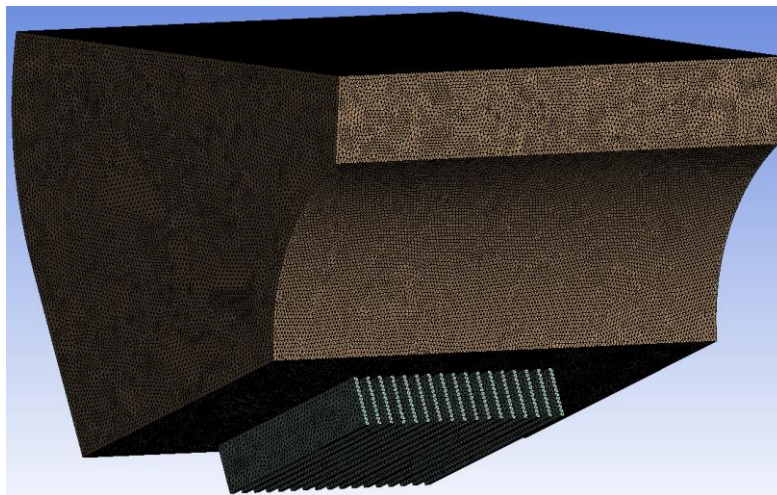
(a)



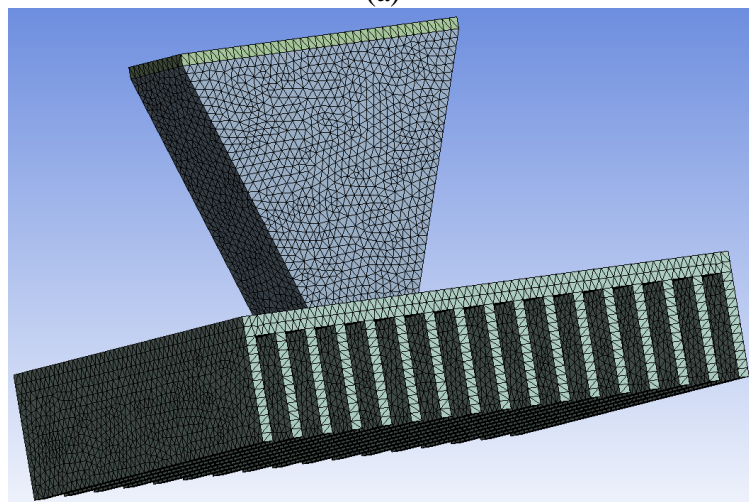
(b)

**Figure 43** - Assembly in Study: (a) Outside; (b) Inside

To create a mesh, in order to get the most accurate results, the components were joined in just one element as if they were all just one body. This action ensures the sharing of nodes between bodies, which means that the heat will be conducted among them. With that said, it was generated an appropriate mesh for a thermal analysis, setting the physics preference as CFD and defining the solver preference as Fluent (figure 44). As the components have quite complex shapes to be meshed in squares, the base element is called SOLID72 which is a tetrahedron defined by 4 nodes in which the minimum size used was 0.1 mm and the maximum 3 mm. In the bodies, smoothing was established to be high with the purpose of having more iterations and, consequently, a better element to simulate with. The transition between cells was defined as slow, where it was adopted a growth rate of 1, and the span angle centre was detailed as fine ( $12^\circ$  to  $36^\circ$ ), which means that curved regions will be divided in more elements.



(a)



(b)

**Figure 44** - Mesh: (a) Outer Parts; (b) Inner Components



The final mesh is constituted by 3663060 cells and 714373 nodes. Its quality can be evaluated based on 2 characteristics: element quality and skewness. The average value presented for the first aspect is 0.82 and skewness is set as 0.26. According to ANSYS Meshing User's Guide (ANSYS, Inc., 2013), these values manifest that the base elements of this mesh possess very good quality and it was decided not to refine more as it would increase much the number of cells as well as the computation time.

The initial temperature of the whole assembly was defined as 20°C. The only heat source, in this situation, is the LED whose power is, according to its datasheet on appendix B, 4.6 W. The heat phenomena involved in this simulation are conduction between the different bodies and, convection which occurs upon the element faces. Conduction happens among all the elements since the generated heat is diffused to the other areas due to the connection of the mesh nodes. Bearing that in mind, it is not necessary to define additional characteristics. On the other hand, it is obligatory to specify a convection heat transfer coefficient in order to provide heat dissipation through the air. In addition, this value was defined as 8 W/m<sup>2</sup>K to an ambient temperature of 20 °C, and its derivation can be found in section 4.2.1..

In figure 45, it can be seen the boundary condition applied to the LED.

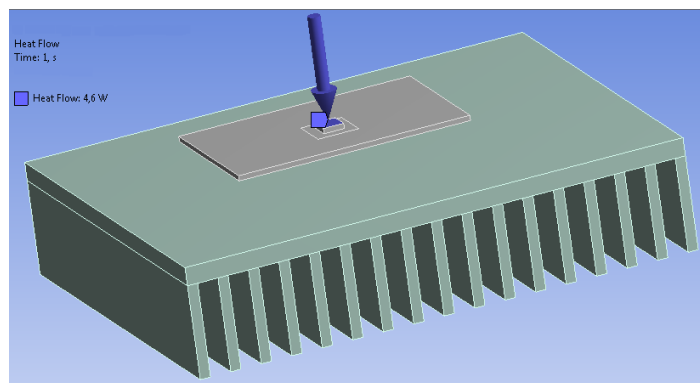


**Figure 45** – Power of the LED

In order to solve the problem, it was employed a sparse solver (direct) and this mode is recommended if enough physical memory is presented to accommodate all of the solver data.

Next, the results of the simulation are displayed and analysed for all the components. These outcomes show a situation of equilibrium for the studied problem. The central carrier was partially affected by the heat flow, although most of it maintained the initial temperature of 20 °C. The temperature of heatsink increased since the heat is being dissipated by this part and reaches values of, approximately, 30 °C. These facts are shown in figure 46.

Inside the box, it is possible to visualise that the heat generated by the LED is being propagated in both ways and that is why PGU has also a lighter blue colour (around 25 °C) on

the extremity closer to the heat source.

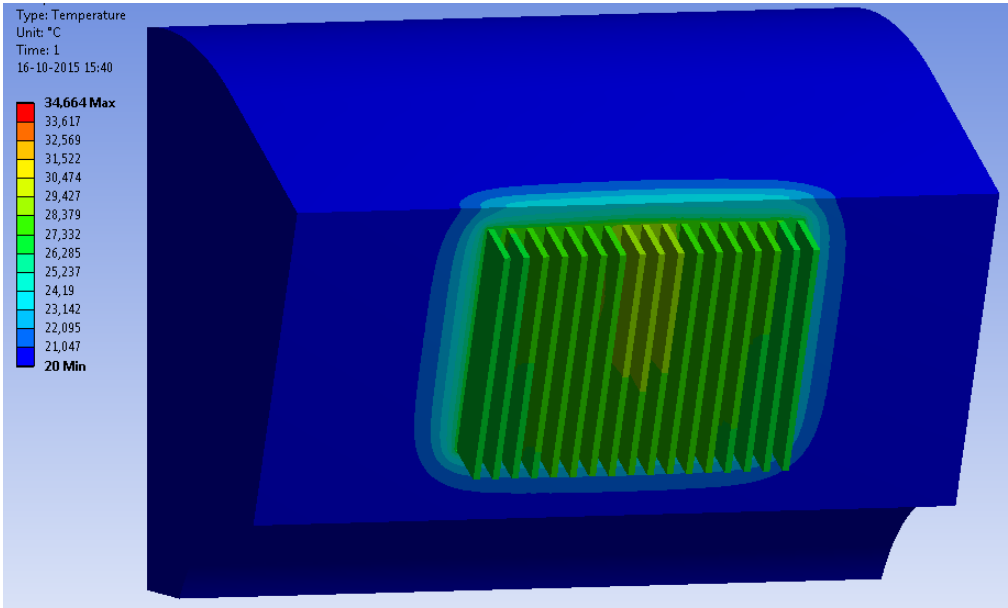


Figure 46 - Results of Temperature at 20 °C

It is essential to note that the quantity of heat going to the heatsink is much higher than that is heading to PGU. This fact is explained by the difference of materials used on the pieces. On one side, the LED has the PCB and, next, in the same direction, there is the heatsink, which are constituted of aluminium. On the other direction, there is the PGU composed by a polymer which presents a very low value of thermal conductivity. As this characteristic is more elevated in aluminium than in polymers, the heat follows the path which offers less resistance and, for that reason, goes to the side of the heatsink.

The maximum temperature registered inside the PGU is, approximately, 28.7 °C and the value at the tip of the fins is around 28 °C. Figure 47 presents this information.

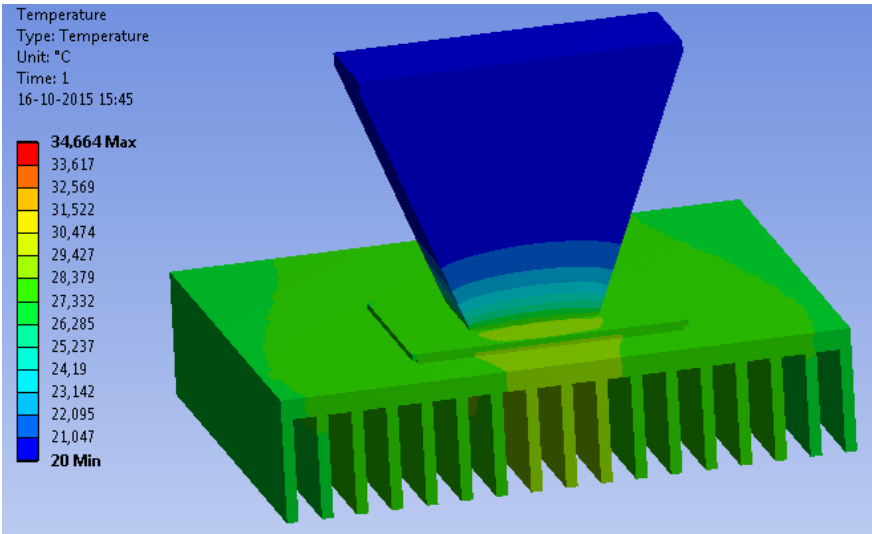
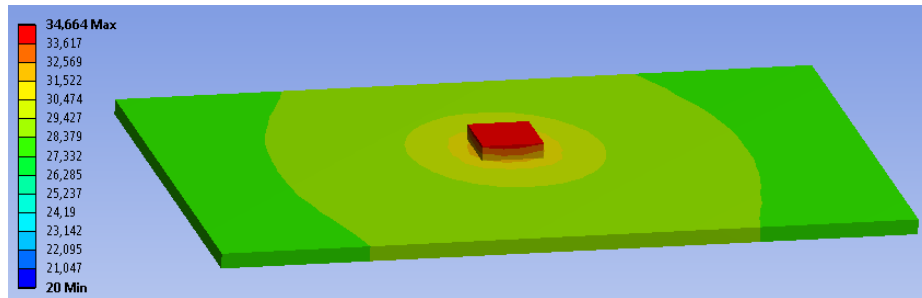


Figure 47 - Temperature Distribution at 20 °C

The maximum temperature presented in the whole assembly is on the LED, where the heat flow was applied and reaches the value of approximately 35 °C.

Nearby the component, it can be noted the difference of temperatures which represent the heat distribution. Firstly, there is the orange part, after the red face of the LED, then, there are the yellow surroundings with the format of a circle and, finally, the green area where the temperature is lower, around 28 °C. Figure 48 shows what was previously referred.



**Figure 48** - Temperature of the LED at 20 °C

Through the interpretation of the results, it was possible to conclude that gears were not important to be included in the examination as the heat did not overcome the lens. In addition, the temperature of gears, in a state of equilibrium, would be not much more than 20 °C. Finally, and keeping in mind the objective of this simulation, it is important to refer that the LED is not able to significantly increase the temperature of gears.

The situation was repeated in the same conditions, except the initial temperature was changed for 90 °C, maintaining the heat transfer coefficient. The results are presented in figure 49, where it is shown that the distribution of heat is the same as before. However, the maximum temperature registered is of, approximately, 105 °C. Bearing that in mind, the tip of the fins are at 98-99 °C and inside the PGU it is presented a value of 99 °C. This leads to the conclusion that the heatsink is correctly performing its function as it is dissipating the heat applied on the system. If gears had been included in this examination, its final temperature would be of 90 °C, wherein can be concluded by the figure, which is considered a dangerous value since it is not known what happen with this mechanism at that temperature.

In these steady-state thermal analyses, there were calculated the effects of steady thermal loads on a system. These studies were considered to be linear as the properties of the materials were constant.

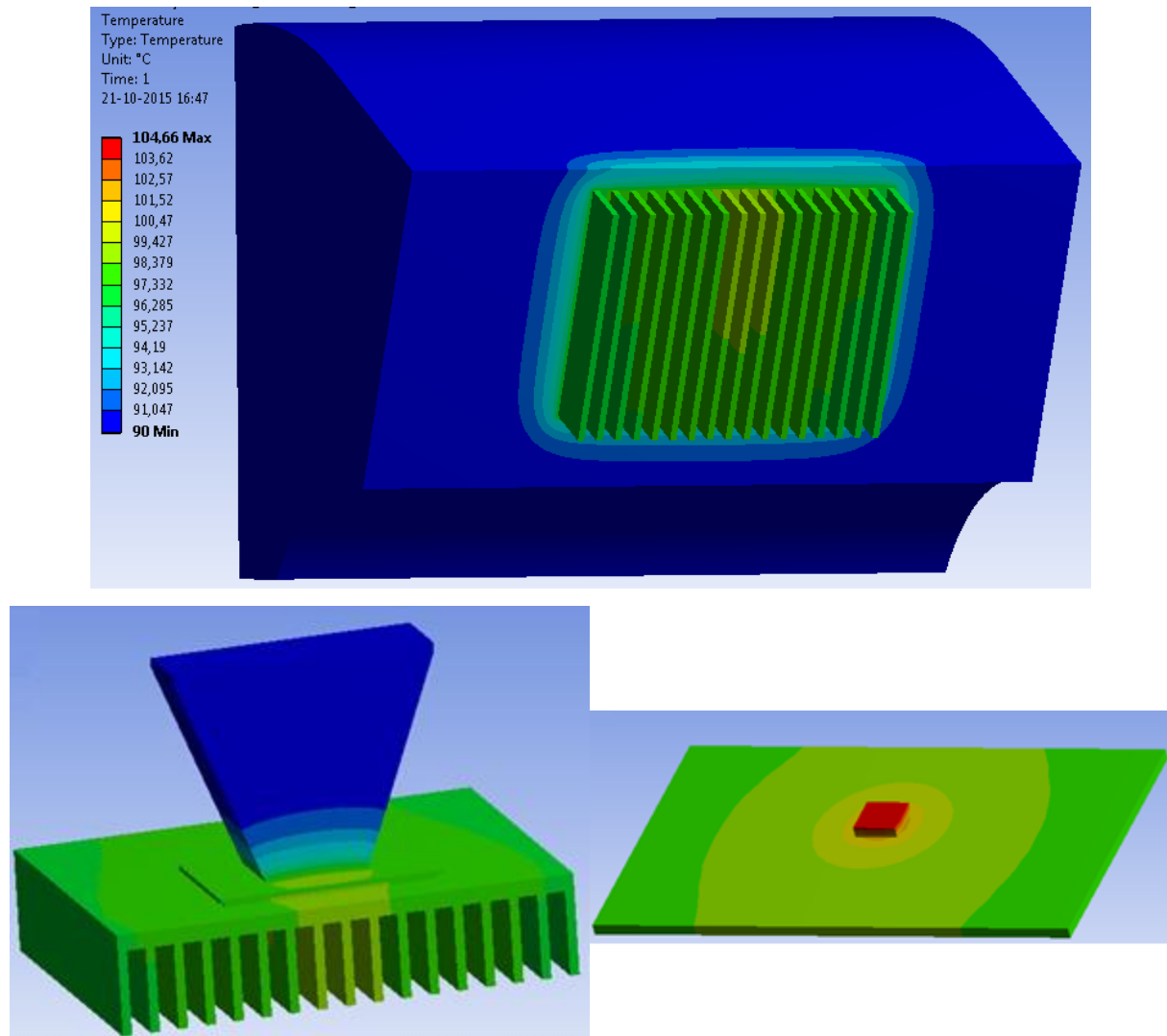


**Figure 49** - Results for the Simulation at 90 °C

#### 4.2.4. Simulations on One Gear

In order to execute this investigation, the simulations of thermal and static structural are coupled as it was previously performed in section 4.2.2. (see figure 35).

Next, it is presented the geometry which will be examined in figure 50. On the left, it can be visualised the front where some paths are incorporated which increase the rigidity of the component as well as the complexity of the geometry. On the right, there is the rear part where the piece of angular adjustment is inserted as well as a structure which contains a pin. In order to allow the correct measurement of the displacements on the teeth, few auxiliary lines were added to the CAD model.

To construct a mesh for this gear, it was indispensable to set the advanced size function to on, using curvature with the purpose of having a refined mesh on the teeth, according to the complexity they represent. The smoothing was established as high and the transition as slow

which results in a dense mesh.

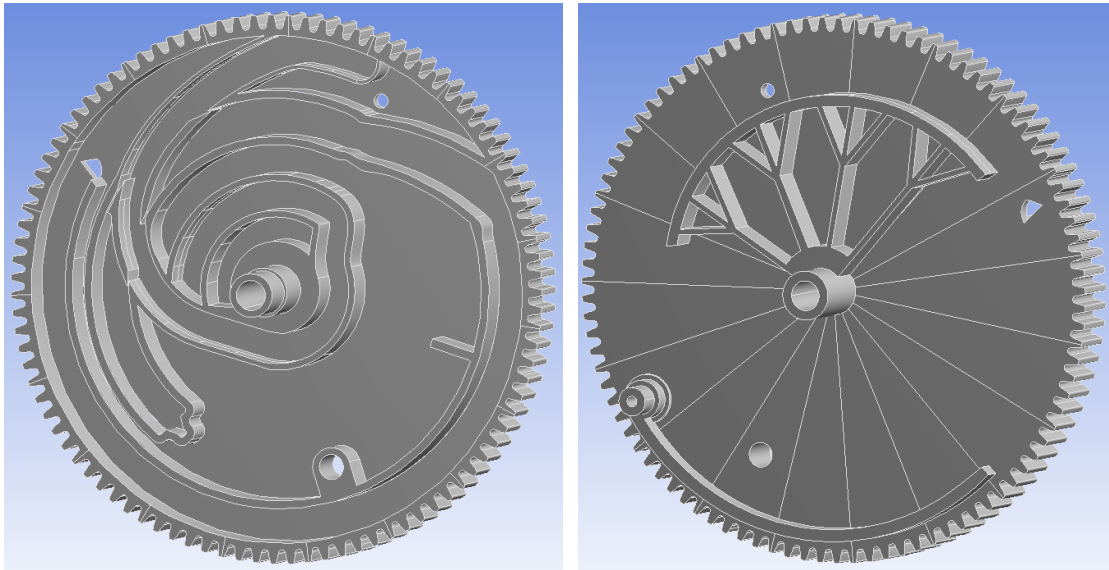


**Figure 50** - Geometry of the Gear on the Front (left) and on the Back (right)

It is mandatory to apply these methods due to the singularities that characterise this element. The element used on this mesh was SOLID92 which is a tetrahedron defined by 10 nodes, 4 on the vertices and 6 in the middle of the edges. The minimum size employed in the cells was 0.015 mm and the maximum 3 mm. The curvature normal angle was chosen to be high and the growth rate was defined as 1.1. As the mesh characterised by these criteria was not refined enough, specifically on the teeth it was applied a sizing method on all the teeth faces using 0.15 mm as the element size and  $15^\circ$  as the curvature normal angle. These characteristics are presented in figure 51.

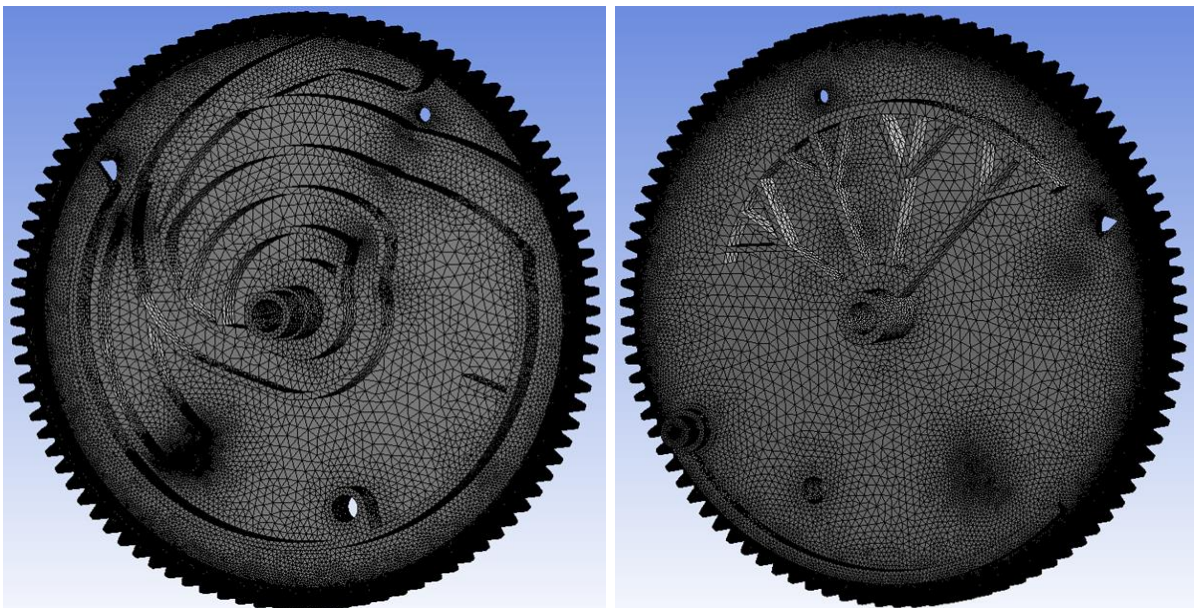


**Figure 51** - Gear Mesh on the Front and on the Rear

Two meshes were created with the same parameters although defined to different physics preference, being CFD to steady-state thermal and mechanical to static structural. After this, the guidelines to evaluate mesh quality (ANSYS, Inc., 2013) were checked and it was discovered that the element quality was 0.85 and the skewness 0.22.

These values along with the global mesh physical appearance expressed a very good quality in which it is concluded that it is not necessary to refine more. Finally, it is important to mention that this mesh is constituted by 8 077 602 elements and 11 504 295 nodes.

Through an attentive observation of figure 52, it can be inspected how the teeth are meshed with the variation of size elements. It must be noted that there is a uniformity of the cells which means this mesh is well suited on the gear teeth.

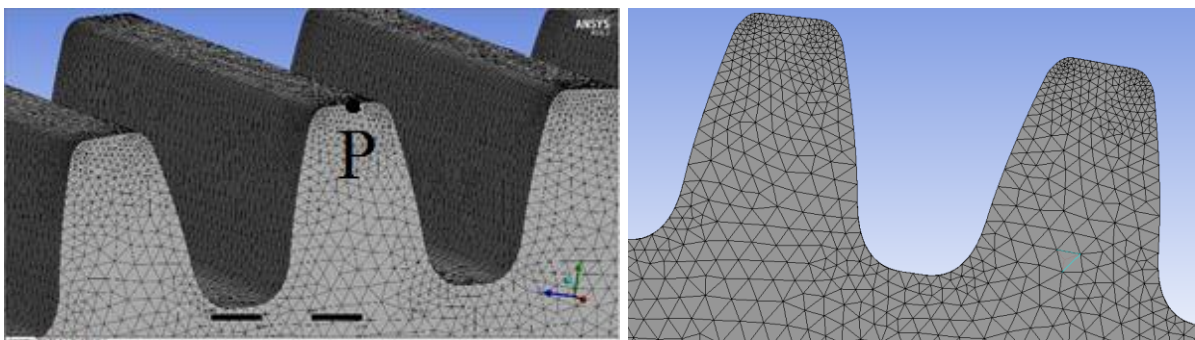


**Figure 52** – Details about the Mesh Teeth

The boundary conditions applied in the thermal simulation were the same of the previous study: 20 °C as the initial temperature, the whole body subjected to 90 °C and the definition of a convection coefficient of 8 W/m<sup>2</sup>K to the faces of the component at an ambient temperature of 90 °C. The previous examination was performed using 20 °C and 90 °C as ambient temperatures. In this case, it is only adopted the 20 °C for the environment since the second temperature is applied to the mechanism. Consequently, if the same temperature was employed for the mechanism and air, there would be no heat transfer or changes in the system.

This analysis was solved using an iterative solver chosen by the software and, then, these results were imported to the static structural simulation as it was explained in the beginning of this section.

The axis of the gear was fixed and the initial temperature was also defined as 20 °C. The mechanical study was completed with the preconditioned conjugate gradient solver using a convergence tolerance of  $1 \times 10^{-8}$ . The results of this thermal-stresses simulation are presented in figure 53.

It can be concluded that the displacements assume higher values on the teeth being null at the centre since the axis is fixed. The maximum value registered for total deformation (which

considers the 3 directions) is, approximately, 0.27 mm which is only presented on the teeth. With the scale located on the left of the figure, the gradient of colours can be understood and it is possible to match these colours with values of displacements.

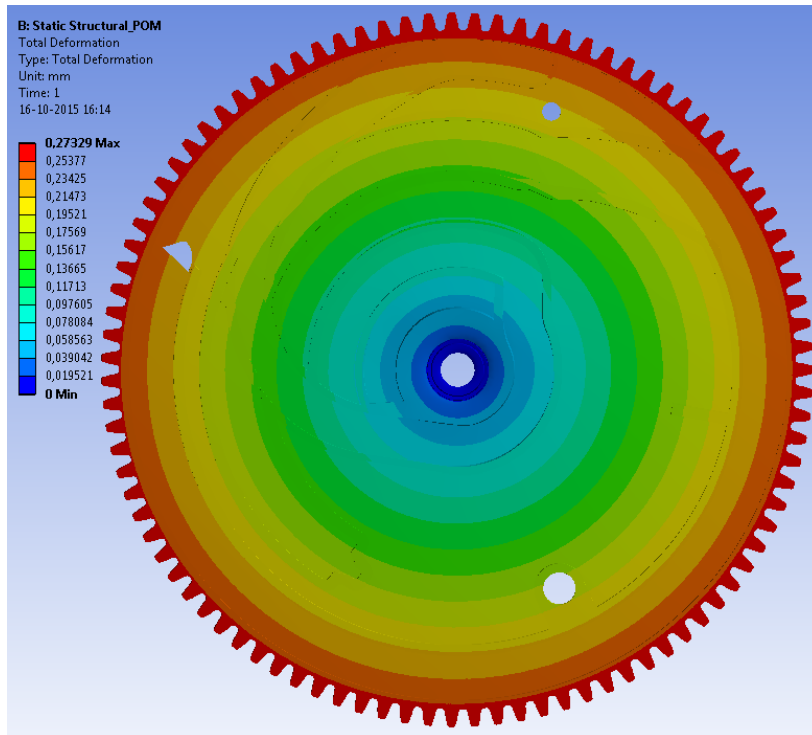


**Figure 53** - Total Deformation for Material POM

For the material PP, the procedure in regard to the mesh, boundary conditions and solvers was exactly the same. However, the results are different and they are presented in figure 54.

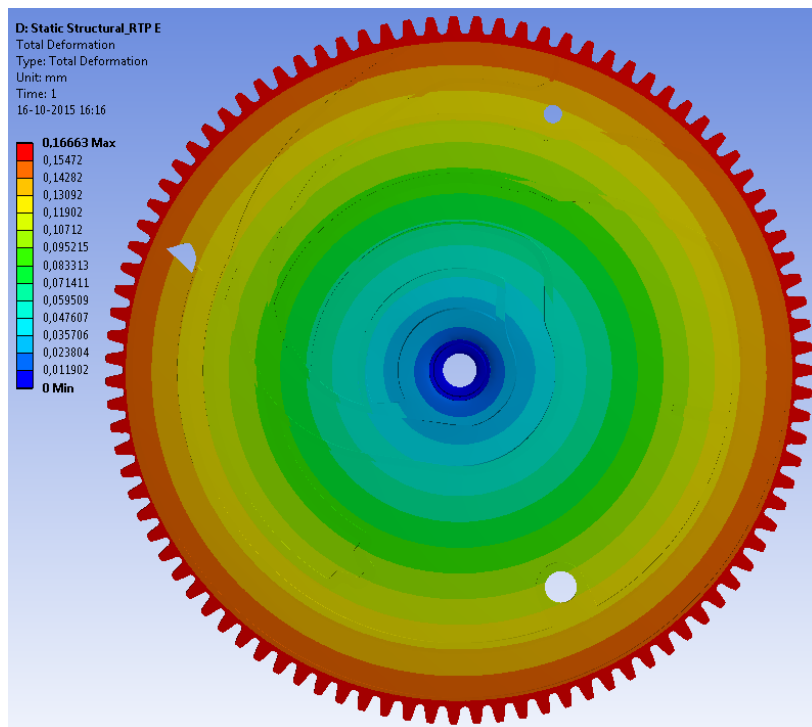


**Figure 54** - Total Deformation for Material PP

The maximum value for the displacements caused by the temperature is around 0.17 mm, which is 48.5 % inferior to the value verified for POM. From the examination of both figures, it is possible to ascertain that the gradient of colours is similar and they are located in the same places. Bearing that in mind, it is possible to conclude that the results are the same but in smaller proportions since the tensile modulus of PP is much higher comparing with POM which leads to inferior displacements. These outcomes will be analysed and compared among each other in a section further on.

### Fluid-Structure Interaction Simulation

Instead of using Steady-State Thermal module, it was treated the same process with Fluent which is other thermal operator provided by ANSYS. The main difference between them is that Fluent allows the user to add a volume of fluid which simulates the air while, in the previous, although the air is considered, it does not exist physically in the simulation. In figure 55, it can be observed the geometry of the gear surrounded by the air and, on the right, the entire CFD mesh of the assembly.

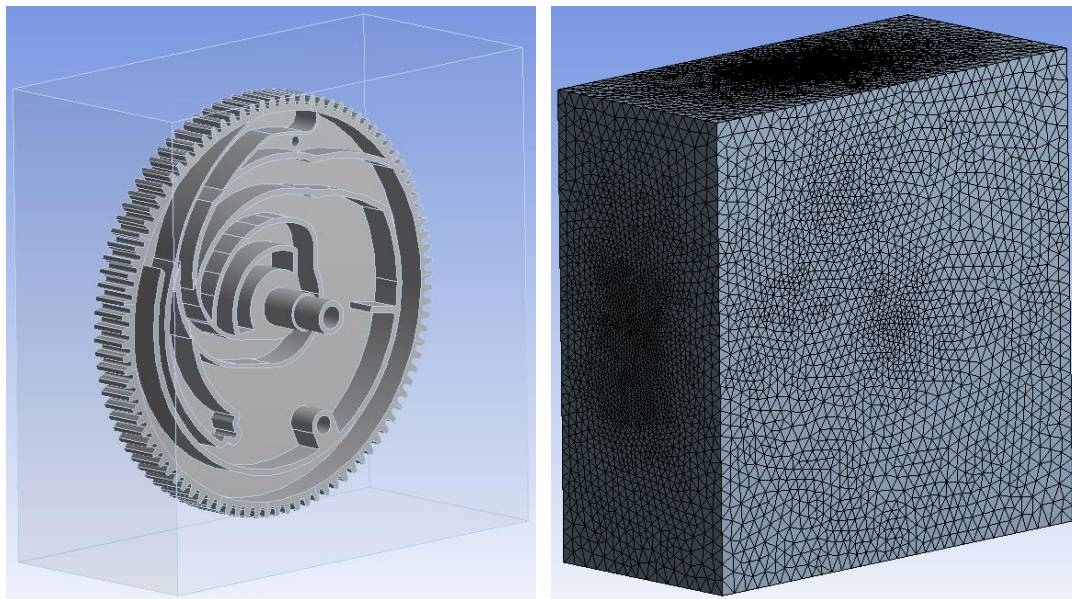


**Figure 55** - Geometry of the Gear with Enclosure and Respective Mesh

The dimensions of the fluid volume are 85×85×40 mm. In regard to this subject, it is important to mention that both parts are joined together as if they were only one body. This method allows to correctly evaluate the heat transfer in the simulation. In fact, all the meshes constructed during this project shared this characteristic. Concerning the qualitative features (advanced size function, smoothing, transition and span angle centre), this mesh was detailed with the same as the ones in the previous analysis. However, the constitutive element is



SOLID72 which is a tetrahedron defined by 4 nodes, 1 per each vertex. The minimum element size was established as 0.2 mm and the maximum 3 mm, with a growth rate of 1.1. Ideally, the minimum length would be smaller due to the difficulty in meshing the transition air-component, which is the hardest task to perform. However, the total number of elements of this structure and, consequently, the computation time are also a concern which cannot be ignored. Nevertheless, the overall amount of nodes on this mesh is 2 886 960 and of cells is 17 204 221. The average value for element quality of these cells, which varies between 0 and 1, is 0.85 and the higher the better, according to (ANSYS, Inc., 2013). The parameter skewness determines how close to ideal a face or a cell is and the perfect value is 0 being the maximum also 1. In this study, this characteristic fixed its value in 0.21 which implies that cell quality is excellent (ANSYS, Inc., 2013). The mechanical mesh used was the same as in the previous simulation.

After some primary simulations, few zones were identified as potential causes of error due to geometric discontinuities. With that said, instead of diminishing the minimum element size, it was decided to employ local refinement, therefore, 2 spheres of influence were created in places with very small thickness, having 7.5 mm of diameter as it is represented in figure 56 on the left. The elements inside these spheres have 0.18 mm of length and the difference of density can be visualised in figure 56 on the right.

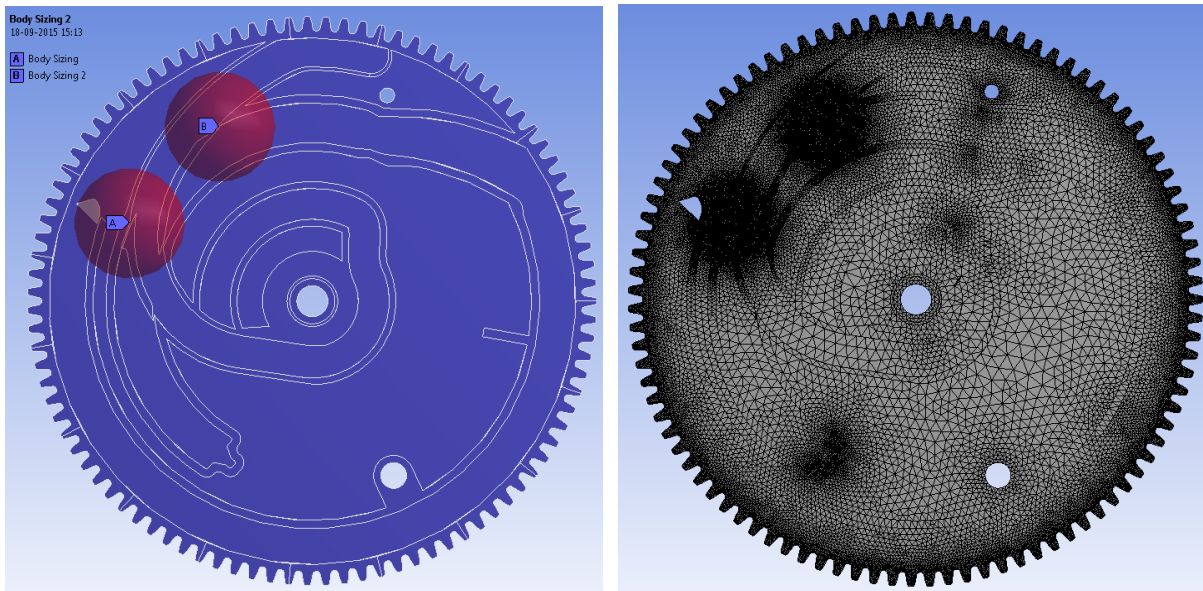


**Figure 56** - Method of Spheres of Influence

Next, the boundary conditions applied in this simulation will be explained in detail. Firstly, it is a steady-state formulation in which it is considered the action of gravitational acceleration of  $-9.8 \text{ m/s}^2$ . Regarding the thermal modules, the energy equation was set to on and it was adopted a laminar regime for the heat transfer process. To define the area of entrance and

exit of the air to the software, two named selections were created, inlet in the face of the air next to the front of the gear and outlet in the face next to the rear side, according to figure 55. This way, it is ensured that the air follows that trail and goes through the body in the intended mode (Xu et al., 2014). It is detailed that the whole volume of fluid is at 90 °C which means the air enters and exits the gear at that temperature. For the outlet it was defined an outflow boundary condition which is used to model flow exits where the details of the flow velocity and pressure are not known prior to solving the flow problem (ANSYS, Inc., 2009a). The user does not define any conditions at outflow boundaries, which means that ANSYS Fluent extrapolates the required information from the interior. Finally, it was applied a convection coefficient of 8 W/m<sup>2</sup>K at an ambient temperature of 90 °C.

Regarding the solvers, in this simulation was used a pressure-based solver as well as a standard procedure for calculating cell-face pressures. In addition, a SIMPLE scheme was chosen for pressure-velocity coupling. For pressure it was adopted the second order method, and, at last, the second order upwind procedure was the one employed for momentum and energy.

After finishing the simulation, the graphic of its residuals is presented in figure 57. It is concluded, through the analysis of the figure that the simulation converged and the values registered for the errors are considerably low. The one for energy reaches  $2 \times 10^{-5}$  while continuity approximates of  $3 \times 10^{-2}$  and the others are around  $10^{-3}$ .

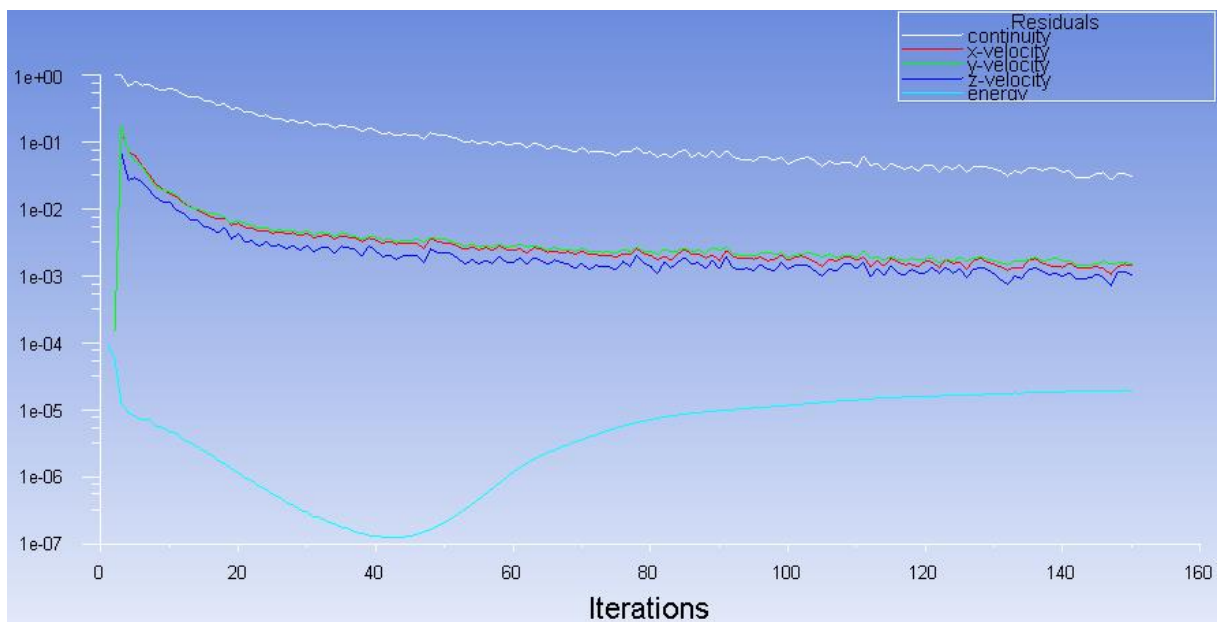


**Figure 57** - Residuals of the Simulation

Although the mesh has been refined in the more critical places, its temperature is not 90 °C in all the extension of the component, as it can be visualised in figure 58.

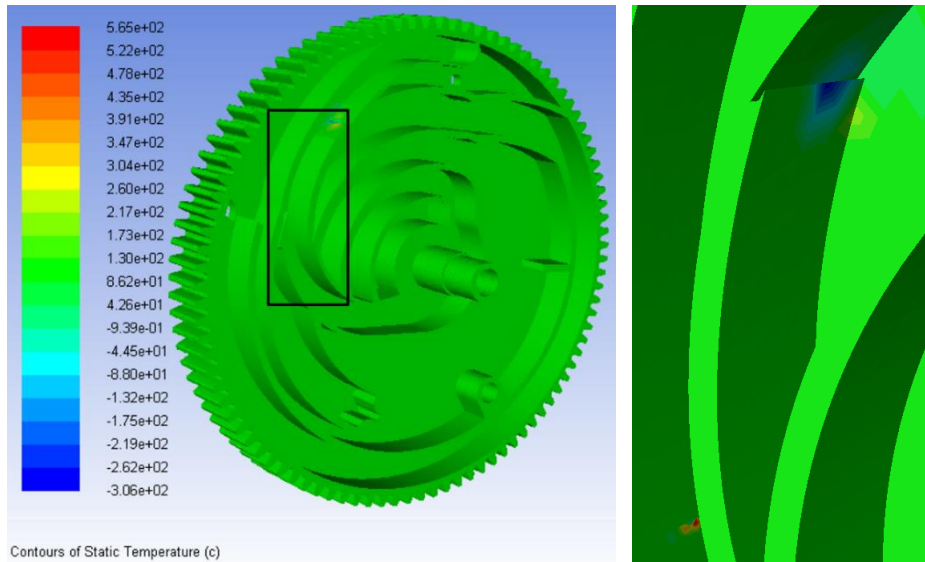


**Figure 58** - Temperature of the Gear

There are 2 areas where illogical values are reached which means the mesh should be even more refined. On the right figure there is an expanded view of what is inside the rectangular on the left. Despite these errors, the remaining piece is at the desired temperature which can be understood by the colour green. Having the thermal results, they were imported to the static structural module and inserted as a boundary condition. Then, the procedure followed was the same of the previous study, which means that, in this part, nothing has been changed.

The results for POM are displayed in figure 59, where it is visible the gradient of radial displacements which are clarified through the scale on the left of the representation.

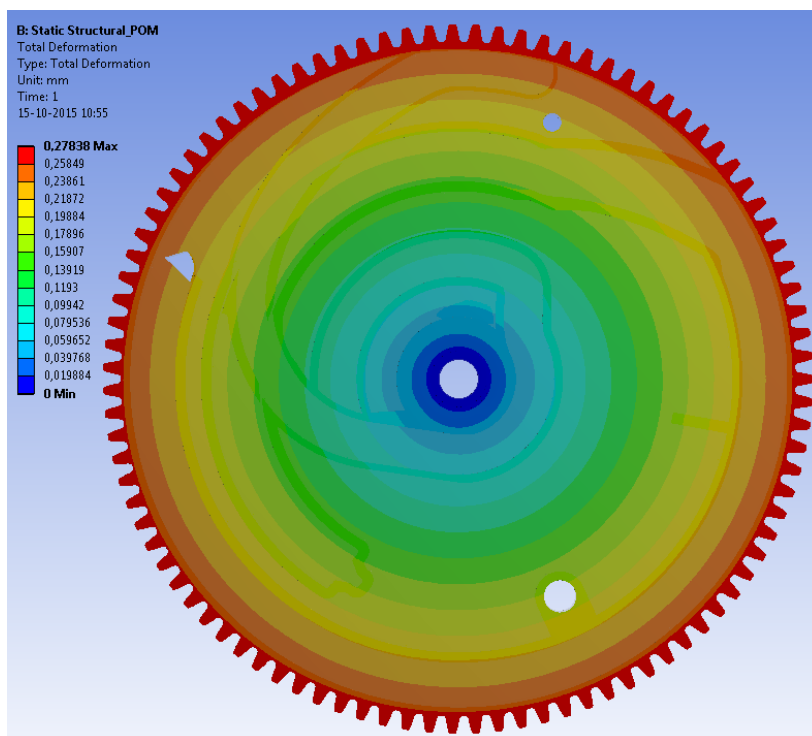


**Figure 59** - Results for the material POM

The maximum value registered for the total deformation is, approximately, 0.27 mm which is the resultant displacement considering the 3 directions, being the radial values the most significant. If both figures are compared, it is drawn the conclusion that this number differs only from the third decimal place on. This fact allows to declare that both modules are suitable to simulate this process of heat transfer, which is not very complex. The differences among both analyses will be compared later, more specifically, on the teeth in order to evaluate the magnitude of the divergences.

For the PP material, everything was performed in the exact same way in both analyses, from the mesh, the boundary conditions until the solvers. The only difference was the application of another material. The results are presented in figure 60.

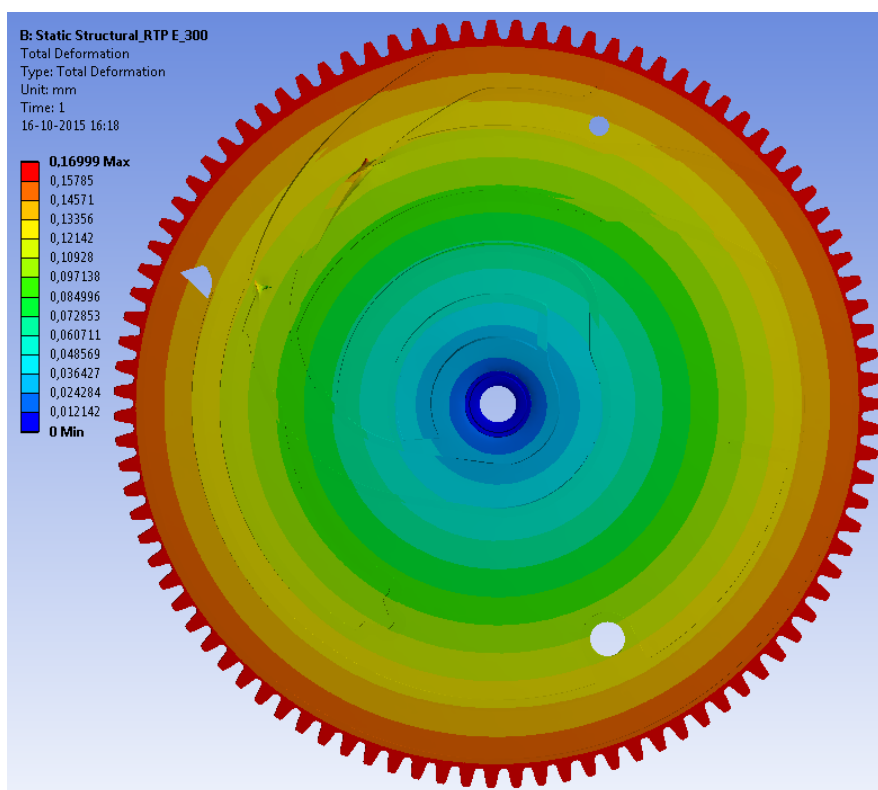


**Figure 60** - Results for the Material PP

The maximum value of deformation in this simulation is, approximately, 0.17 mm. If it is established the comparison between this and the previous maximum displacement, when the steady-state thermal module was used, it can be confirmed that the differences are only registered since the third decimal place. In addition, regarding the higher values, this material reaches displacements around 48 % smaller. A lower coefficient of thermal expansion ( $6.1 \times 10^{-5}$ ) than POM ( $1 \times 10^{-4}$ ) is responsible for the displayed discrepancies.

When the presented outcomes are analysed, it is concluded that it is indifferent to simulate with one thermal module or the other since the registered values are so close among them.

#### 4.2.5. Simulations on the Assembly of Gears

The next simulations that will be presented were executed using ANSYS Workbench through a coupled analysis of steady-state thermal and static structural as in the preceding study. It was decided not to perform this analysis also in ANSYS Fluent since, in the previous section, it was verified the similarity of the results which led to the conclusion it would not be necessary to repeat the study using other approach.

In these investigations was used the assembly of gears presented in section 4.1.2. where its dimensions and specifications were described. It was examined regarding the kinematics and dynamics in section 4.1.3., which means that these components have been referred intensively along this report. In figure 61 it is represented the set of gears in study.

In the figure it can be seen that there are different colours in the different components as they were all sliced, which was already explained in section 4.2.1.. Each colour represents a part and that measure simplified the construction of the mesh enabling the application of different element sizes in the diverse elements. The contacts among the different components were established as no separation, since it was the option provided by the software more in line with reality.

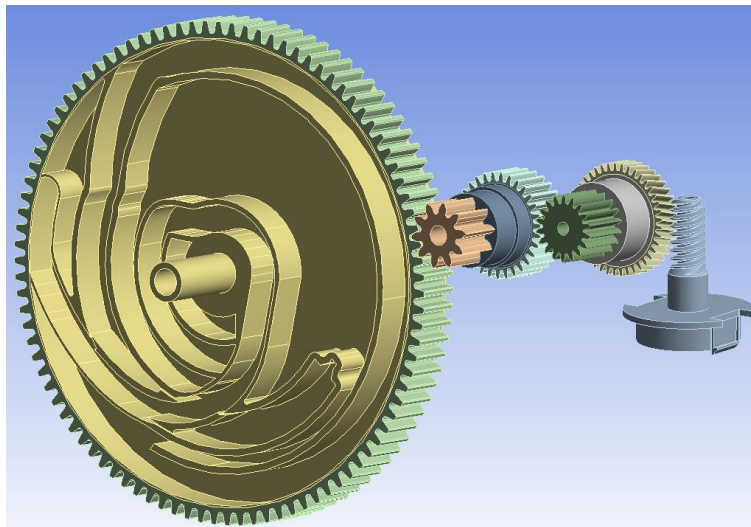


**Figure 61** - Representation of the Assembly Geometry

The main goal of this simulation is to study what happens to this assembly when it is subjected to a temperature of 90 °C. At that temperature, it is important to evaluate if the displacements of the gears causes constraints and, consequently, leads to the malfunction or, even, the stop of the system. In addition, the stresses of the set are assessed in order to verify if the maximum value exceeds the yield strength and, also, the points where the stresses present higher values.

The mesh of this assembly was a difficult task to accomplish due to the geometry complexity of the components which constitutes it. It was constructed 2 meshes, 1 for each analysis performed. The same parameters were applied to both, although the physics preference was different, being CFD for steady-state thermal and mechanical for static structural. The advanced size function adopted was the curvature, which means that the mesh is more refined in the rounded surfaces. In this case it is necessary to employ this method since the assembly consists of gears. The option chosen for smoothing was high and the transition was established as slow in order not to have an abrupt change between the element size of the teeth and the remaining part of the piece, as it can be visualised in figure 62.

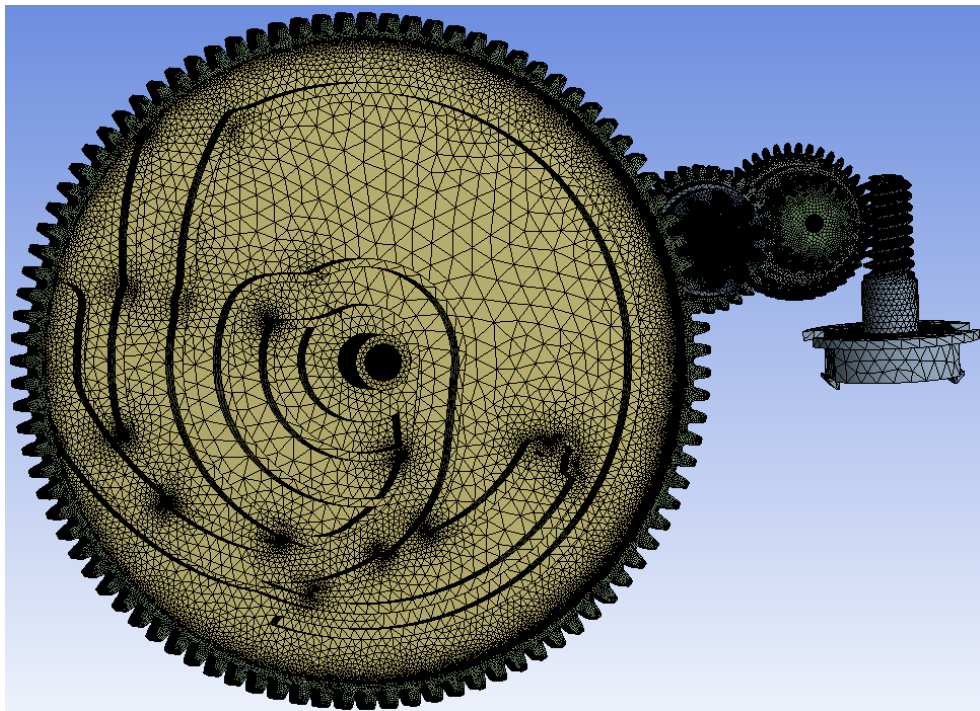


**Figure 62** - Mesh of the Assembly (Front)

The span angle centre was defined as high which means the rounded surfaces will be divided in several parts to be meshed and, with that method, the result will be more uniform. For the same reason, the growth rate of the mesh was defined as 1.20 which maintains an appropriate increase of the cells.

The elements used on the mesh were SOLID92 and SOLID95 which is a tetrahedron defined by 10 nodes and a hexahedron of 20 nodes, respectively. These 3D elements can be regular or irregular according to the shapes of the bodies or the parts where they are inserted. In this specific case, the minimum size applied was 0.15 mm and the maximum was 4 mm. The minimum size of the element was chosen given that, it was necessary to have a small cell to mesh the peculiarities of the teeth without forgetting the number of elements of the assembly.

These characteristics can be seen in figure 63.

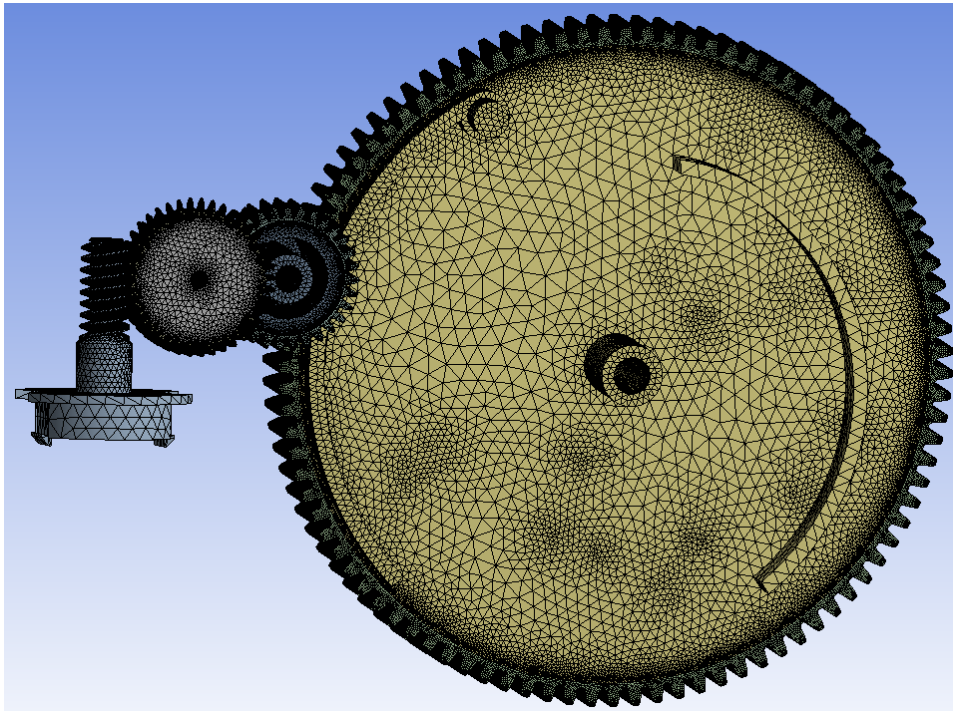


**Figure 63** - Mesh of the Assembly (Back)

The total number of elements is 4 099 988 and of nodes 8 137 724. According to the analysis complexity it is intended to perform, the mesh could not have much more elements, otherwise the computation time would be intolerable. It is important to mention that the element quality of the global mesh is 0.82 and the skewness is 0.25, which indicates it is a mesh close to excellence (ANSYS, Inc., 2013).

To achieve this level of detail, it was necessary to apply the method of face sizing in some of the places where it is established the contact of the teeth. The element size chosen to be applied was 0.05 in order to have the most accurate results. Regarding the worm and the helical gear, it was created a sphere of influence having 2 mm of diameter and the elements which constitutes it have a length of 0.1 mm.

Finally, it was employed a body sizing on the gear meshed with the bigger one, as it was considered that the default mesh was not refined enough. Hereupon, it was applied an element size of 0.15 mm, which installs in every cell of the component and a curvature angle of  $15^\circ$ , which helps to mesh the roundness of the teeth (ANSYS, Inc., 2013). All these details of the mesh can be inspected in figure 64.

To perform the thermal analysis on these components, it was established  $20^\circ\text{C}$  as the initial temperature. The value of  $90^\circ\text{C}$  was not considered for the ambient temperature since this would not create changes in the system, similar to what was explained in section 4.2.4..

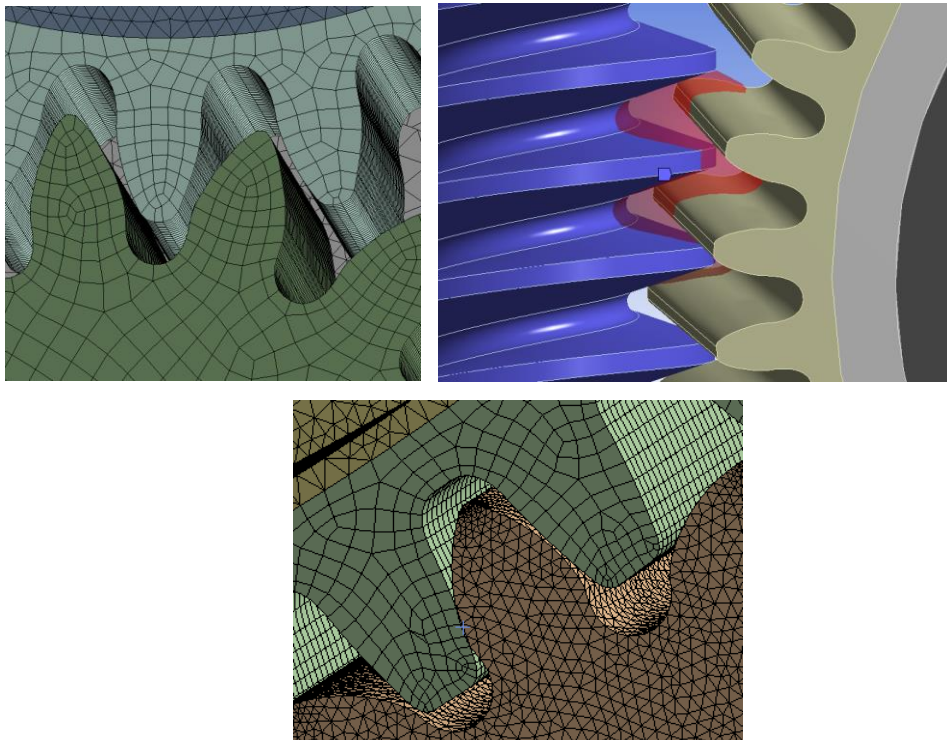


**Figure 64** - Details about the Mesh

Then, all the parts were subjected to a temperature of 90 °C in the complete extension of the bodies. Next, it was applied a convection coefficient of 8 W/m<sup>2</sup>K to all the faces which constitute the 9 parts, at an ambient temperature of 90 °C. Lastly, this 3D investigation was executed as a static problem and it was used an automatic iterative solver chosen by the software in order to perform what is intended. After the simulation is finished, the structural module is coupled and it is necessary to import the results from the first to the second study. The thermal results are one of the boundary conditions employed in the mechanical analysis. Then, the initial temperature of this examination is the same as in the previous situation, and the central axes of all the components are fixed.

The mechanical simulation was completed using the preconditioned conjugate solver, described in the third chapter of this dissertation, with a convergence tolerance of  $1 \times 10^{-8}$ .

The results obtained through this analysis are presented in figure 65. As it can be visualised, figure shows a colour gradient which can be understood through the scale located on its left. The presented total displacements are more significant in the bigger gear where it is registered the maximum value of 0.40 mm. The total deformation considers the 3 directions x, y and z. It can also be mentioned that the displacements are higher as the distance to the centre of the gear increases. In the axes of the different components, the deformation is zero due to the constraint applied. It can also be observed in the gear with higher dimensions that teeth there are



diverse values for the displacements, as in the upper part exists a region more red and the remaining parts present more yellow tones and even green.

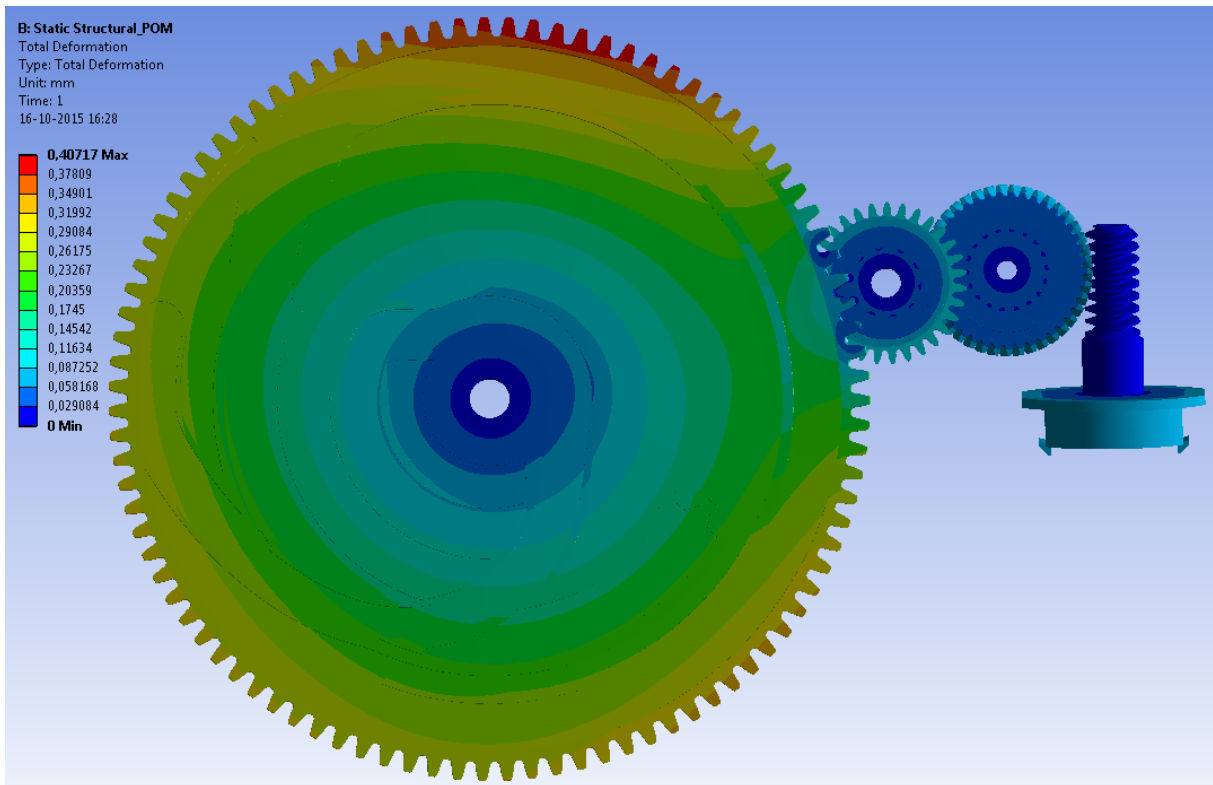


Figure 65 - Results of Total Deformation for Material POM

Regarding the stresses, it is crucial to refer that the maximum presented value is 1166 MPa, which is registered on the contacts between the teeth, being on the left the contact of gears 5 and 6 and on the right the worm and helical gear. In figure 66 it is displayed the contacts where these stresses are maximum and it can be concluded that these values are reached in certain points.

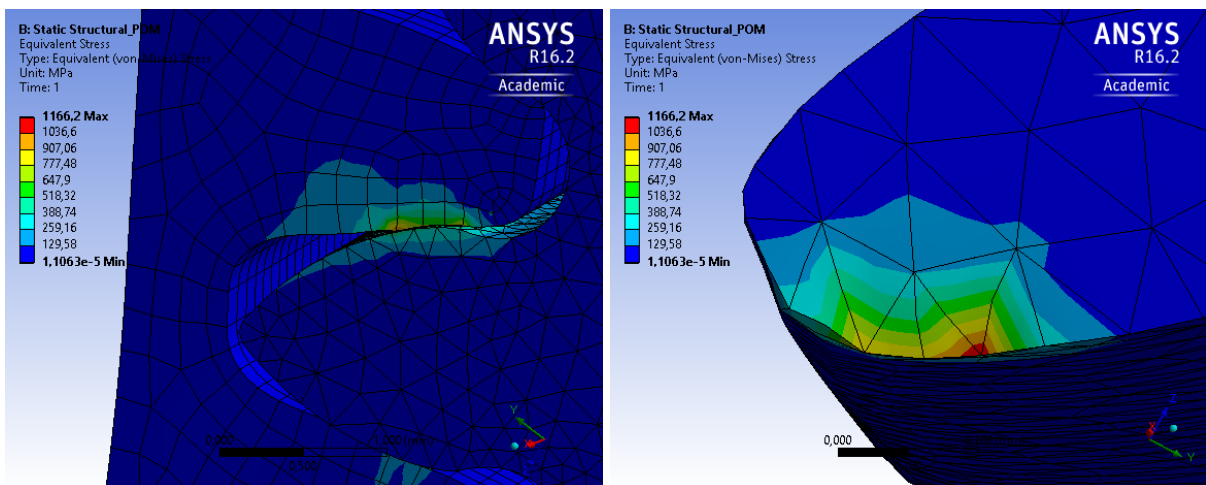


Figure 66 - Von-Mises Stresses for POM Simulation

Those points are called of singularities of the simulation and should not be considered as they do not make sense having in mind that this investigation was performed on the linear range of the material. However, the obtained values for the remaining parts of the component should be taken into consideration. The other components do not display significant values of stress. These results allow to conclude that, at this temperature the teeth reach some values of stress which produce some concern as the yield strength of POM is 61 MPa.

Next, it was analysed the material PP for the same situation. To do so, the exact same boundary conditions were applied to the components, whether in the thermal or the mechanical simulation. In addition, the same solvers were employed to determine the solutions. The objective is to compare both situations and conclude about the differences in the behaviour of the materials.

The analysis for the new material produced the results displayed in figure 67. After an attentive examination over both figures, it can be concluded that they are similar and the gradient of colours does not change much among each other. In this case, the maximum value registered for the displacements is, approximately, 0.25 mm which is around 46 % inferior to the one presented for POM. This may be explained by the fact that, as it can be verified in section 4.2.1., the coefficient of thermal expansion is lower for PP which results in smaller displacements. Once again, the gears have null deformations on the axes and the maximum values on their teeth.

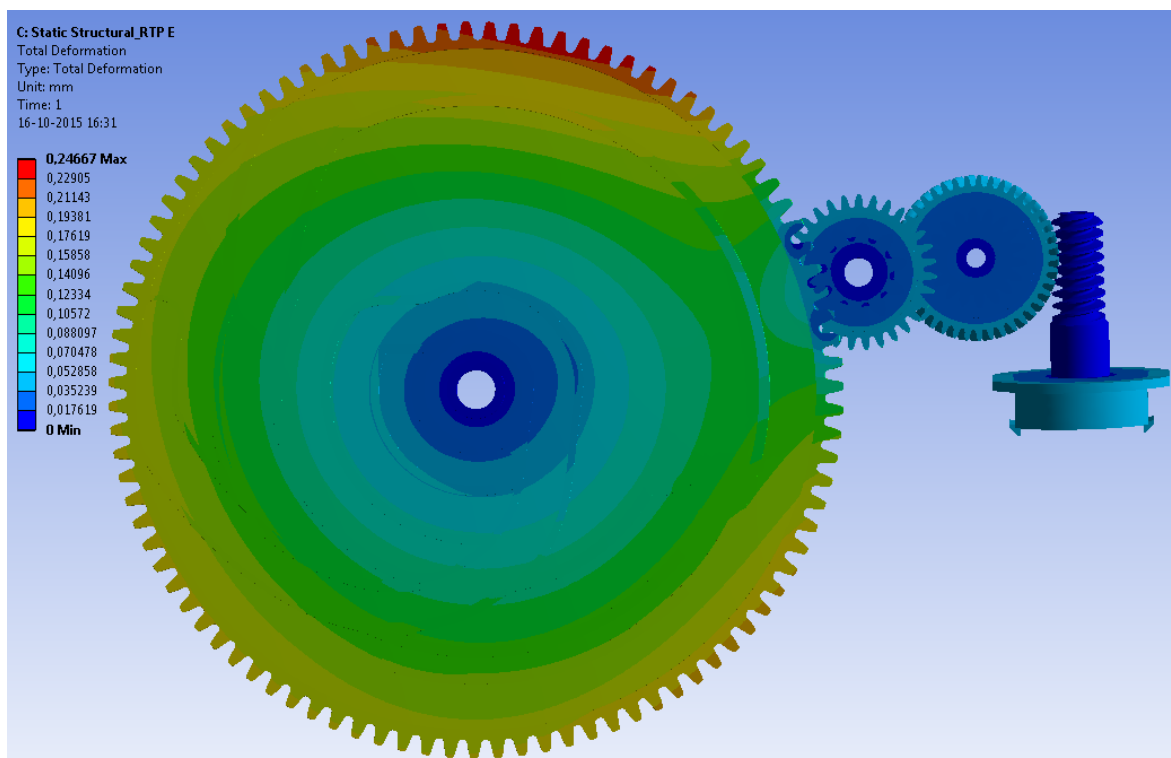


Figure 67 - Results of Total Deformation for Material PP

In what concerns to the stresses, it can be mentioned that the maximum registered value is, approximately, 2478 MPa and it is also in the contacts of the teeth, as it follows in figure 68. The displayed contacts are the same of the previous situation.

This value is higher than what was registered by POM which can be clarified by the higher tensile modulus for the material PP which is 9450 MPa, while the one of POM is 2700 MPa. The remaining parts of the components do not exhibit significant values of stress. With these outcomes it can be concluded, once again, that at this temperature the pieces would enter in the plastic region, suffering permanent deformations. This does not make sense since the simulation was performed on the elastic region and the yield strength of PP is 82 MPa. Like what was already mentioned, these values should not be considered as they present errors of the simulation. However, that does not mean that everything is wrong and the remaining areas of the component should be considered.

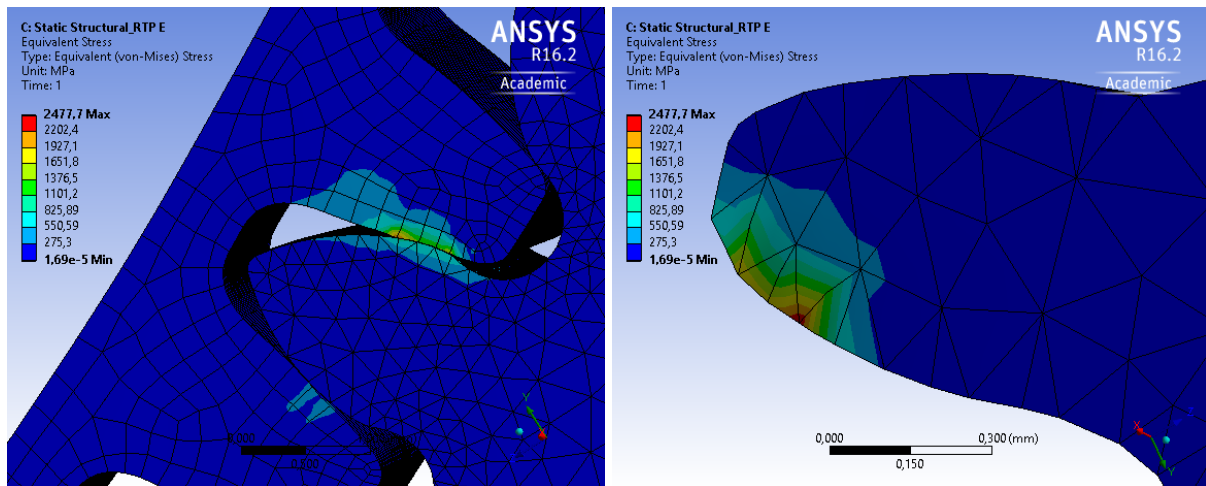


Figure 68 - Von-Mises Stresses for PP Simulation

#### 4.2.6. Comparison and Discussion of the Numerical Results

##### Comparison of the Numerical Results

Since there are 4 sets of results, they were all brought together in table 9 in order to be possible to compare them. The values presented are the 19 points marked on figure 50 on the right where the radial displacements were measured on the extremity of every 5 teeth of the analysed gear (see the point P figure 52). To compare the software modules, the outcomes of both simulations using POM were analysed and they are displayed in the fifth column, being the higher difference of 2.3 %. The same was considered for PP material and the maximum divergence is 2.2 %. Considering these values which are very good, it is proved that steady-state thermal reproduce similar results, in this situation, although they operate with different approaches.

On the other hand, simulations performed with the same method were compared in order to evaluate the discrepancies among materials. For the steady-state, the percentages are displayed on the seventh column and, for fluent, in the last one. The variations round the value of 49 % which means that the use of PP instead of POM represents a very significant difference in regard to the resultant displacements due to thermal loads.

Then, the determined percentages will be displayed in the form of graphic. However, it is only showed a representation for the module and one other for the materials since it is not necessary to examine the same 2 times.

**Table 9** - Results of the Radial Displacements

Steady-State POM (mm)	Fluent POM (mm)	Steady-State PP (mm)	Fluent PP (mm)	Difference between Steady-State POM and Fluent POM	Difference between Steady-State PP and Fluent PP	Difference between Steady-State POM and PP	Difference between Fluent POM and PP
0.27328	0.27737	0.16662	0.16903	1.5%	1.4%	48.5%	48.5%
0.27303	0.27838	0.16646	0.16884	1.9%	1.4%	48.5%	49.0%
0.27203	0.27738	0.16587	0.16864	1.9%	1.7%	48.5%	48.8%
0.27143	0.27577	0.16549	0.16803	1.6%	1.5%	48.5%	48.6%
0.27016	0.27441	0.16473	0.16750	1.6%	1.7%	48.5%	48.4%
0.26977	0.27369	0.16453	0.16750	1.4%	1.8%	48.5%	48.1%
0.26991	0.27361	0.16467	0.16765	1.4%	1.8%	48.4%	48.0%
0.27035	0.27389	0.16502	0.16785	1.3%	1.7%	48.4%	48.0%
0.27090	0.27452	0.16545	0.16813	1.3%	1.6%	48.3%	48.1%
0.27130	0.27516	0.16576	0.16834	1.4%	1.5%	48.3%	48.2%
0.27120	0.27535	0.16573	0.16820	1.5%	1.5%	48.3%	48.3%
0.27052	0.27507	0.16531	0.16773	1.7%	1.5%	48.3%	48.5%
0.26950	0.27476	0.16466	0.16726	1.9%	1.6%	48.3%	48.6%
0.26863	0.27462	0.16411	0.16703	2.2%	1.8%	48.3%	48.7%
0.26844	0.27457	0.16397	0.16708	2.3%	1.9%	48.3%	48.7%
0.26910	0.27478	0.16434	0.16755	2.1%	1.9%	48.3%	48.5%
0.27040	0.27585	0.16507	0.16835	2.0%	2.0%	48.4%	48.4%
0.27172	0.27686	0.16582	0.16955	1.9%	2.2%	48.4%	48.1%
0.27287	0.27719	0.16643	0.16993	1.6%	2.1%	48.5%	48.0%

The circles exhibited in figure 69 show a high level of accordance among them and, even though some values are more distinct than others, it is maintained the consistency since the red

circle has a bigger diameter than the blue in every point. With that said, for this situation, there is no difference in executing the simulation in steady-state or fluent. However, the later presents much more possibilities in regard to the boundary conditions and the solvers employed to perform the studies.

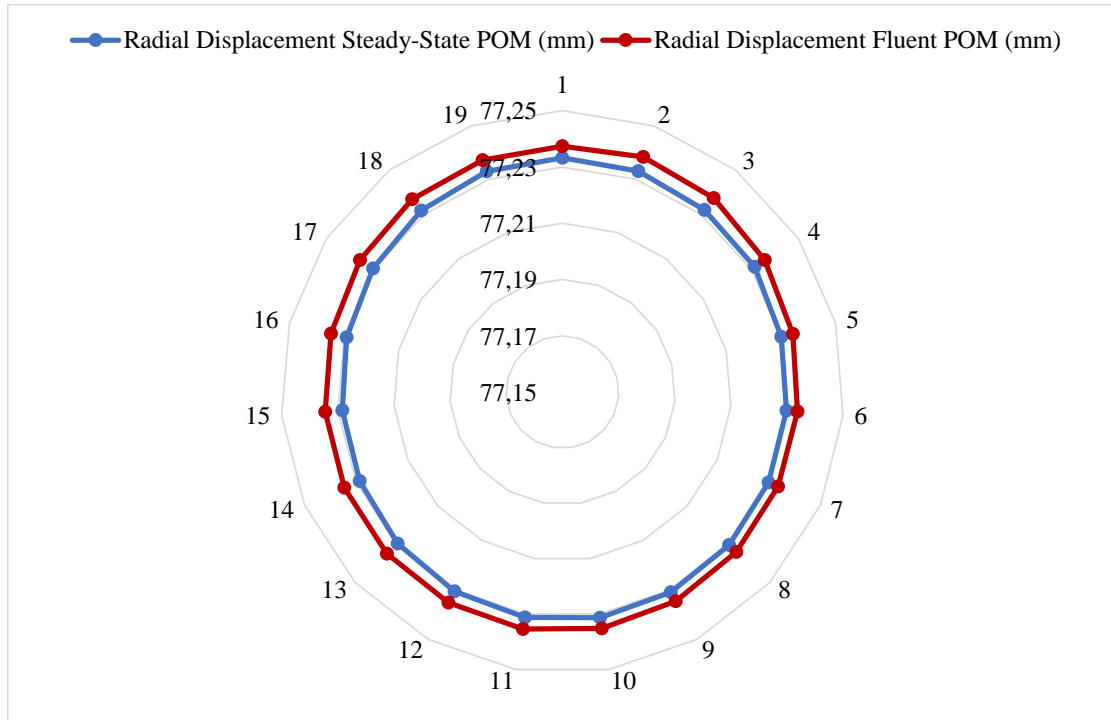


Figure 69 - Comparison of the Software Module

Figure 70 contains a graphic in green which is the real gear whose diameter is 76.96 mm.

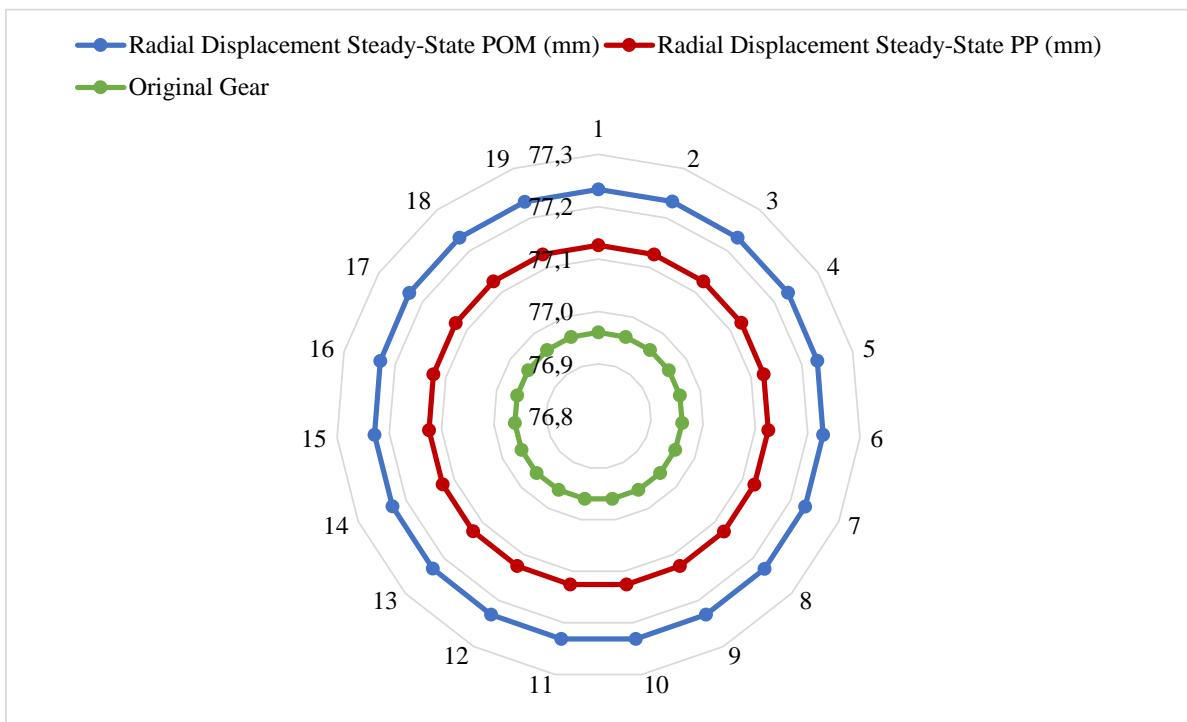


Figure 70 - Comparison of the Materials

Then, the displacements were added to that feature and the graphics of the radial displacements for POM and PP were created. The values are different but the shape is the same, maintaining the proportions among the circles. The change of using a polymer to a polypropylene reinforced with carbon fibres is beneficial as there a huge divergence in adopting one or the other. However, the cost of the polypropylene is much higher than the polymer, which means that pros and cons must be balanced before choosing.

### Analysis of Mesh Convergence

With the intention of evaluating the convergence of the mesh, it was performed a simple analysis on the software. In general 5 simulations were formulated with the purpose of having enough points to draw some conclusions. The geometry used was the gear with higher dimensions and the chosen modules were steady-state thermal and static structural. In addition, it was used the default mesh, in regard to quality, although the element size has been changed between 0.5 and 2 mm with the objective of obtaining different numbers of cells on the component. Then, the same boundary conditions of the previous studies were applied and, once the coupled simulation was finished, the outcomes were evaluated.

In the 5 analyses, it was verified the displacement on the exact same point. In table 10, there are the number of mesh cells used as well as the results of the displacements.

**Table 10** - Number of Mesh Cells and Results

Number of Mesh Elements	Displacement (mm)
249 342	0.27247
490 449	0.27293
1 068 822	0.27304
1 447 652	0.27306
1 954 945	0.27306

Then, with the points of the table it was constructed a graphic where it is simple to evaluate the convergence of the mesh. As the number of elements increases, the value of the displacement is approaching the equilibrium which means it is heading to the final result. Through the analysis of the table, it can be confirmed that, with the amount of decimal numbers available, the last 2 values of deformation are the same. This fact leads to the conclusion that the mesh is converging, as it can be verified in figure 71. It can also be stated that with a much smaller amount of cells (approximately  $10 \times 10^5$ ), the obtained results would be very similar. However, in order to perform a simulation in the module Fluent the mesh needs to be very dense, as the

one used in the investigations, since the interaction with the air forces the elements to be smaller. Consequently, the same density of mesh was implemented in the module Steady-State Thermal or otherwise, it would not be possible to compare the results determined in both examinations.

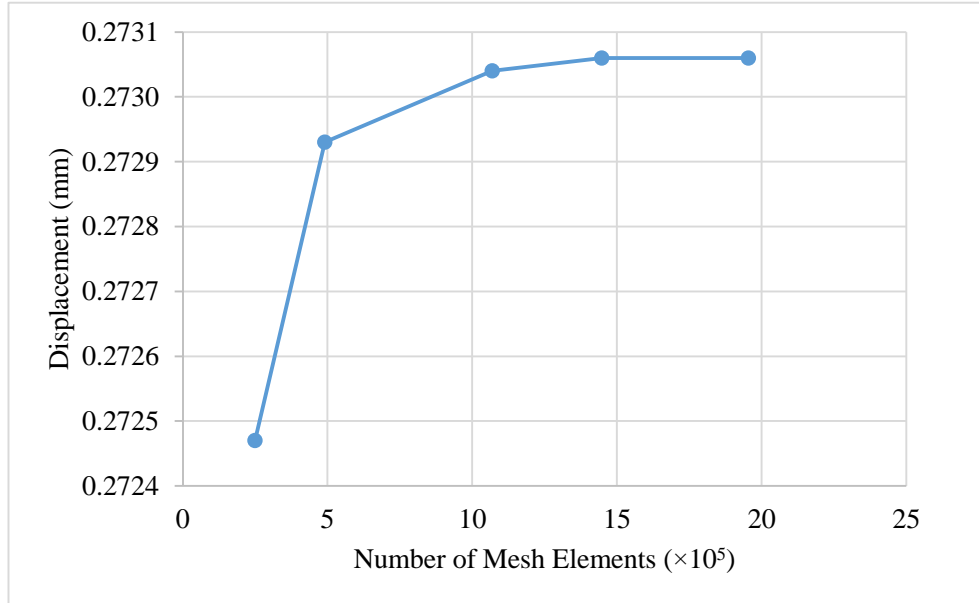


**Figure 71** - Results about Convergence of the Mesh





“No amount of experimentation can ever prove me right; a single experiment can prove me wrong.”

Albert Einstein

## 5. EXPERIMENTAL VALIDATION

It is fundamental to perform experimental activities as, in this situation, it is intended to compare the outcomes which means that the numerical results must be validated. The main goal of performing two types of analysis is to try to understand what sort of errors are inherent to each of the studies. There are diverse sources of errors, where from the experimental activity or the numerical analysis. With the comprehension of their characteristics, it is possible to conclude about how to diminish or eliminate them.

In this chapter it will be described and summarised what was performed in the experimental activity. Firstly, the conditions are detailed in order to clarify the parameters which may influence the final results as well as the whole procedure followed during the experiments. Then, the outcomes are displayed and analysed in regard to the background acquired along the past chapters. Consequently, it is established a comparison between the numerical and experimental results, with the presentation of graphics and tables. Finally, some recommendations are mentioned about the functional dimensions of manufacturing with the purpose of studying if the applied tolerances are in agreement with the correct operation of the system.

### 5.1. DESCRIPTION OF THE EXPERIMENT

The experimental activity was executed at Bosch Car Multimedia, in their metrology laboratory and it was handled by an experienced technician. The equipment used is displayed in figure 72 and it is a 3D sensor called COMET 6 16M, produced by Steinbichler (STEINBICHLER - Inspiring Innovation, s.d.).

The sensors include the proven single-camera-technology which allows a fast, precise and easy adaptation of the field-of-view to the application in study. The compact sensor design and new handling system are designed to offer maximum user friendliness and ergonomic operation.

COMET 6 features a powerful LED and innovative projection optics. A technology called 3D Intelligent Light Control (ILC) is the adaptive projection which locally adapts the light quantity projected onto the object surface. This equipment presents a high-resolution 16 megapixel camera features a previously unprecedented precision for the digitization of objects with fine structures or for applications requiring the highest level of detail. Paired with the fast measurement time, COMET 6 offers maximum efficiency. The datasheet of this equipment can be consulted in the appendix C.



**Figure 72** - Equipment used in the Experimental Activity (STEINBICHLER - Inspiring Innovation, s.d.)

The main goal was to analyse the gear of higher dimensions and evaluate the consequences of thermal loads on it. Basically, the point was to determine the displacements caused by heating from 20 °C to 90 °C using the same conditions and adopting an equal process as well. The most important parts to be inspected are: the teeth because they establish the contact with other gears; the paths located in the front of the gear (see figure 62) as there is a pin which shifts inside of it; the component of angular adjustment (see figure 63) since it could threaten

this function.

This activity was performed in 2 distinct phases: (i) check if the CAD model was in agreement with the real component and (ii) the deformations of the part are calculated at the high temperature. It is fundamental to compare the 3D model with the piece as it is required to have the same reference and positions in order to measure the displacements.

It is necessary to apply a spray to the component as the teeth of the gear are very small and this will contribute to perform an experimental activity with more precision. Two pages of the spray datasheet can be consulted in appendix D since they are the most important. It can be verified that this substance is constituted by 74 to 78 % of acetone and 18 to 19.5 % of propanol. Its boiling temperature is located between 54 °C and 84 °C and, in this range is also included the acetone's boiling point, which is around 56 °C. When that occurs, a white layer deposits in the part, whose thickness is, at maximum, 0.01 mm and that helps to reveal the details of the gear teeth.

The execution of the primary part of the experiment is represented in figure 73. The component is held on a support and the laser is shot in order to detect the material and create an image of the gear on that side. The substance attached to the plate where the part is being supported is used as a reference to match the figures in a later phase. The temperature inside the laboratory is maintained at 20 °C and the humidity is of 60 %.

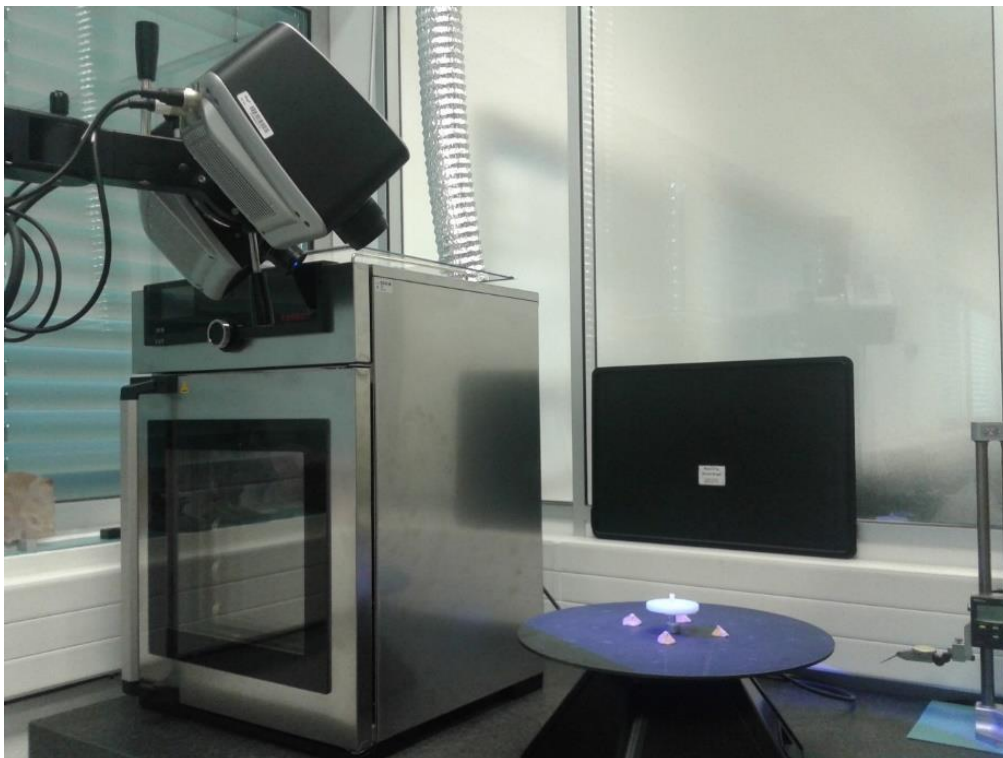


**Figure 73** - Experimental Activity of the Gear at 20 °C

Next, the gear was inserted in a chamber and the temperature was established at 90 °C, as it can be seen in figure 74. In order to ensure that the temperature in the component was stable during the measurements, the gear was maintained inside the chamber for one hour after the equipment reached the target temperature. Then, with the laser the software creates a 3D model of the component which can be compared with the object modelled using the design software called NX. It is important to mention that, for the measurements of points in both sides of the gear, the component was rotated inside the chamber with the help of a mechanism specially manufactured for this experiment. This solution allowed to avoid the manual rotation of the component that may introduce positioning errors which lead to an unacceptable comparison of results.

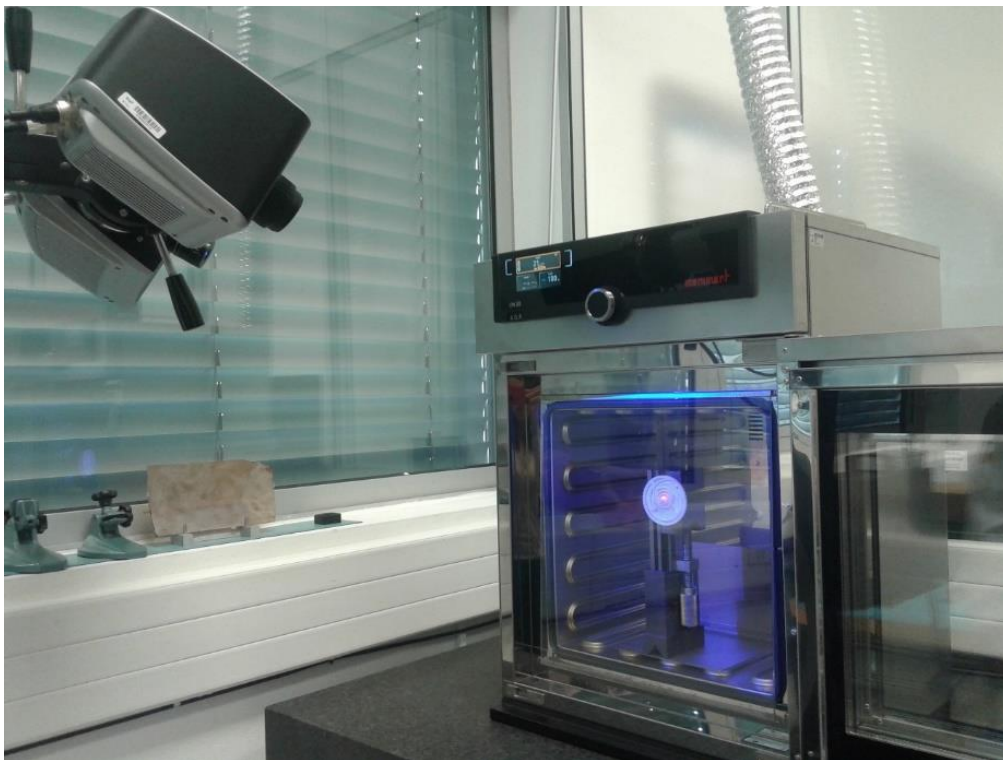


**Figure 74** - Experimental Activity of the Gear at 90 °C

### 5.2. PRESENTATION OF THE RESULTS

In the next 8 figures (75-82) the results of the experimental activity are showed for the different parts analysed. According to the legend, the first corresponds to 20 °C and the second to 90 °C.

It is important to explain the figures and the displayed information in order to clarify the parameters of the experimental activity. On the left there is a scale which allows to understand

the magnitude of the displacements installed in the piece. It is only considered the radial displacements since they are the most significant, which is why the displacements of direction x are null. In every box, attributed to each point, there is a nominal value which corresponds to the length in the 3D model while the actual cell is occupied with measure obtained in the experiment. Then, the deviation between them is calculated for the 3 coordinates x, y and z. In the line called 3D it is the module of the vector constructed with the 3 values of deviation. This is calculated for both analyses which means that, in the final, it is possible to determine the vectors of displacement and conclude what the real values for the displacements are. If they are both compared to the 3D model, the difference between them coincide with the displacements occurred during the experiment due to the thermal loads. The first 2 figures concern the teeth displacements measured on the extremity of it, the next 4 figures regard the paths of the gear being 2 from one perspective and the other 2 in the opposite direction. Finally, the last 2 are about the component for angle adjustment which is similar to half of a circle.

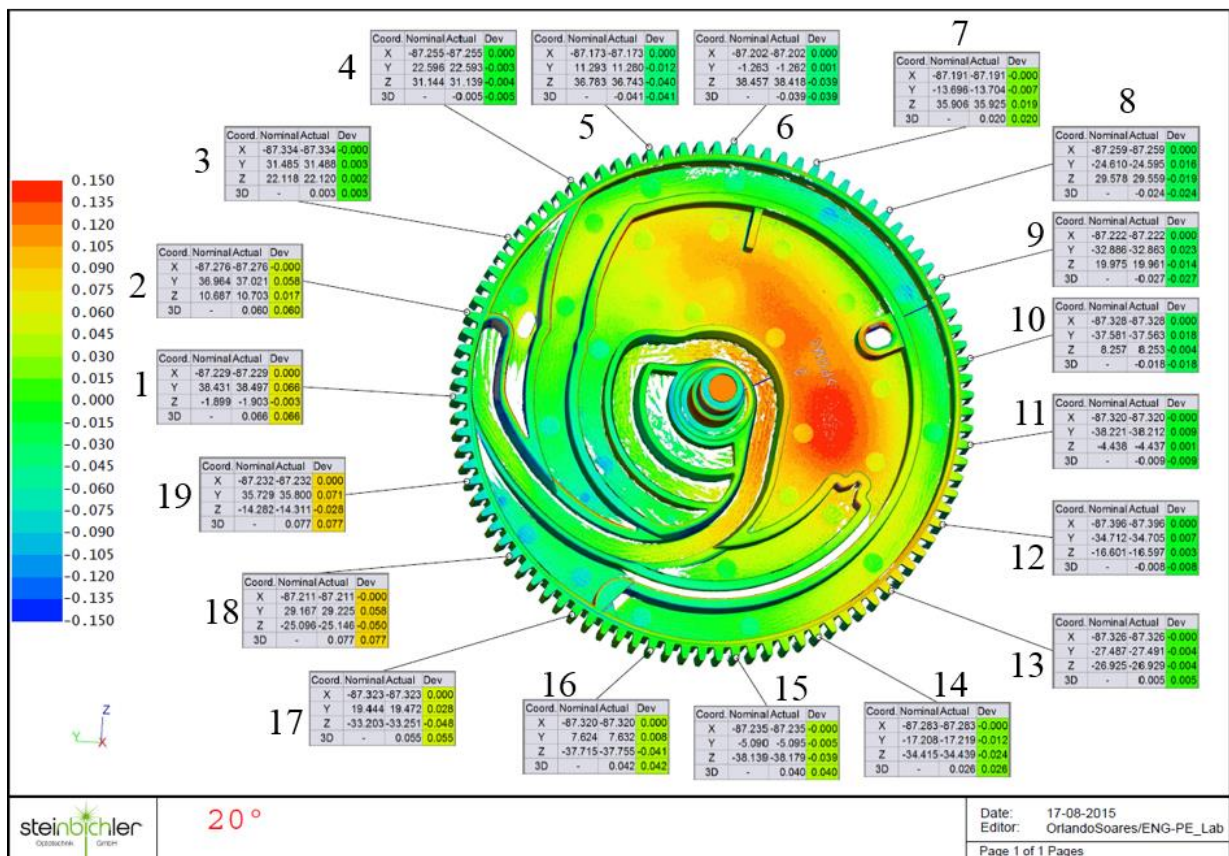


Figure 75 - Experimental Results for the Teeth at 20 °C (mm)

## 5. EXPERIMENTAL VALIDATION

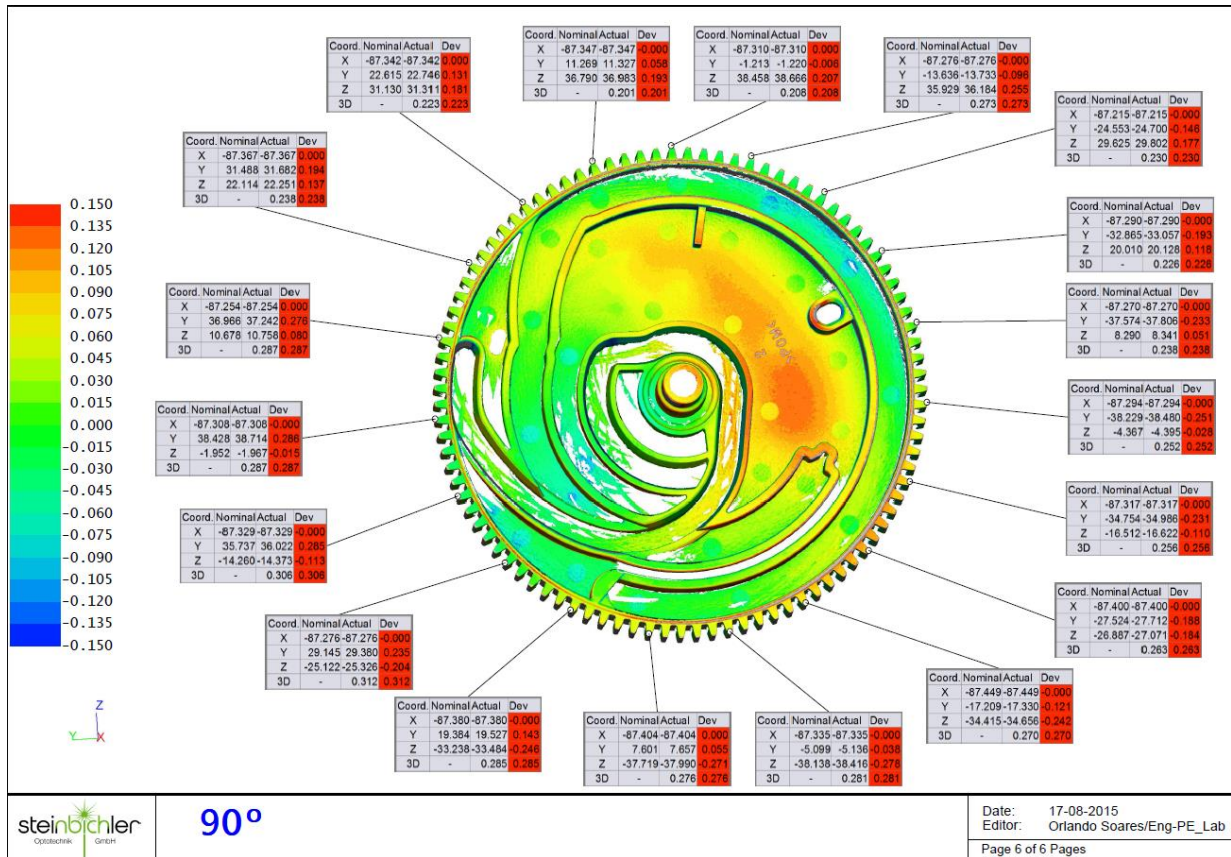


Figure 76 - Experimental Results for the Teeth at 90 °C (mm)

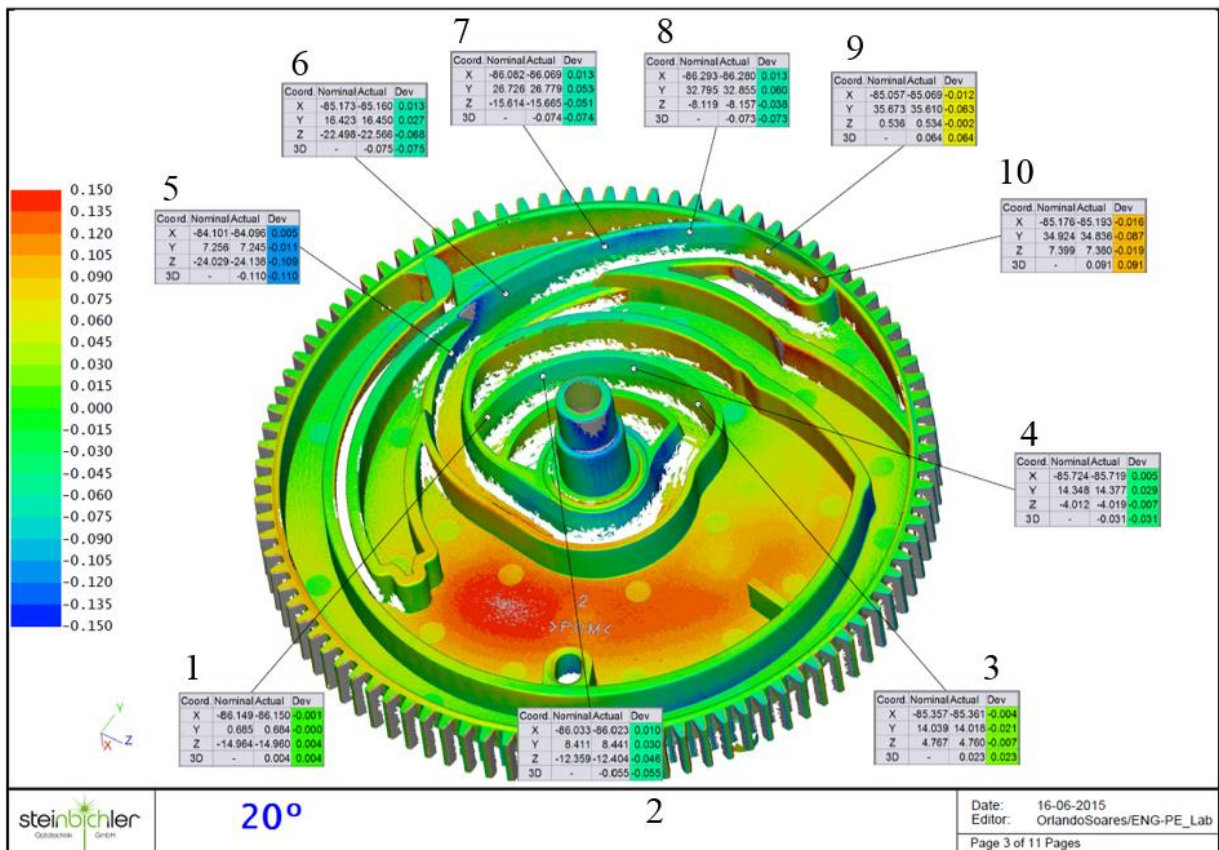


Figure 77 - Experimental Results for the Path of the Pin at 20 °C (mm)

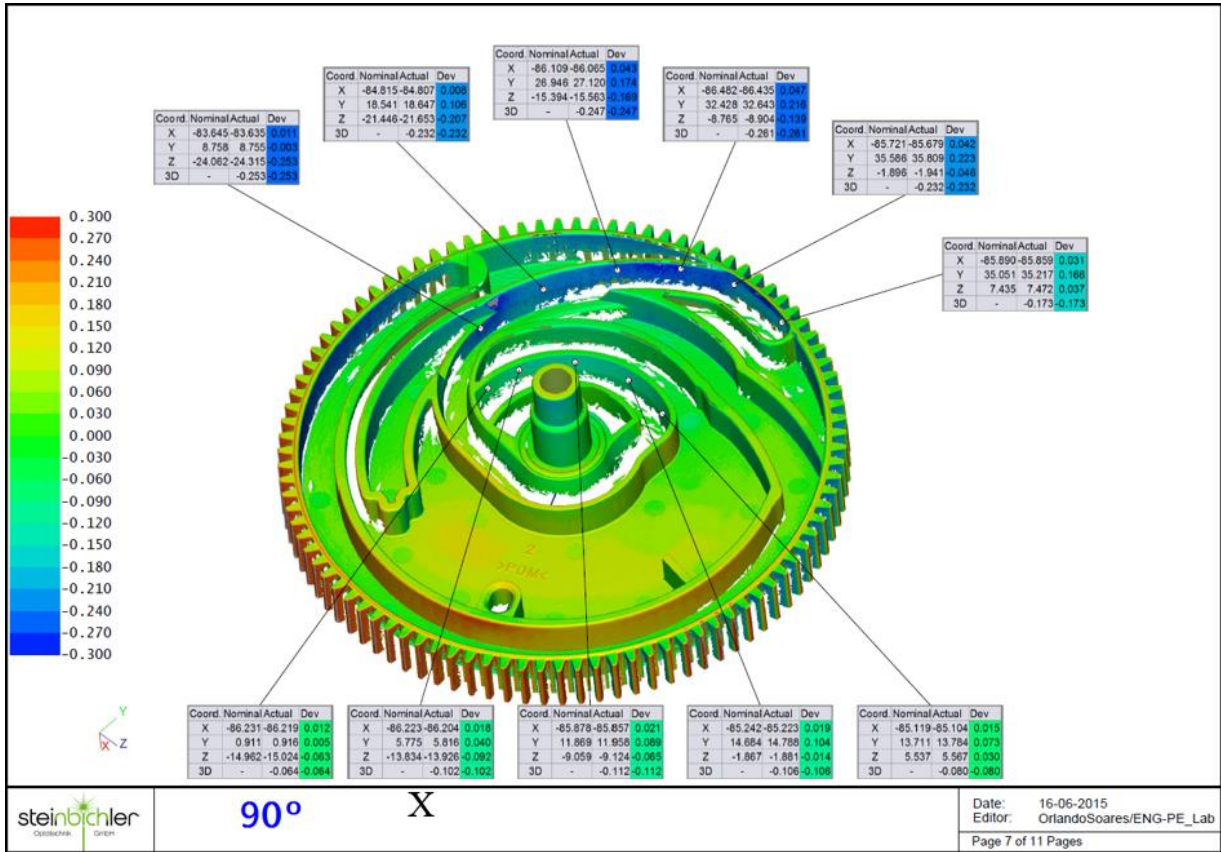


Figure 78 - Experimental Results for the Path of the Pin at 90 °C (mm)

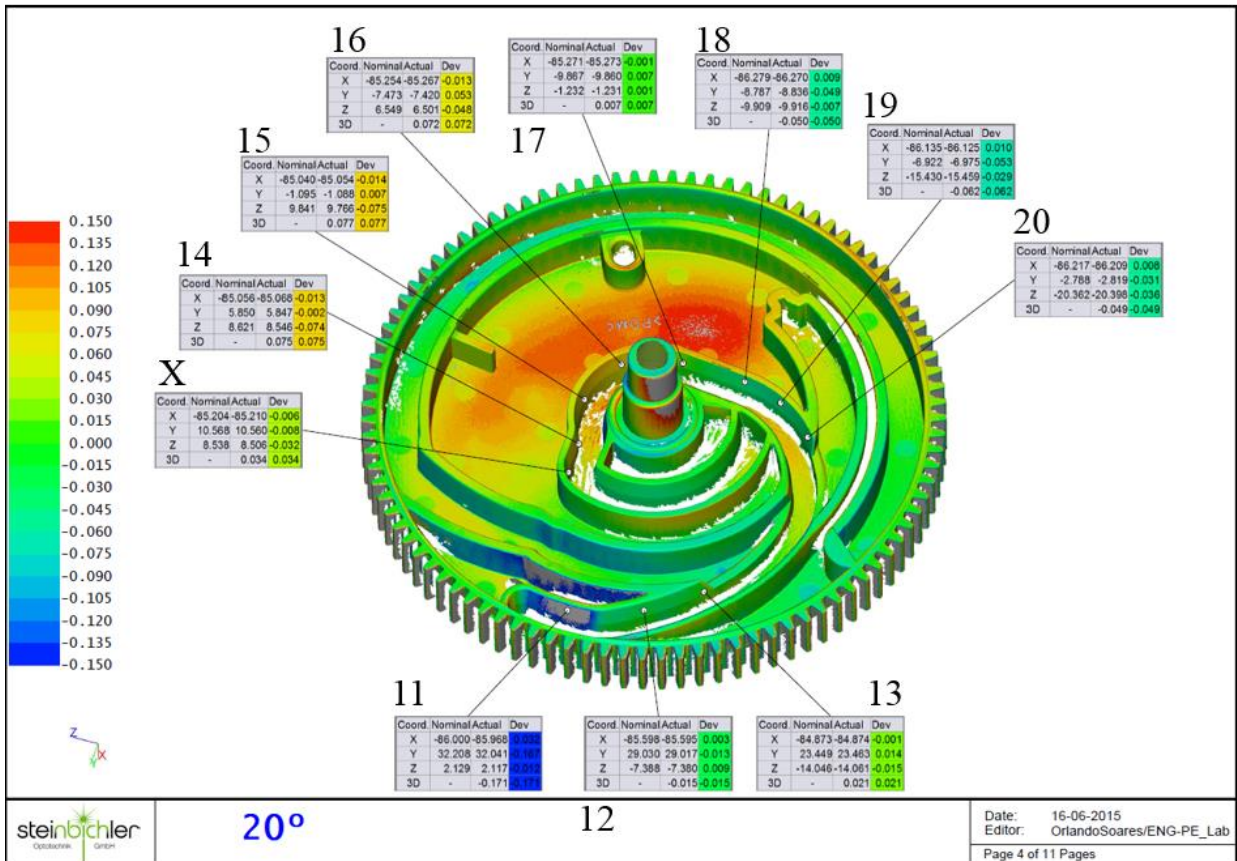


Figure 79 - Experimental Results for other part of the Pin Path at 20 °C (mm)

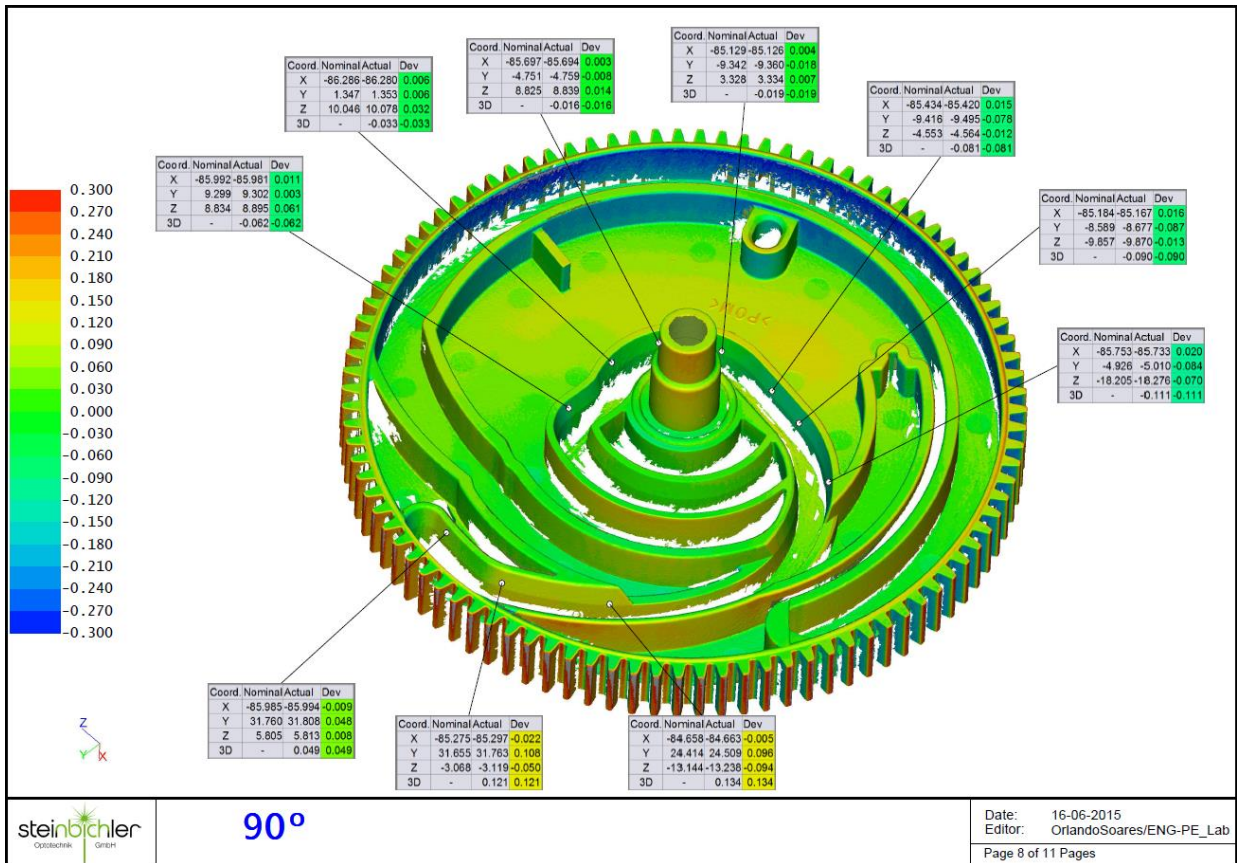


Figure 80 - Experimental Results for other part of the Pin Path at 90 °C (mm)

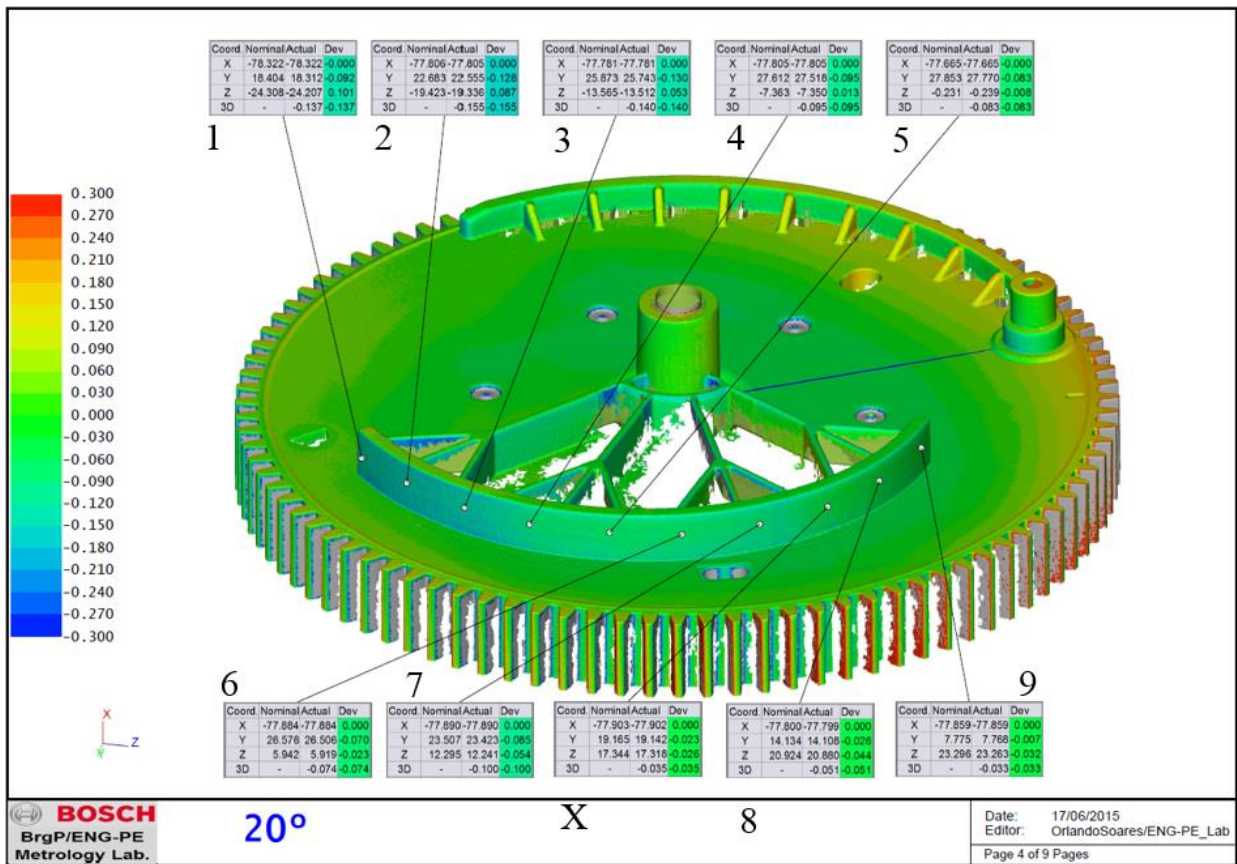


Figure 81 - Experimental Results for the Angular Adjustment Component at 20 °C (mm)



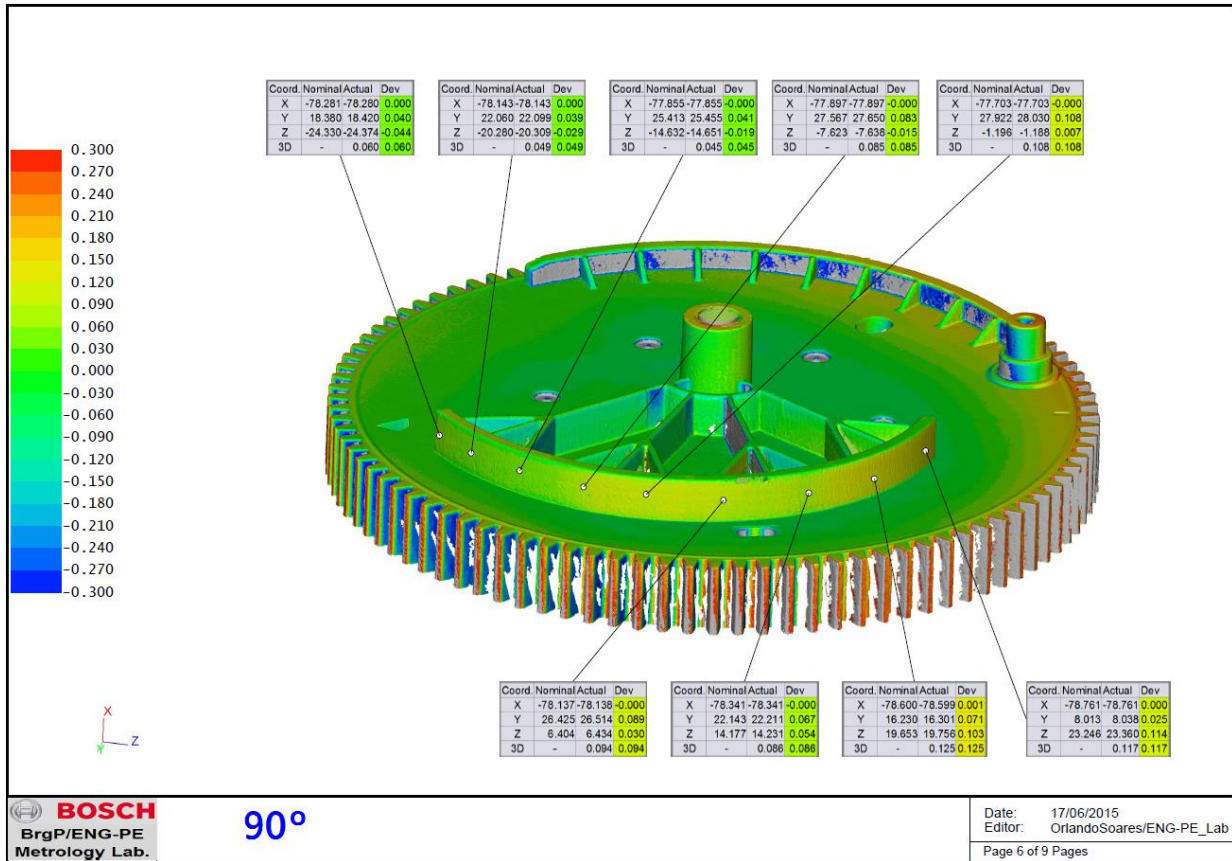


Figure 82 - Experimental Results for the Angular Adjustment Component at 90 °C (mm)

### 5.3. COMPARISON OF THE NUMERICAL AND EXPERIMENTAL RESULTS

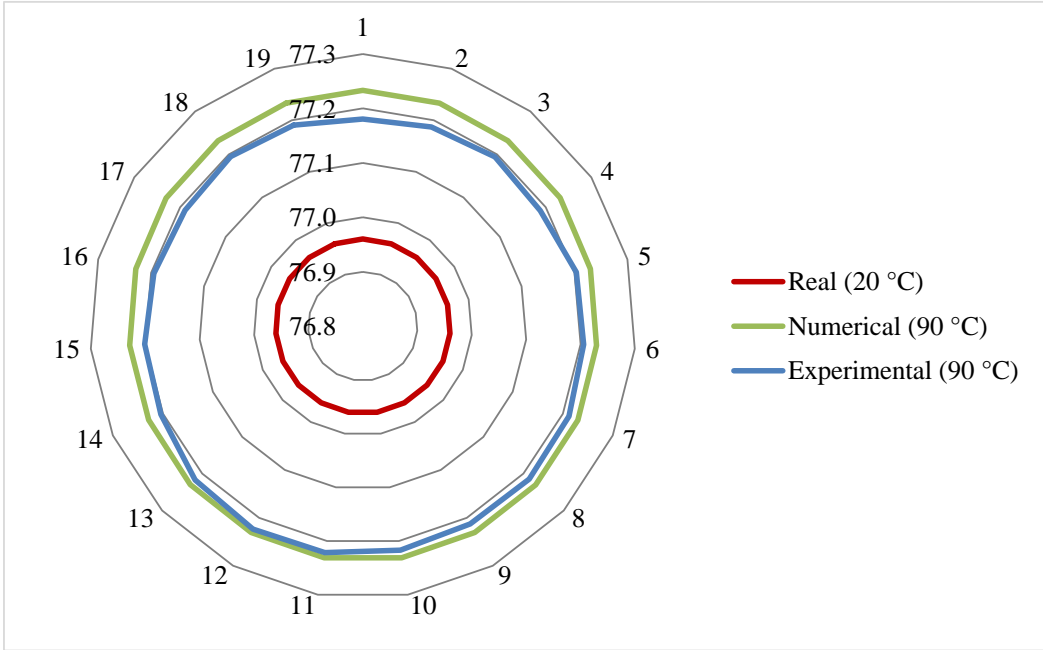
After having all the numerical studies as well as the experimental activities finished, the results are collected and joined in tables and graphics to conduct a simpler analysis. In this section, these elements are displayed and discussed to be possible of drawing some conclusions from the performed tasks.

Table 11 concerns the teeth of the gear which are represented on figures 75 and 76. The measurements of the radial displacements were performed every 5 teeth which results in 19 points. It must be mentioned that the values for the radial displacements are always higher for the numerical analysis. From the column called difference, it can be noted that the biggest divergence among both analyses is of 21 %. From the work previously performed, which was already studied in the background, this value represents that the results are in agreement with each other (Li et al., 2012; Wang et al., 2013; Fratila & Radu, 2010).

**Table 11** - Comparison between Numerical and Experimental Teeth Results

Points	Numerical (mm)	Experimental (mm)	Difference
1	0.273	0.220	21%
2	0.273	0.227	18%
3	0.272	0.234	15%
4	0.271	0.228	17%
5	0.270	0.243	10%
6	0.270	0.246	9%
7	0.270	0.252	7%
8	0.270	0.254	6%
9	0.271	0.253	7%
10	0.271	0.257	5%
11	0.271	0.262	4%
12	0.271	0.263	3%
13	0.270	0.257	5%
14	0.269	0.244	10%
15	0.268	0.241	11%
16	0.269	0.235	14%
17	0.270	0.229	17%
18	0.272	0.235	15%
19	0.273	0.230	17%

In figure 83, it is the graphical representation of the data previously presented in table 11.



**Figure 83** - Teeth Displacement Results (mm)

The circle of the real gear component (in red) at 20 °C is characterised by a diameter of 76.96 mm which is the real external diameter and it will be used to understand the magnitude of the displacements from the numerical and experimental analyses at 90 °C.

These figures present a similar behaviour, although the element during the numerical examination registers higher values of radial displacements in comparison with the experimental one. In contrast, from the information obtained in both analyses, it is concluded that the gear does not increase its diameter the same way in the various directions, even though, these divergences are more noticeable in the experimental activity results. The differences between the values of both examinations are registered in table 11.

In table 12 the results for the points along the path are presented. The points marked with an X in figures 78 and 79 were not used as there were more in some figures than in others. The numbers of the figures coincide with the ones on the table in order to be simple to identify them.

**Table 12** - Comparison of the Numerical and Experimental Path Results

Points	Numerical (mm)	Experimental (mm)	Difference
1	0.106	0.068	43%
2	0.107	0.063	52%
3	0.108	0.127	17%
4	0.109	0.058	61%
5	0.180	0.144	22%
6	0.199	0.160	22%
7	0.215	0.172	22%
8	0.236	0.189	22%
9	0.251	0.294	16%
10	0.251	0.263	5%
11	0.224	0.220	2%
12	0.215	0.137	44%
13	0.193	0.114	52%
14	0.091	0.137	40%
15	0.074	0.035	72%
16	0.073	0.052	34%
17	0.074	0.062	18%
18	0.077	0.098	24%
19	0.095	0.107	13%
20	0.119	0.111	7%

From the analysis of the displayed information, it is noted that some high differences were registered. In this case it was a little complicated to measure the radial displacements in the exact same places which can explain these variations. In this situation it was not possible to construct a polar graphic as the points does not belong to the same circle and, for that reason, the distance between the point and the centre of the circle is different for every one of them.

Even though the results were not so good, the differences for the points between 5 and 10 were acceptable which means this segment of the path presented the smallest differences. Concerning the others, it is possible to mention that, in general, the values of the numerical analyses are higher than the experimental ones, although there has been some exceptions.

Next, there is the analysis of the results for the angle adjustment component whose figures are 81 and 82. The points marked with an X in figure 81 were not used as there were more in some figures than in others. Just to remember that this component allows the angular adjustment of the combiner which is where the image is projected to the driver. The percentages determined for these outcomes can be seen in table 13 and they are very good wherein the maximum value is 16 % which proves that the numerical and experimental results are in agreement (Li et al., 2012; Wang et al., 2013; Fratila & Radu, 2010).

**Table 13** - Comparison of the Numerical and Experimental Angle Adjustment Component Results

Points	Numerical (mm)	Experimental (mm)	Difference
1	0.218	0.196	11%
2	0.213	0.203	5%
3	0.209	0.186	12%
4	0.202	0.180	11%
5	0.198	0.192	3%
6	0.193	0.168	14%
7	0.188	0.186	1%
8	0.184	0.176	4%
9	0.175	0.149	16%

In order to finish the presentation of the numerical and experimental outcomes, the graphic correspondent to the previous table is displayed in figure 84. In a similar way to the first graphic, there is the red line, whose diameter is 27.5 mm, wherein it is correlated to the original component. Moreover, this is used to establish a visual comparison between the values of the radial displacements and conclude about their differences.

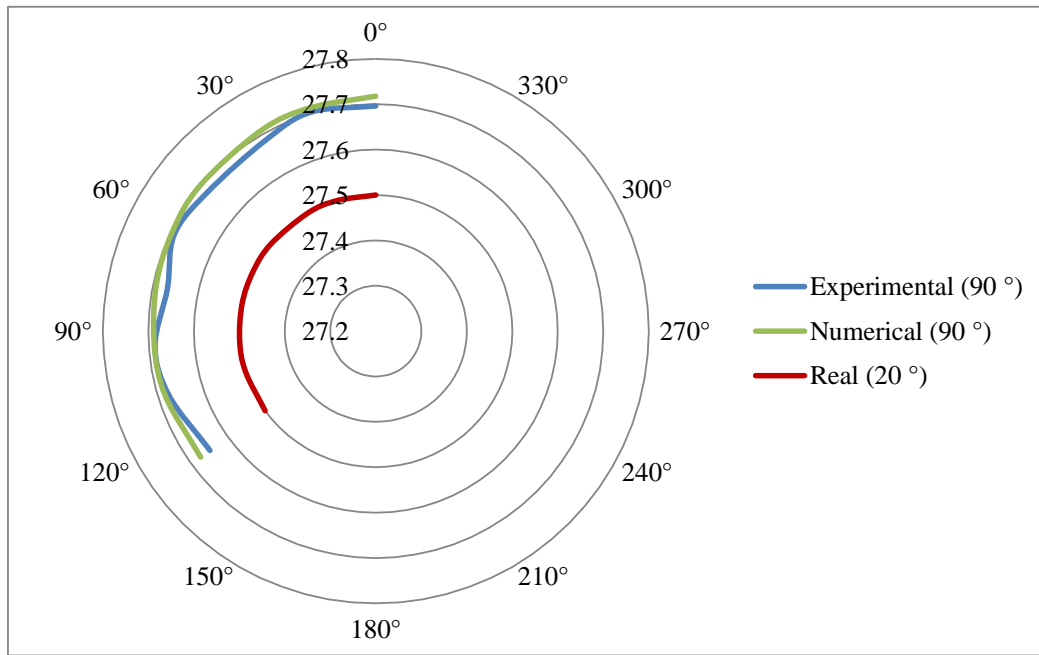


**Figure 84** - Angular Adjustment Component Displacements (mm)

Then, there is a green one for the numerical results which maintains the same shape as the original, while the blue line (experimental) presents some changes in its format. These variations could interfere with the correct function of the system and not fulfil entirely what is intended. Even if that does not happen, it could also diminish the lifetime of the component as some damages would be caused over time. Through the analysis of the figure, it can be concluded that the numerical results are superior to the experimental in each point.

Considering that it has been performed a comparison between two types of results, it is important to refer some sources of error. Whenever something is measured or simulated, there is an error associated with it. The equipment used, the experimental parameters, the software, the component, the conditions and the procedure, among others are just some of the factors which will, next, be explained in detail.

The equipment presented in the section 5.1. has an associated error of 50  $\mu\text{m}$  in every measurement it performs. That plus the spray pulverised on the component can alter the values of the experimental activity.

Similarly to the equipment, the software also introduces a correlated error in every simulation it performs since the numbers are always rounded in the results and, even in the data inserted by the user in the material properties, for example. It is understandable that a computational programme presents some limitations when compared to real situations.

One other source is the conditions applied to each situation, in which it is very difficult to reproduce in the exact same way what happened in the experiment and what was employed

in the numerical model. There could have been a boundary condition or a solver which reproduced some divergence between either cases or, even, some parameter of the experiment which was not possible to be included in the software.

It is also important to mention that, for example, if for some reason the temperature is not the same in every point of the gear inside the chamber, this would interfere the results. One cannot be sure if that happened as there is no method to control it, while in the software it is certain that was the situation since the user defines the conditions of the simulation.

Thereafter, it is crucial to refer that the tested component could be a defective one or be altered somehow. If that was the case, the use of a different gear would produce distinct results in the experimental activity.

Finally, in a simulation, it is possible to follow a node and, with that, the user knows perfectly what occurred on that point. On the other hand, in a real piece that cannot be done and it is more difficult to be ensure if it is being measured the same point. This source of error is very plausible and understandable, however, in order to be eliminated, it would introduce some complex method on the experiments.

In general, the results obtained in the numerical analyses are higher than the experimental ones and that differences might have been caused by the aforementioned sources of error.

### 5.3.1. Recommendations for the Functional Dimensions of Manufacturing

In this section are presented the tolerances applied on some measures of the gears which were collected in table 14. They were provided by the company Pioneer which, as it was already been referred, is the producer and supplier of these mechanisms.

**Table 14** - Tolerances Applied on the Gears

	Measure (mm)	Tolerance (mm)
External Diameter of Gear 1	5.57	+/- 0.03
External Diameter of Gear 2	17.28	+/- 0.05
External Diameter of Gear 3	10.40	+/- 0.05
External Diameter of Gear 4	16.40	+/- 0.05
External Diameter of Gear 5	10.40	+/- 0.05
External Diameter of Gear 6	76.96	+/- 0.05
Centre Distance of Gears 1 and 2	10.63	+/- 0.05
Centre Distance of Gears 3 and 4	12.25	+/- 0.05
Width of the Component for Angle Adjustment	4.40	+/- 0.10
Width of the Path	3.00	+/- 0.05

The displayed values will be used to investigate some conditions and mention some recommendations about the functional dimensions of manufacturing.

Next, it is evaluated the situation of the contact between the bigger gear (6) and the one to which it is attached (5). The tolerance for the external diameters of gears 5 and 6 is of +/- 0.05 mm, as it can be confirmed in table 14. The tolerance of the centre distance for gears 5 and 6 was not provided which means that the situation is analysed without this information. Although it could change the scenario of the contact, the conclusions have to be drawn without this data.

Firstly, some geometrical dimensions are introduced before mentioning the determination of the clearances. The term  $h_f$  refers to the radial height of the gear teeth, since the root until the primitive circle and it can be calculated with the equation 5.1.

$$h_f = \frac{d_p - d_i}{2} \quad (5.1)$$

where  $d_p$  refers to the primitive diameter and  $d_i$  to internal diameter.

Furthermore,  $h_a$  characterises the radial distance from the pitch circle until the beginning of the teeth. The expression 5.2 shows how to determine this parameter.

$$h_a = \frac{d_e - d_p}{2} \quad (5.2)$$

where  $d_e$  represents the external diameter.

With that said, the difference between them results in the gap from the top of a gear tooth until the root of the meshed tooth. Hereupon, and using the information of table 3 on the section 4.1.2.,  $h_f$  is 0.72 mm for the gear 5 and 1.44 for the gear 6. In addition,  $h_a$  presents the value of 1.20 mm and 0.48 mm for gears 5 and 6, respectively.

After explaining these parameters, there are conditions to estimate the values of the clearances. If it is considered the space between the root of gear 5 and head of gear 6, the calculated value for the average radial clearance ( $\bar{c}_r$ ) is 0.24 mm, by equation 5.3.

$$\bar{c}_r = h_{f5} - h_{a6} = 0.24 \text{ mm} \quad (5.3)$$

Otherwise, if it is examined the gap between gear 5 head and gear 6 root, the result is also 0.24 mm which can be proved by the next calculation.

$$\bar{c}_r = h_{f6} - h_{a5} = 0.24 \text{ mm} \quad (5.4)$$

Finally, it can be concluded that if both tolerances are 0.05 mm, then the situation for the total clearance ( $c$ ) is the one presented in formula 5.5:

$$\bar{c}_r - 0.1 < c < \bar{c}_r + 0.1 \quad (5.5)$$

Analysing the first segment of the relation,  $c > \bar{c}_r - 0.1$ , if the radial clearance is of 0.24 mm and to this is subtracted 0.1 mm as the pieces were manufactured bigger, then there is only 0.14 mm of space between the parts. Having in mind that the maximum displacements registered for this gear were 0.27 mm, the area left is not enough for the teeth to expand. In addition, the system cannot work properly, with the existence of noise and high damage of the polymer components especially in the course of time. In order to solve the aforementioned problems, one of two procedures could be performed. First, for the system not to present interference between the pieces, the clearance must be increased which it is possible by maintaining the same gears, diminishing the size of the tooth, more specifically the measure  $h_a$ . The analysis of the equations 5.3 and 5.4 allow to conclude that lowering the length  $h_a$  leads to the increment of the clearance. The problem is that it may threaten the continuity of the engagement. Another option is to redraw the whole train and change the gear size as well as the number of teeth, maintaining the transmission ratio. That would conduct to the adoption of gears of different sizes which must be in consideration considering the final global dimensions of the system. A third solution for this problem could be the substitution of the materials being employed on the pieces by polypropylene. This alternative material was studied during this project and it was proved that it suffers much less displacements when it is subjected to very high thermal loads. Therefore, there would be no problems of interference among the teeth which would lead to no noise.

For the second portion of the equation  $c < \bar{c}_r + 0.1$ , it is not the same situation. If it is summed 0.24 mm of clearance with 0.1 of tolerance, it results in 0.34 mm of space between the teeth. So, even with a displacement of 0.27 mm, there are no constraints produced in the components which means they continue to function in the same conditions.

As the value of clearance is the same for either gears, the aforementioned conclusions are applied for both. It could be considered other cases, given the values of tolerances. However, it is not necessary since the most critical situation was already studied.

In an analogous way, it can be calculated the transversal clearance, on the sides of the teeth, although for that measure there is no tolerance presented. However, it can be estimated how high the maximum displacements can be in order to not have any problems in the contact of the gear teeth. According to the table where the characteristics of the gears are displayed, the tooth thickness ( $s$ ) of components 5 and 6 are 1.47 mm and 0.95 mm, respectively. In regard to the width of space ( $e$ ), it is registered as 1.04 mm for gear 5 and 1.56 mm for gear 6. Moreover,



the transversal clearance ( $c_t$ ) of the contact on the sides of the teeth can be estimated by the equations 5.6 and 5.7. This is an average value for which there is no tolerance to be considered.

$$\bar{c}_t = e_5 - s_6 = 0.09 \text{ mm} \quad (5.6)$$

$$\bar{c}_t = e_6 - s_5 = 0.09 \text{ mm} \quad (5.7)$$

The presented values also contribute to the concern about the function of the mechanism since the teeth are in contact and there is no space for them to expand, even 0.09 mm.

It was chosen to analyse this contact since it is a critical one and it presents much difficulty in being created since it is established a high transmission ratio among the gears.

Bearing that in mind, the other presented values will not be used in any evaluation. However, it was decided to exhibit them in order to show the magnitude of the tolerances applied on the measures. Nevertheless, the other measures does not influence directly the correct function of the mechanism, which means that it was not considered much important to study them.



“Our beliefs determine our actions and it is our consistent actions that will produce results.”

Billy Cox

## 6. CONCLUDING REMARKS

In this section it is intended to include all the relevant information about this dissertation, describing what was performed during the past few months and stating the conclusions drawn in every chapter. After that, it will be detailed some directions that could be followed by someone who had the objective of pursuing this theme and continue exploring it, specifying particular aspects which could be studied and types of simulations that could be performed.

This report was initiated with the explanation about what motivated the author to investigate this area. Then, it was presented the company where the whole work was produced, referring its principles, the products they develop and manufacture as well as the internal organisation. The objectives which must be accomplished by the end of the project and the adopted methodology in order to achieve these goals were also mentioned. Finally, there is the overview of the dissertation content where it is detailed what constitutes the chapters, including the progresses achieved in this work.

The second chapter is divided in 2 parts, technical and technological component, and concerns the fundamental background the readers must understand in order to interpret the following sections. Firstly, it is reported some facts related to gear history, referring names of the ones who contributed more for the development of this area over time. Thereafter, it is explained

the importance of these mechanisms in the quotidian, where it is concluded that this type of system have been evolved much mostly due to the horology industry, with new capabilities and precision. However, nature was the first to discover gears and it had been incorporated into animals. Moreover, it is enunciated some examples of applications of these systems in industry, since toys, home appliances, watches, automobile differentials, industrial mixers, among others. In the second segment of this chapter it is mentioned previous articles written about this subject in which it was presented a succinct description of the most recent contributions on the thermal study of different types of gears namely, spur, bevel, helical, etc. Nowadays, the possibility of using polymers to manufacture gears is increasingly growing although these materials are described as unpredictable in dimensional variations. For that reason, this area of interest is the focus of many articles. Therefore, some examples of papers about coupled simulations are displayed in order to show the examination of processes, materials, prediction of behaviours and modification of parameters. When it is necessary to assess conditions or procedures, it is beneficial to perform simulations like these to understand better what may happen in certain circumstances.

The theoretical introduction comprises 6 sections where are included the themes, subjects and topics necessary to understand chapters 4 and 5. This part describes the finite element method which is the basis for some types of numerical simulations. It is also referred the finite volume method, highlighting the differences among them. The steps of these approaches are reviewed and detailed, praising the most important aspects. Next, the clarifications are focused on the heat transfer and mechanical phenomena as well as the concepts of deformation and stress. Later, it is introduced the methods used on the mesh in order to obtain the best structure possible which will be employed to get the most accurate results. The most appropriate type of elements to be applied depends on the simulation performed and the results which is intended to reach. The sixth section covers the models employed in order to perform the simulations in the 3 modules of ANSYS which are Steady-State Thermal, Fluent and Static Structural. It was concluded that some solvers can be applied for different areas and, most of the times, they are chosen according to the accuracy it is expected for an analysis. The last segment summarises some concepts related to 3D scanning in order to detail how the experimental activities were performed. In addition, some techniques that can be employed to obtain 3D models of pieces were explained in detail, mainly triangulation. This methodology enables the creation of three-dimensional representations of objects by considering triangles between the laser, the camera and the point to be measured.

The chapter 4 includes the description of the system being analysed, referring the most

relevant characteristics. It is also important to describe the components that constitute the assembly and the specifications required by the client. Consequently, it is performed a kinematic and a dynamical analysis with the purpose of having some notion of the velocities involved and the forces applied in the system. In the first analysis, it was concluded that the speed is decreasing as you progress along the mechanism. This can be explained by the fact that the number of teeth increases in all engagements as well as the size of the components. In the dynamical study, it can be declared that the forces involved does not present high values, and after determining the efficiency of the whole assembly, it was drawn the conclusion that most of the power transmitted by the engine is lost in the first stage due to the low performance of the worm gear. Besides, some considerations are defined and explained such as the assembly used in the work, the materials and contacts, among others. Then, the second issue is related to the validation of the software where some simple experiments are executed on ANSYS. Consequently, it is concluded that geometry influences the errors which result from these studies since the errors decrease with the size reduction. On the other hand, it can be assumed that material properties contribute to the error between theoretical and numerical results, in which, for this situation, the tensile modulus and the coefficient of thermal expansion are the most relevant factors. Next, the total assembly is taken into consideration with the purpose of performing thermal simulations using Steady-State Thermal module of ANSYS. It is understood that the temperature reached during this study is of 35 °C, which is not critical and it is registered on the LED. After that, it was performed an intensive study on the bigger gear, with both fluid-structure interface and thermal-stress simulations, using 2 different processes of heating the component. It was also tested how this piece would behave if it was constituted of another material. From the results obtained, there is no difference in simulating the heating procedure with one module or the other. Regarding the materials, the polypropylene produces better outcomes about the occurrence of displacements due to thermal loads although implies more costs. At another time the study includes only the 6 gears to execute thermal-stress simulations and it is intended to evaluate how they behave when facing high temperatures. It is concluded that the registered values for the maximum displacements can put in danger the correct function of the mechanism and damage the pieces over time.

In what concerns the experimental activity, it was firstly described and summarised what was performed as well as detailed the conditions in order to clarify the parameters which may influence the final results. Thereafter, the outcomes are displayed along with the respective interpretation. The most important part is the comparison established between numerical and experimental values where it is concluded that the results are very good in some cases, while in

others they are not so much. Finally, some recommendations are mentioned about the functional dimensions of manufacturing with the purpose of studying if the applied tolerances are in agreement with the correct operation of the system. Through the analysis of all the factors, including displacements and tolerances, it is understood that the most critical contact of the gears can create interferences and endanger the appropriate operating conditions of the system.

In regard to the future work, there several possibilities considering this could be a very complex problem. It would be very interesting to perform a dynamical analysis with only the gears and evaluate what occurs after 30 000 cycles of operating since this is a specification for the system. The displacements and stresses, in this case, would be more reliable as they are more in line with reality.

As the module fluent of ANSYS allows diverse options for boundary conditions and solvers, it could also be investigated if the ones used were the most appropriate which means that it would be a possibility to test other conditions. A new model would be created in order to verify the outcomes of that studies.

The area of materials is fundamental since different types present various behaviours which are more convenient to certain cases. In addition, it could be performed simulations integrating materials with other characteristics. The aim would be to reduce the costs and eliminate the problems related to the interference between gears.

Something also very interesting which could be performed was transient analyses of the problem in study using ANSYS. With time, the properties change considering that the situation is not the same and, then, the results would be more reliable.

Nevertheless, these are the main conclusions of the work produced along the past few months. Many were the difficulties presented in every step but, one by one, they were resolved and, in the end, the objectives were achieved and it was presented an objective, organised and well thought dissertation.

“If I have seen further than others, it is by standing upon the shoulders of giants.”

Isaac Newton

## REFERENCES

- Abaqus*. (2015). (Dassault Systèmes) Retrieved from <http://www.3ds.com/products-services/simulia/products/abaqus/>
- Algor*. (2011). (Autodesk, Inc) Retrieved from [http://www.algor.com/service\\_support/customer/default.asp](http://www.algor.com/service_support/customer/default.asp)
- ANSYS. (2005). *Chapter 6 - Steady-State Thermal Analysis (Training Manual)*. USA: ANSYS, Inc.
- ANSYS. (2015). (ANSYS, Inc) Retrieved from <http://www.ansys.com/>
- ANSYS, I. (2010). Brochure ANSYS v13.0. USA.
- ANSYS, Inc. (2009). *ANSYS FLUENT 12.0 - Theory Guide*. USA: SAS IP.
- ANSYS, Inc. (2009). *Structural Analysis Guide*. USA: SAS IP.
- ANSYS, Inc. (2009). *Thermal Analysis Guide*. USA: SAS IP.
- ANSYS, Inc. (2013). *ANSYS Meshing User's Guide*. USA: SAS IP.
- Antunes, F. (2012). *Mecânica Aplicada*. Lidel.
- Atan, E. (2005). On the prediction of the design criteria for modification of contact stresses due to thermal stresses in the gear mesh. *Tribology International*, 38, 227-233.
- Atan, E., & Ozdemir, S. (2005). Intelligence modeling of the transient asperity temperatures in meshing spur gears. *Mechanism and Machine Theory*, 40, 119-127.
- Bagnoli, F., Dolce, F., Colavita, M., & Bernabei, M. (2008). Fatigue fracture of a main landing gear swinging lever in a civil aircraft. *Engineering Failure Analysis*, 15, 755-765.
- Barglik, J., Smalcerz, A., Przylucki, R., & Doležel, I. (2014). 3D modeling of induction hardening of gear wheels. *Journal of Computational and Applied Mathematics*, 270, 231-240.
- Behnke, R., & Kaliske, M. (2015). Thermo-mechanically coupled investigation of steady state rolling tires by numerical simulation and experiment. *International Journal of Non-Linear Mechanics*, 68, 101-131.
- Belhocine, A., & Bouchetara, M. (2013). Thermal-Mechanical Coupled Analysis of a Brake Disk Rotor. *Journal of Failure Analysis and Prevention*, 13, 167-176.
- Blok, H. (1937). Theoretical study of temperature rise at surfaces of actual contact under oiliness lubricating conditions. *Proceedings of the General Discussion on Lubrication and Lubricants IMechE*, 2, 222-235.

- BMW Technology Guide: Head-Up Display*. (n.d.). (BMW) Retrieved February 2015, from [http://www.bmw.com/com/en/insights/technology/technology\\_guide/articles/head\\_up\\_display.html](http://www.bmw.com/com/en/insights/technology/technology_guide/articles/head_up_display.html)
- Bobach, L., Beilicke, R., Bartel, D., & Deters, L. (2012). Thermal elastohydrodynamic simulation of involute spur gears incorporating mixed friction. *Tribology International*, 48, 191-206.
- Bosch Car Multimedia. (2014). *Order Specification: Kinematic Module of Automotive Combiner Head-Up Display*. Braga.
- Bosch Group. (2014). *Annual Report*. Stuttgart: Robert Bosch GmbH Corporate Communications.
- Bosch S.A. (2011). *Bosch: 125 Years Invented for Life*. Stuttgart: Robert Bosch GmbH Corporate Communications.
- Branco, C. M., Ferreira, J. M., da Costa, J. D., & Ribeiro, A. S. (2009). *Projecto de Órgãos de Máquinas*. Lisbon: Fundação Calouste Gulbenkian.
- Budynas, R. G., & Nisbett, J. K. (2014). *Shigley's Mechanical Engineering Design*. New York: McGraw-Hill.
- Butaud, P., Placet, V., Klesa, J., Ouisse, M., Foltête, E., & Gabrion, X. (2015). Investigations on the Frequency and Temperature Effects on Mechanical Properties of a Shape Memory Polymer. *Mechanics of Materials*, 87, 50-60.
- Caggiano, A., & Etse, G. (2015). Coupled thermo-mechanical interface model for concrete failure analysis under high temperature. *Computer Methods in Applied Mechanics and Engineering*, 289, 498-516.
- Castilla, R., Gamez-Montero, P. J., Ertürk, N., Vernet, A., Coussirat, M., & Codina, E. (2010). Numerical simulation of turbulent flow in the suction chamber of a gearpump using deforming mesh and mesh replacement. *International Journal of Mechanical Sciences*, 52, 1334-1342.
- Childs, P. (2013). *Mechanical Design Engineering Handbook*. Butterworth-Heinemann.
- Chironis, N. P., & Sclater, N. (1996). *Mechanisms and Mechanical Devices SourceBook*. New York: McGraw-Hill.
- Cho, J. R., Kang, W. J., Kim, M. G., Lee, J. H., Lee, Y. S., & Bae, W. B. (2004). Distortions induced by heat treatment of automotive bevel gears. *Journal of Materials Processing Technology*, 153-154, 476-481.
- Coda, H. B., Sampaio, M. S., & Paccola, R. R. (2015). A FEM Continuous Transverse Stress Distribution for the Analysis of Geometrically Nonlinear Elastoplastic Laminated Plates and Shells. *Finite Elements in Analysis and Design*, 101, 15-33.
- Cook, R. D., Malkus, D. S., Plesha, M. E., & Witt, R. J. (2002). *Concepts and Applications of Finite Element Analysis*. Winesconsin: John Wiley and Sons.



- Crosher, W. F. (2014). *A Gear Chronology: Significant Events and Dates Affecting Gear Development*. London: Xlibris Corporation.
- DEFORM. (2015). (Scientific Forming Technologies Corporation) Retrieved from <http://www.deform.com/>
- Denkena, B., Köhler, J., Schindler, A., & Woiwode, S. (2014). Continuous generating grinding - Material engagement in gear tooth root machining. *Mechanism and Machine Theory*, 81, 11-20.
- Drago, R. J. (1988). *Fundamentals of Gear Design*. London: Butterworths.
- Durley, R. J. (1903). *Kinematics of Machines*. New York: John Wiley and Sons.
- Düzçükoglu, H. (2009). Study on development of polyamide gears for improvement of load-carrying capacity. *Tribology International*, 42, 1146-1153.
- Elhosni, M., Elmazria, O., Talbi, A., Aissa, K. A., Bouvot, L., & Sarry, F. (2014). FEM Modelling of Multilayer Piezo-Magnetic Structure Based Surface Acoustic Wave Devices for Magnetic Sensor. *Procedia Engineering*, 87, 408-411.
- Engineering Information*. (n.d.). (Boston Gear) Retrieved February 2015, from <http://www.bostongear.com/>
- England, B. (2014, January 9). *The New Mini Vision - Coming Soon to the DC / Baltimore Metro Area*. (British American Auto) Retrieved February 2015, from <http://www.britishamericanauto.com/car-repair-education-and-info-blog/bid/88490/The-New-Mini-Vision-Coming-Soon-to-the-DC-Baltimore-Metro-Area>
- Fallah, N., Bailey, C., Cross, M., & Taylor, G. (2000). Comparison of Finite Element and Finite Volume Methods. *Applied Mathematical Modelling*, 24, 439-455.
- Fernandes, C. M., Battez, A. H., González, R., Monge, R., Viesca, J. L., García, A., . . . Seabra, J. H. (2015). Torque loss and wear of FZG gears lubricated with wind turbine gear oils using an ionic liquid as additive. *Tribology International*, 90, 306-314.
- Fernandes, C. M., Martins, R. C., & Seabra, J. H. (2014). Torque loss of type C40 FZG gears lubricated with wind turbine gear oils. *Tribology International*, 70, 83-93.
- Flores, P. (2009). *Projecto de Mecanismos Came-Seguidor*. Porto: Publindústria.
- Flores, P., & Claro, J. C. (2007). *Cinemática de Mecanismos*. Coimbra: Edições Almedina.
- Flores, P., & Gomes, J. (2015). *Cinemática e Dinâmica de Engrenagens: Teoria e Exercícios de Aplicação*. Porto: Publindústria.
- FloTHERM. (2015). (Mentor Graphics) Retrieved from <http://www.mentor.com/products/mechanical/flotherm/flotherm/>
- Fratila, D., & Radu, A. (2010). Modeling and comparing of steady thermal state at gear milling by conventional and environment-friendly cooling method. *The International Journal of Advanced Manufacturing Technology*, 47, 1003-1012.

- Frisani, A., & Hassan, Y. A. (2015). On the Immersed Boundary Method: Finite Element versus Finite Volume Approach. *Computers and Fluids*, 121, 51-67.
- Gauruva, & Shankar, V. (2015). Manipulation of Interfacial Instabilities by using a Soft, Deformable Solid Layer. *Sadhana*, 40(3), 1033-1048.
- Geethamma, V. G., Asaletha, R., Kalarikkal, N., & Thomas, S. (2014). Vibration and Sound Damping in Polymers. *Resonance Journal of Science Education*, 19(19), 821-833.
- Gopinath, K., & Mayuram, M. (n.d.). *Machine Design II - Lecture 15 (Worm Gears)*.
- Gualdi, S., Morandini, M., & Ghiringhelli, G. L. (2008). Anti-skid induced aircraft landing gear instability. *Aerospace Science and Technology*, 12, 627-637.
- Haj-Fraj, A., & Pfeiffer, F. (2001). Optimal control of gear shift operations in automatic transmissions. *Journal of the Franklin Institute*, 338, 371-390.
- Henriot, G. (1979). *Traité Théorique et Pratique des Engrenages*. Dunod.
- Heyns, T., Godsill, S. J., de Villiers, J. P., & Heyns, P. S. (2012). Statistical gear health analysis which is robust to fluctuating loads and operating speeds. *Mechanical Systems and Signal Processing*, 27, 651-666.
- Hirsch, C. (2007). Chapter 5 - Finite Volume Method and Conservative Discretization with an Introduction to Finite Element Method. In *Numerical Computation of Internal and External Flows* (pp. 203-248). USA: Butterworth Heinemann.
- Holman, J. P. (2009). *Heat Transfer*. New York: McGraw-Hill.
- Hoskins, T. J., Dearn, K. D., Chen, Y. K., & Kukureka, S. N. (2014). The wear of PEEK in rolling-sliding contact - Simulation of polymer gear applications. *Wear*, 309, 35-42.
- Hu, H., Zhang, D., Pan, F., & Yang, M. (2009). Thermal-stress Simulation of Direct-chill Casting of AZ31 Magnesium Alloy Billets. *Journal of Wuhan University of Technology - Materials Science*, 24, 376-382.
- Hu, X. (1998). Tribological Behaviour of Modified Polyacetal against MC Nylon without Lubrication. *Tribology Letters*, 5(4), 313-317.
- Huebner, K. H., Dewhurst, D. L., Smith, D. E., & Byrom, T. G. (2001). *The Finite Element Method for Engineers*. Canada: John Wiley and Sons.
- Huson, M. G., & Maxwell, J. M. (2006). The Measurement of Resilience with a Scanning Probe Microscope. *Polymer Testing*, 25(1), 2-11.
- Hutton, D. V. (2004). *Fundamentals of Finite Element Analysis*. Pullman: McGraw-Hill.
- Hwang, W.-M., & Huang, Y.-L. (2011). Connecting clutch elements to planetary gear trains for automotive automatic transmissions via coded sketches. *Mechanism and Machine Theory*, 46, 44-52.
- Incropera, F. P., DeWitt, D. P., Bergman, T. L., & Lavine, A. S. (2013). *Principles of Heat and Mass Transfer*. Singapore: John Wiley and Sons.

- International Organisation for Standardisation. (1988). *ISO Standards HandBook - Mechanical Transmissions*. Switzerland.
- Jeon, J., Muliana, A., & Saponara, V. L. (2014). Thermal stress and deformation analyses in fiber reinforced polymer composites undergoing heat conduction and mechanical loading. *Composite Structures*, *111*, 31-44.
- Jiang, Q. Y., & Barber, G. C. (2000). Experimental Determination of Bulk Temperature and Critical Temperature in Scuffing Resistance Evaluation of Gears. *Tribology Transactions*, *43*, 21-26.
- Juvinall, R. C., & Marshek, K. M. (2006). *Fundamentals of Machine Component Design*. New York: John Wiley and Sons.
- Kadashevich, I., Beutner, M., Karpuschewski, B., & Halle, T. (2015). A novel simulation approach to determine thermally induced geometric deviations in dry gear hobbing. *Procedia CIRP*, *31*, 483-488.
- Kadmiri, Y., Rigaud, E., Perret-Liaudet, J., & Vary, L. (2012). Experimental and numerical analysis of automotive gearbox rattle noise. *Journal of Sound and Vibration*, *331*, 3144-3157.
- Kansal, G., Pao, P. N., & Atreya, S. K. (2001). Study: temperature and residual stress in an injection moulded gear. *Journal of Materials Processing Technology*, *108*, 328-337.
- Khan, K. A., Barello, R., Muliana, A. H., & Lévesque, M. (2011). Coupled heat conduction and thermal stress analyses in particulate composites. *Mechanics of Materials*, *43*, 608-625.
- Khapane, P. D. (2006). Gear walk instability studies using flexible multibody dynamics simulation methods in SIMPACK. *Aerospace Science and Technology*, *10*, 19-25.
- Kim, S.-H., Choi, J.-B., Park, J.-S., Choi, Y.-H., & Lee, J.-H. (2013). A coupled CFD-FEM analysis on the safety injection piping subjected to thermal stratification. *Nuclear Engineering and Technology*, *45*, 237-248.
- Kurokawa, M., Uchiyama, Y., Iwai, T., & Nagai, S. (2003). Performance of plastic gear made of carbon fiber reinforced polyamide 12. *Wear*, *254*, 468-473.
- Lee, H.-C., Hwang, Y.-H., & Kim, T.-G. (2003). Failure analysis of nose landing gear assembly. *Engineering Failure Analysis*, *10*, 77-84.
- Li, H., Wei, W., Liu, P., Kang, D., & Zhang, S. (2014). The kinematic synthesis of involute spiral bevel gears and their tooth contact analysis. *Mechanism and Machine Theory*, *79*, 141-157.
- Li, M.-J., Pan, J.-H., Ni, M.-J., & Zhang, N.-M. (2015). Heat transfer and thermal stress analysis in fluid-structure coupled field. *Applied Thermal Engineering*, *88*, 473-479.
- Li, Y., Liu, W. Y., & Frimpong, S. (2012). Effect of ambient temperature on stress, deformation and temperature of dump truck tire. *Engineering Failure Analysis*, *23*, 55-62.

- Lima, C. R., Souza, N. F., & Camargo, F. (2013). Study of Wear and Corrosion Performance of Thermal Sprayed Engineering Polymers. *Surface & Coatings Technology*, 220, 140-143.
- Lingamanaik, S. N., & Chen, B. K. (2012). The effects of carburising and quenching process on the formation of residual stresses in automotive gears. *Computational Materials Science*, 62, 99-104.
- LMI Technologies. (2013). A Simple Guide To Understanding. Canada: LMI Technologies, Inc.
- Luo, R. K., Wu, X. P., & Mortel, W. J. (2014). Rubber Unloading-Behaviour Evaluation Using Product-Orientated Specimen Based on a Resilience Test. *Polymer Testing*, 34, 49-57.
- Mabie, H. H., & Reinholtz, C. F. (1987). *Mechanisms and Dynamics of Machinery*. New York: John Wiley and Sons.
- Maitra, G. M. (2010). *Handbook of Gear Design*. New Delhi: Tata McGraw-Hill Education.
- Malkin, A. Y. (2008). Surface Instabilities. *Colloid Journal*, 70(6), 673-689.
- Mao, K. (2007). A numerical method for polymer composite gear flash temperature prediction. *Wear*, 262, 1321-1329.
- Mao, K., Langlois, P., Hu, Z., Alharbi, K., Xu, X., Milson, M., . . . Chetwynd, D. (2015). The wear and thermal mechanical contact behaviour of machine cut polymer gears. *Wear*, 332-333, 822-826.
- Mao, K., Li, W., Hooke, C. J., & Walton, D. (2009). Friction and wear behaviour of acetal and nylon gears. *Wear*, 267, 639-645.
- Mao, K., Li, W., Hooke, C. J., & Walton, D. (2010). Polymer gear surface thermal wear and its performance prediction. *Tribology International*, 43, 433-439.
- Mechanical Gears Seen for the First Time in Nature*. (2013, September 18). (Astrobiology Magazine) Retrieved February 2015, from <http://www.astrobio.net/topic/origins/origin-and-evolution-of-life/mechanical-gears-seen-for-the-first-time-in-nature/>
- Meng, F., Tao, G., Zhang, T., Hu, Y., & Geng, P. (2015). Optimal shifting control strategy in inertia phase of an automatic transmission for automotive applications. *Mechanical Systems and Signal Processing*, 60-61, 742-752.
- Moaveni, S. (1999). *Finite Element Analysis, Theory and Application with ANSYS*. New Jersey: Prentice-Hall.
- Moukalled, F., Mangani, L., & Darwish, M. (2015). *The Finite Volume Method in Computational Fluid Dynamics*. USA: Springer.
- MSC Nastran*. (2015). (MSC Software Corporation) Retrieved from <http://www.mscsoftware.com/product/msc-nastran>
- Murashov, M. V., & Panin, S. D. (2015). Numerical Modelling of Contact Heat Transfer Problem with Work Hardened Rough Surfaces. *International Journal of Heat and Mass Transfer*, 90, 72-80.

- Nakano, H., Omiya, Y., Sekiguchi, Y., & Sawa, T. (2014). Three-Dimensional FEM Stress Analysis and Strength Prediction of Scarf Adhesive Joints with Similar Adherends Subjected to Static Tensile Loadings. *International Journal of Adhesion and Adhesives*, 54, 40-50.
- Nathi, M. G., Charyulu, T. N., Gowtham, K., & Reddy, P. S. (2012). Coupled Structural/Thermal Analysis of Disc Brake. *International Journal of Research in Engineering and Technology*, 1, 539-553.
- Nejad, A. R., Gao, Z., & Moan, T. (2014). On long-term fatigue damage and reliability analysis of gears under wind loads in offshore wind turbine drivetrains. *International Journal of Fatigue*, 61, 116-128.
- Niemann, G. (1971). *Elementos de Máquinas - Volume 2*. São Paulo: Edgard Blucher.
- NX. (2015). (Siemens PLM Software) Retrieved from [http://www.plm.automation.siemens.com/en\\_us/products/nx/](http://www.plm.automation.siemens.com/en_us/products/nx/)
- Ossa, E. A. (2006). Failure analysis of a civil aircraft landing gear. *Engineering Failure Analysis*, 13, 1177-1183.
- Pogosian, A. K., Hovhannisyan, K. V., & Isajanyan, A. R. (2010). Friction Transfer and Self-Lubrication of Polymers. *Journal of Friction and Wear*, 31(1), 81-88.
- Qiu, X., Han, Q., & Chu, F. (2015). Load-sharing characteristics of planetary gear transmission in horizontal axis wind turbines. *Mechanism and Machine Theory*, 92, 391-406.
- Ranjbaran, M. M. (2010). A Comparative Experimental Study of Interfacial Wave Instability and Mechanical Properties of Two-Layer Polymer Extrudate. *Fibres and Polymers*, 11(3), 448-454.
- Rao, J. S., & Dukkipati, R. V. (1992). *Mechanism and Machine Theory*. New Delhi: New Age International Publishers.
- Rohsenow, W. M., Hartnett, J. R., & Cho, Y. I. (1998). *Handbook of Heat Transfer*. USA: McGraw-Hill.
- Saifullah, A. B., Masood, S. H., & Sbarski, I. (2012). Thermal-structural analysis of bi-metallic conformal cooling for injection moulds. *The International Journal of Advanced Manufacturing Technology*, 62, 123-133.
- Savaria, V., Monajati, H., Bridier, F., & Bocher, P. (2015). Measurement and correction of residual stress gradients in aeronautical gears after various induction surface hardening treatments. *Journal of Materials Processing Technology*, 220, 113-123.
- Seireg, A., & Atan, E. (2002). On the prediction of transient temperature in the gear mesh. *VDI Berichte*, 1665, 615-626.
- Sfakiotakis, V. G., Katsareas, D. E., & Anifantis, N. K. (1997). Boundary element analysis of gear teeth fracture. *Engineering Analysis with Boundary Elements*, 20, 169-175.
- Shigley, J. E., & Mischke, C. R. (1989). *Mechanical Engineering Design*. New York: McGraw-Hill.

- Shigley, J. E., & Uicker, J. J. (1995). *Theory of Machines and Mechanisms*. New York: McGraw-Hill.
- Shilong, W., Yang, Y., Li, X., Zhou, J., & Kang, L. (2013). Research on thermal deformation of large-scale computer numerical control gear hobbing machines. *Journal of Mechanical Science and Technology*, *27*, 1393-1405.
- Simões, F., & Rodrigues, D. M. (2014). Material flow and thermo-mechanical conditions during Friction Stir Welding of polymers: Literature review, experimental results and empirical analysis. *Materials and Design*, *59*, 344-351.
- Simon, V. V. (2014). Optimization of face-hobbed hypoid gears. *Mechanism and Machine Theory*, *77*, 164-181.
- SolidWorks. (2015). (Dassault Systèmes SolidWorks Corp.) Retrieved from <http://www.solidworks.com/>
- South, D. W., & Mancuso, J. R. (1994). *Mechanical Power Transmission Components*. New York: Marcel Dekker.
- Spotts, M. F., & Shoup, T. E. (1998). *Design of Machine Elements*. New Jersey: Prentice-Hall.
- Stander, C. J., Heyns, P. S., & Schoombie, W. (2002). Using vibration monitoring for local fault detection on gears operating under fluctuating load conditions. *Mechanical Systems and Signal Processing*, *16*, 1005-1024.
- Stark, S., Beutner, M., Lorenz, F., Uhlmann, S., Karpuschewski, B., & Halle, T. (2013). Heat flux and temperature distribution in gear hobbing operations. *Procedia CIRP*, *8*, 456-461.
- STEINBICHLER - Inspiring Innovation. (n.d.). (Steinbichler) Retrieved June 2015, from <http://www.steinbichler.com/>
- Strandh, S. (1979). *A History of the Machine*. New York: A&W Publishers, Inc.
- Subramanian, N., Sinha, B. R., Blum, F. D., Chen, Y.-R., & Dharani, L. R. (2006). Glass Fiber Based Friction Materials. *Polymeric Materials and Polymeric Biomaterials*, *15*(2), 93-102.
- Taburdagitan, M., & Akkok, M. (2006). Determination of surface temperature rise with thermo-elastic analysis of spur gears. *Wear*, *261*, 656-665.
- Technical Drawings of the Combiner Head-Up Display. (n.d.).
- Tevruz, T. (1997). Experiments of scoring and the calculation of scoring on gears by heat method. *Wear*, *206*, 204-213.
- Tevruz, T. (1998). Experimental investigations on scoring of gears and calculation by temperature method. *Wear*, *217*, 81-94.
- Umanskii, É. S., Shidlovskii, N. S., Kryuchkov, V. V., Grishko, S. V., & Stezhko, L. L. (1990). Load-Carrying Capacity of Polymer Tape Rolls under Impact Loads. *Strength of Materials*, *22*(4), 611-617.

- Vera, L. C. (1996). *Documentos Biográficos de Juanelo Turriano*. Madrid: Fundación Juanelo Turriano.
- Versteeg, H. K., & Malalasekera, W. (2007). *An Introduction to Computational Fluid Dynamics: The Finite Volume Method*. Glasgow: PEARSON Prentice Hall.
- Wang, G., Schwöppe, A., & Heinrich, R. (2010). Comparison and Evaluation of Cell-Centred and Cell-Vertex Discretisation in the Unstructured Tau-Code for Turbulent Viscous Flows. *European Conference on Computational Fluid Dynamics*. Lisbon.
- Wang, H., Xing, J. T., Price, W. G., & Li, W. (2008). An investigation of an active landing gear system to reduce aircraft vibrations caused by landing impacts and runway excitations. *Journal of Sound and Vibration*, 317, 50-66.
- Wang, S., Yang, Y., Li, X., Zhou, J., & Kang, L. (2013). Research on Thermal Deformation of Large-Scale Computer Numerical Control Gear Hobbing Machines. *Journal of Mechanical Science and Technology*, 27, 1393-1405.
- Wen, Z., Zhi, Z., Qidan, Z., & Shiyue, X. (2009). Dynamics Model of Carrier-based Aircraft Landing Gears Landed on Dynamic Deck. *Chinese Journal of Aeronautics*, 22, 371-379.
- Wilson, C. E., & Sadler, J. P. (1993). *Kinematics and Dynamics of Machinery*. New York: Harper Collins College Publishers.
- Wu, Y., Ming, T., Li, X., Pan, T., Peng, K., & Luo, X. (2014). Numerical simulations on the temperature gradient and thermal stress of a thermoelectric power generator. *Energy Conversion and Management*, 88, 915-927.
- Xia, M. (2015). Thermo-mechanical coupled particle model for rock. *Transactions of Nonferrous Metals Society of China*, 25, 2367-2379.
- Xiao, R., & Nguyen, T. D. (2015). An effective Temperature Theory for the Nonequilibrium Behaviour of Amorphous Polymers. *Journal of the Mechanics and Physics of Solids*, 82, 62-81.
- Xin, L., Gaoliang, P., & Zhe, L. (2014). Prediction of seal wear with thermal-structural coupled finite element method. *Finite Elements in Analysis and Design*, 83, 10-21.
- Xu, L., Lu, W.-G., Lu, L.-G., Dong, L., & Wang, Z.-F. (2014). Flow Patterns and Boundary Conditions for Inlet and Outlet Conduits of Large Pump System with Low Head. *Applied Mathematics and Mechanics*, 35(6), 675-688.
- Yakut, R., Düzcükoglu, H., & Demirci, M. T. (2009). The load capacity of PC/ABS spur gears and investigation of gear damage. *Archives of Materials Science and Engineering*, 40, 41-46.
- Yang, Q., & Li, G. (2015). Temperature and Rate Dependent Thermomechanical Modelling of Shape Memory Polymers with Physics based Phase Evolution Law. *International Journal of Plasticity*.
- Yazdani, M., & Soteriou, M. C. (2014). A novel approach for modeling the multiscale thermo-fluids of geared systems. *International Journal of Heat and Mass Transfer*, 72, 517-530.

- Yazdani, M., Soteriou, M. C., Sun, F., & Chaudhry, Z. (2015). Prediction of the thermo-fluids of gearbox systems. *International Journal of Heat and Mass Transfer*, *81*, 337-346.
- Zhang, C. S., & Li, L. (2009). A Coupled Thermal-Mechanical Analysis of Ultrasonic Bonding Mechanism. *METALLURGICAL AND MATERIALS TRANSACTIONS B*, *40*, 196-207.
- Zhigun, V. I. (1991). Experimental Validation of the Load-Carrying Capacity of Composites with a Circular Hole when subjected to Combined Loading in Interlaminar Shear and Transverse Compression. *Mechanics of Composite Materials*, *27*(1), 54-58.
- Zhou, S., Zhang, Q., Wu, C., & Huang, J. (2013). Effect of carbon fiber reinforcement on the mechanical and tribological properties of polyamide6/polyphenylene sulfide composites. *Materials and Design*, *44*, 493-499.



“Some people dream of success while others wake up and work hard at it.”

Winston Churchill

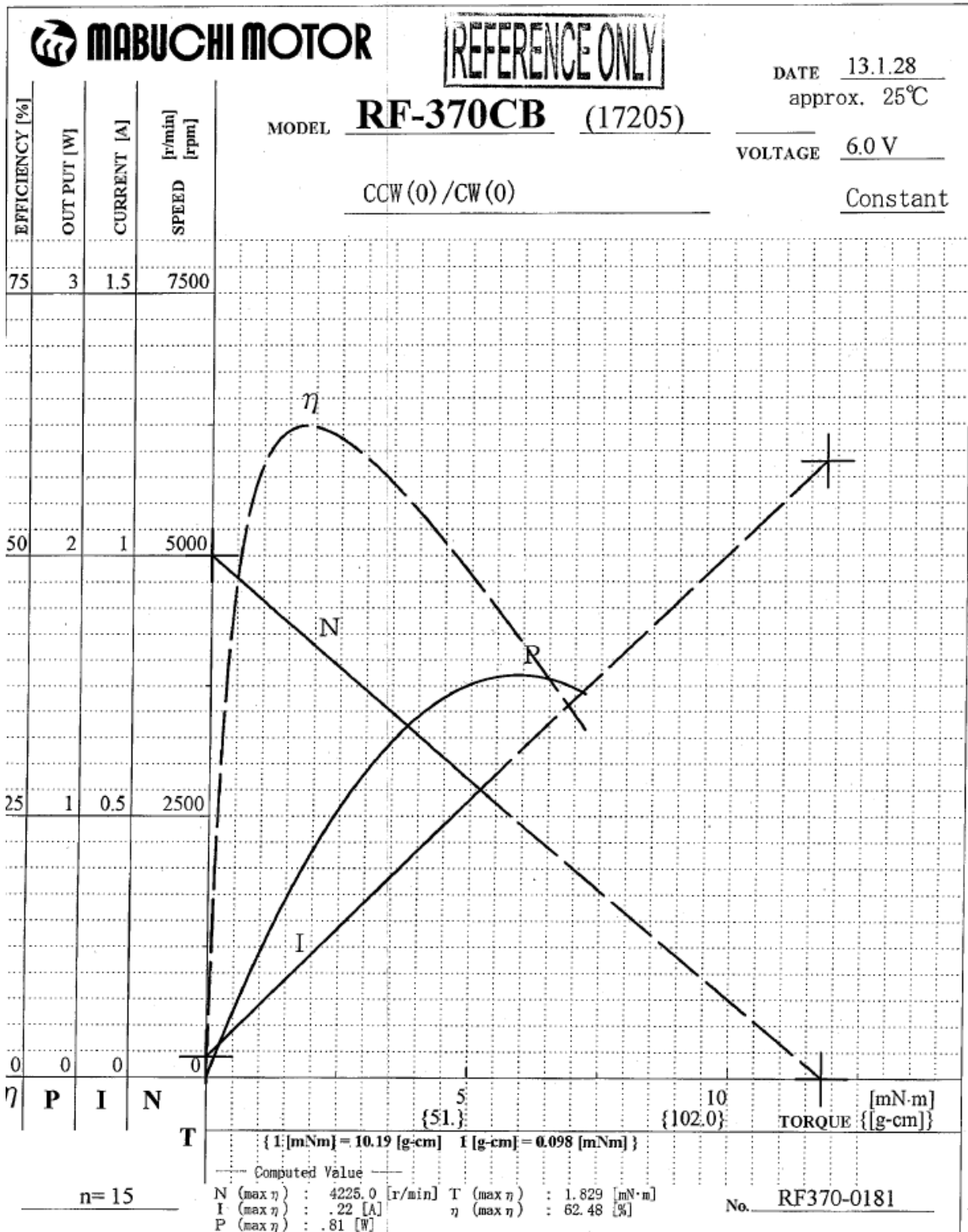
# APPENDICES



## Appendix A

### Datasheet of the D. C. Motor







## Appendix B

### LED Specifications





1. SPECIFICATIONS

(1) Absolute Maximum Ratings (Ts=25°C)

Item	Symbol	Absolute Maximum Rating	Unit
Forward Current	IF	400	mA
Pulse Forward Current	IFP	500	mA
Allowable Reverse Current	IR	85	mA
Power Dissipation	PD	4.6	W
Operating Temperature	Topr	-40 ~ +100	°C
Storage Temperature	Tstg	-40 ~ +100	°C
Dice Temperature	Tj	150	°C
Soldering Temperature	Tstd	Reflow Soldering : 260°C for 10sec.	

IFP Conditions : Pulse Width ≤ 10msec. and Duty ≤ 1/10

(2) Initial Electrical/Optical Characteristics (Ts=25°C)

Item	Symbol	Condition	Typ.	Max.	Unit
Forward Voltage	VF	IF=350[mA]	(10.5)	11.5	V
Luminous Flux*	φv	IF=350[mA]	(350)	-	lm
Chromaticity Coordinate**	x	IF=350[mA]	0.344	-	-
	y	IF=350[mA]	0.355	-	-

\* Luminous flux value is traceable to the CIE 127:2007-compliant national standards.

\*\* Please refer to CIE 1931 chromaticity diagram.

(3) Ranking (Ts=25°C)

Item	Symbol	Condition	Min.	Max.	Unit	
Forward Voltage	Rank H	VF	IF=350[mA]	11.0	11.5	V
	Rank M			10.5	11.0	
	Rank L			10.0	10.5	
	Rank K			9.5	10.0	
Luminous Flux	Rank D360	φv	IF=350[mA]	360	380	lm
	Rank D340			340	360	
	Rank D320			320	340	
	Rank D300			300	320	
	Rank D280			280	300	

\* Forward Voltage Measurement allowance is ± 3%.

\* Luminous Flux Measurement allowance is ± 7%.



## Appendix C

### Datasheet of the 3D Sensor



# STEINBICHLER COMET® 6 8M / 16M

INNOVATIVE HIGH-END SENSORS  
FOR EFFICIENT AND HIGH PRECISION 3D DIGITIZING



New:  
COMET 6 8M  
High-Speed



High-End technology for your demanding digitizing applications: Do your projects require maximum measurement speed or highest resolution for measuring detailed/complex-shaped parts? The COMET 6 sensors are the ideal choice, offering uncompromising flexibility and data quality.

#### HIGH LIGHT POWER AND INTELLIGENT 3D ILC TECHNOLOGY

COMET 6 features an extremely powerful LED and innovative projection optics. The adaptive projection technology (3D ILC - Intelligent Light Control) locally adapts the light quantity projected onto the object surface; undesired effects such as glare are therefore minimized.

#### COMET 6 8M: THE NEW SENSOR FOR ULTIMATE MEASUREMENT SPEED

The new high-speed fringe projection sensor COMET 6 8M excites with a stunningly short measurement time which is even in high resolution mode less than one second. The outstandingly powerful projection module sets new standards with maximum efficiency for the acquisition of 3D data.

#### COMET 6 16M: HIGH RESOLUTION FOR HIGHEST LEVEL OF DETAIL

COMET 6 16M with a high-resolution 16 Megapixel camera features a previously unprecedented precision for the digitization of objects with fine structures or for applications requiring the highest level of detail.

#### MODULAR DESIGN FOR EFFICIENCY AND FLEXIBILITY

The unique design of the STEINBICHLER COMET 6 sensors is based on a modular set-up with the proven single-camera-technology which allows a fast and easy adaptation of the field-of-view to the application at hand.



steinbichler  
INSPIRING  
INNOVATION

# STEINBICHLER COMET® 6 8M / 16M

INNOVATIVE HIGH-END SENSORS  
FOR EFFICIENT AND HIGH PRECISION 3D DIGITIZING



TECHNICAL DATA		COMET 6 8M	COMET 6 16M
Camera resolution		3296 x 2472	4896 x 3264
Field-of-view		Measurement volume 86 x 64 x 40 mm³ 142 x 106 x 80 mm³ 283 x 213 x 160 mm³ 386 x 289 x 200 mm³ 666 x 499 x 400 mm³ 1216 x 912 x 600 mm³	Measurement volume 81 x 54 x 40 mm³ 145 x 97 x 80 mm³ 274 x 193 x 160 mm³ 382 x 254 x 200 mm³ 656 x 437 x 400 mm³ 1235 x 823 x 600 mm³
Field-of-view	80 / 150 250 / 400 700 / 1200	3D point distance 26 µm / 43 µm 86 µm / 117 µm 202 µm / 369 µm	3D point distance 16 µm / 30 µm 56 µm / 78 µm 134 µm / 252 µm
Field-of-view	80 / 150 250 / 400 700 / 1200	Working distance 420 mm / 600 mm 600 mm / 785 mm 785 mm / 1400 mm	Working distance 420 mm / 600 mm 600 mm / 785 mm 785 mm / 1400 mm
Fastest measuring time in seconds		< 1 sec.	1.2 sec.
PC		64Bit HighEnd Workstation with Windows 7	64Bit HighEnd Workstation with Windows 7
Sensor positioning		Tripod or column stand with manual rotary/swivel axis	Tripod or column stand with manual rotary/swivel axis
Automatic object-positioning		Rotary tables COMETrotary, COMETdual rotary	Rotary tables COMETrotary, COMETdual rotary
Available software		STEINBICHLER colin3D	STEINBICHLER colin3D

### HIGH FLEXIBILITY AND EFFICIENCY FOR WIDE APPLICATION RANGE

Choose between higher resolution and maximum measurement speed at any time and achieve optimal performance for your specific usage with the COMET 6 sensors. The short working distance even with large measuring fields enables simple, time-saving handling, especially in confined spaces.

Adapting the field-of-view only requires a few simple steps by exchanging the objective lens - within shortest time, the modular digitizing system is available for your next application.

Without the need of any elaborate hardware modifications or additional sensors, you can take full advantage of the exceptionally high flexibility provided by the COMET 6 high-end sensors.



### USER-ORIENTED, ERGONOMIC SENSOR HANDLING

The compact sensor design and new handling system are designed to offer maximum user friendliness and ergonomic operation. The sensor can be adjusted particularly easy, precise and quick – enabling the user to operate the system intuitively and conveniently. Paired with the sensorially fast measurement time, COMET 6 offers maximum efficiency.



STEINBICHLER OPTOTECHNIK GmbH  
Georg-Wiesböck-Ring 12 • 83115 Neubuern • Germany  
fon: +49-8035-8704-0 • fax: +49-8035-1010  
sales@steinbichler.de  
www.steinbichler.de

International Branch Offices:  
USA • BRAZIL • P.R. CHINA • INDIA  
FRANCE • PORTUGAL • UK • AUSTRIA • RUS  
© Steinbichler-Optotechnik GmbH 04\_2015

## Appendix D

### Datasheet of the Spray





	<b>CGM CIGIEMME S.r.l.</b>	Revisão n. 10
	<b>02011200 - R2.82-ROTRIVEL U</b>	Data de revisão 13/11/2013 Imprimida a 16/07/2014 Página n. 2/11

<b>R36</b>	IRRITANTE PARA OS OLHOS.
<b>R66</b>	PODE PROVOCAR SECURA DA PELE OU FISSURAS, POR EXPOSIÇÃO REPETIDA.
<b>R67</b>	PODE PROVOCAR SONOLÊNCIA E VERTIGENS, POR INALAÇÃO DOS VAPORES.
<b>S 9</b>	MANTER O RECIPIENTE NUM LOCAL BEM VENTILADO.
<b>S16</b>	MANTER AFASTADO DE QUALQUER CHAMA OU FONTE DE IGNIÇÃO - NÃO FUMAR.
<b>S25</b>	EVITAR O CONTACTO COM OS OLHOS.
<b>S26</b>	EM CASO DE CONTACTO COM OS OLHOS, LAVAR IMEDIATA E ABUNDANTEMENTE COM ÁGUA E CONSULTAR UM ESPECIALISTA.
<b>S33</b>	EVITAR ACUMULAÇÃO DE CARGAS ELECTROSTÁTICAS.
<b>S43</b>	EM CASO DE INCÊNDIO, UTILIZAR ... (MEIOS DE EXTINÇÃO A ESPECIFICAR PELO PRODUTOR. SE AÁGUA AUMENTAR OS RISCOS, ACRESCENTAR "NUNCA UTILIZAR ÁGUA").

### 2.3. Outros perigos.

Informações não disponíveis.

## SECÇÃO 3. Composição/informação sobre os componentes.

### 3.1. Substâncias.

Informação não pertinente.

### 3.2. Misturas.

Contém:

Identificação.	Conc. %.	Classificação 67/548/CEE.	Classificação 1272/2008 (CLP).
<b>ACETONA</b>			
CAS. 67-64-1	74 - 78	R66, R67, F R11, Xi R36	Fam. Liq. 2 H225, Eye Irrit. 2 H319, STOT SE 3 H336, EUH065
CE. 200-662-2			
INDEX. 606-001-00-8			
<b>2-PROPANOL</b>			
CAS. 67-63-0	16 - 19,5	R67, F R11, Xi R36	Fam. Liq. 2 H225, Eye Irrit. 2 H319, STOT SE 3 H336
CE. 200-661-7			
INDEX. 603-117-00-0			

Nota: Valor superior do range excluído.

O texto completo das frases de risco (R) e das indicações de perigo (H) consta da secção 16 da ficha.

T+ = Muito Tóxico(T+), T = Tóxico(T), Xn = Nocivo(Xn), C = Corrosivo(C), Xi = Irritante(Xi), O = Comburente(O), E = Explosivo(E), F+ = Extremamente Inflamável(F+), F = Facilmente Inflamável(F), N = Perigoso para o Ambiente(N)

## SECÇÃO 4. Primeiros socorros.

### 4.1. Descrição das medidas de primeiros socorros.

**OLHOS:** Eliminar eventuais lentes de contacto. Lavar-se de imediato e com bastante água por pelo menos 15 minutos, abrindo bem as pálpebras. Se o problema persistir consultar um médico.

**PELE:** Tirar as roupas contaminadas. Lavar-se imediatamente e com bastante água. Se a irritação persistir, consultar um médico. Lavar o vestuário contaminado antes de o voltar a utilizar.

**INALAÇÃO:** Transportar o sujeito ao ar livre. Se a respiração for difícil, chamar de imediato um médico.

**INGESTÃO:** Consultar de imediato um médico. Provocar o vômito só sobre indicação do médico. Não subministrar nada por via oral se o sujeito estiver inconsciente e se não autorizados pelo médico.

	<b>CGM CIGIEMME S.r.l.</b>	Revisão n. 10
	<b>02011200 - R2.82-ROTRIVEL U</b>	Data de revisão 13/11/2013 Imprimida a 16/07/2014 Página n. 5/11

(C) = CEILING ; INALÁV = Fracção Inalável ; RESPIR = Fracção Respirável ; TORAX = Fracção Torácica.

TLV da mistura solventes: 926 mg/m<sup>3</sup>.

## 8.2. Controlo da exposição.

Tendo em conta que o uso de medidas técnicas adequadas teria sempre de ter a prioridade em relação aos equipamentos de protecção pessoais, assegurar uma boa ventilação no lugar de trabalho através de uma aspiração eficaz local. Os dispositivos de protecção pessoais devem ser conformes às normas em vigor abaixo indicadas.

### PROTECÇÃO DAS MÃOS

Proteger as mãos com luvas de trabalho de categoria II (ref. Directriz 89/686/CEE e norma EN 374) tais como PVC, neoprene, nitril ou equivalentes. Para a escolha definitiva do material das luvas de trabalho é preciso ter em conta: degradação, tempo de ruptura e permeação. No caso de preparações a resistências das luvas de trabalho tem de ser verificada antes do uso, por não ser previsível. As luvas têm um tempo de desgaste que depende da duração da exposição.

### PROTECÇÃO DOS OLHOS

Usar óculos de protecção herméticos (ref. norma EN 166).

### PROTECÇÃO DA PELE

Usar vestuário de trabalho com mangas compridas e calçado de segurança para uso profissional de categoria II (ref. Directriz 89/686/CEE e norma EN ISO 20344). Lavar-se com água e sabão depois de ter removido o vestuário de protecção.

### PROTECÇÃO RESPIRATÓRIA

Em caso de ultrapassagem do valor de limite de uma ou mais das substâncias presentes no produto, referido à exposição diária no ambiente de trabalho ou a uma fracção estabelecida pelo serviço de prevenção e protecção empresarial, usar uma máscara com filtro do tipo AX ou do tipo universal, cuja classe (1, 2 ou 3) terá de ser escolhida em relação à concentração limite de uso (ref. norma EN 14387).

O uso de meios de protecção das vias respiratórias, como máscaras do tipo acima indicado, é necessário na falta de medidas técnicas para limitar a exposição do trabalhador. A protecção oferecida pelas máscaras é, seja como for, limitada.

No caso em que a substância considerada seja sem cheiro ou o seu limiar olfactivo seja superior ao respectivo limite de exposição e em caso de emergência, ou seja quando os níveis de exposição são desconhecidos ou a concentração de oxigénio no ambiente de trabalho seja inferior a 17% em volume, usar um auto respirador de ar comprimido de circuito aberto (ref. norma EN 137) ou um respirador de tomada de ar exterior para o uso com máscara interna, semi-máscara ou bocal (ref. norma EN 139).

Prever um sistema para a lavagem ocular e chuveiro de emergência.

## CONTROLES DA EXPOSIÇÃO AMBIENTAL.

As emissões de processos de produção, incluídas as de equipamentos de ventilação, deveriam ser controladas de acordo com a normativa de protecção do ambiente.

## SECÇÃO 9. Propriedades físicas e químicas.

### 9.1. Informações sobre propriedades físicas e químicas de base.

Estado Físico	líquido
Cor	branco
Cheiro	característico
Limiar olfactivo.	Não disponível.
pH.	Não disponível.
Ponto de fusão ou de congelação.	Não disponível.
Ponto de ebulição inicial.	> 35 C.
Intervalo de ebulição.	54°C / 84°C
Ponto de inflamação.	< 21 C.
Velocidade de evaporação	Não disponível.